

Artem R. Oganov

Professor, Skoltech

25 June 2020

Mineralogical Crystallography:

Lecture Notes

CONTENTS

1. What to do to be successful
2. Introduction and history
3. How crystals grow. Factors determining crystal shape
4. Geometric macrocrystallography
5. Space groups
6. Crystal Chemistry: Part I. Structure determination. Chemical bonding
7. Crystal chemistry: Part II. Structural motifs. Polyhedral representation of structures. Close packing. Pauling's rules
8. Crystal Chemistry: Part III. Polymorphism, polytypism. Morphotropy. Solid solutions
9. Structure types of minerals
10. Crystallography at extreme conditions
11. Structure-property relations
12. Simulating & predicting structure and properties of crystals
13. Supplementary lecture: Crystallography of nanoparticles
14. Supplementary lecture: Structure of crystalline surfaces

1. What to do to be successful.

- Be active –ask questions!
- Always come to classes!
- These notes.
- A.Putnis “Introduction to Mineral Sciences”. Cambridge, 1992. (main textbook).
- L. Pauling “The Nature of the Chemical Bond”. Cornell Univ. Press, 1960 (masterpiece, although in places outdated. Only for further reading).
- I. Hargittai & M. Hargittai “Symmetry through the eyes of a chemist”. Plenum Press, 1995. (Crystallography as fun – for those who liked this course, good reading in free time).

2. Introduction and history.

What is crystallography? Goethe said:

“Crystallography ... is not productive, it exists only for itself, and has no consequences... As it is nowhere really useful, it has developed largely within itself. It does provide the intellect with a certain limited satisfaction, and its details are so diverse that one can describe it as inexhaustible; that is why it captures even first-rate people so firmly and so long.” (Translation J.D. Dunitz).

Crystallography has greatly changed since – and changed all related sciences, including physics, chemistry, biology, and geosciences. One can say that crystallography is a modern interdisciplinary science dealing with the structure and properties of solids with long-range order. In this course we stress its role in Earth sciences.

History.

Ancient times: In Greek, “crystallos” means “transparent ice”. Greeks believed that rock crystal is a form of ice. Democritos and Lucretius Car develop views that matter consists of particles – “atoms”.

Renaissance: G. Cardano (1501-1576) was probably the first scientist attracted by crystals, he tried to explain their internal structure using ideas about packing of spherical particles. These ideas were developed, and the first attempts to analyse the shape of crystals were made, by Johannes Kepler (1571-1630) in his treatise on snow flakes (1611).

1669 – year of birth of crystallography as a science. Nicholas Steno formulates the first crystallographic law: “Crystals of the same compound, but different shapes, have invariable angles between the corresponding faces”. His work was unknown until much later. His life was dramatic – born to a Lutheran Danish family and converted to Catholicism in mature age, he abandoned science and soon became a bishop. He was renowned for his heroic life and was later proclaimed a Catholic saint.

Steno’s law was later re-discovered by M.V.Lomonoson (his work was also forgotten) and, finally, in 1783 by the French mineralogist J.-B. Rome de L’isle (1736-1790).

French abbot R.-J. Haüy (1743-1822) was the first to introduce the notion of the crystal lattice. This allowed him to formulate a second law of crystallography – the law of rational indices, which we discuss later. Haüy’s life was also remarkable. Being a priest during the French revolution was very risky, but he refused to change his convictions. Revolutionary tribunal, however, saved his life– thanks to Haüy’s scientific achievements.

XIX century was the golden era of geometric crystallography. A. Bravais derives the 32 crystallographic point symmetry groups (1848) and discovers the 14 lattice types (1855) – though the 32 groups were previously derived by J. Hessel (1830) and M. Frankenheim (1826), whose works were quickly forgotten. A.W. Gadolin proved that 5-fold and higher than 6-fold symmetry axes are impossible in crystals and gave an elegant derivation of the 32 groups (1867). In 1890, E.S. Fedorov (1853-1919) has derived the 230 space groups,

which describe the symmetry of periodic crystals. A. Schoenflies (1853-1928) gave a different (and independent) derivation, but completed it slightly later. At this stage geometric crystallography was practically complete. Its major extensions in the XX century include the derivation of antisymmetry space groups by A.V. Shubnikov (1887-1970), colour symmetry by N.V. Belov (1891-1982), and 4-, 5-, and 6-dimensional space groups by a number of different people. End of the XIX century witnessed significant developments in chemical crystallography – by such scientists as L. Pasteur, P. Groth, W. Barlow.

XX century. Atomistic theory was accepted by many people, but it was not possible to prove it until the discovery of X-rays in 1895 by W. Roentgen. In 1906, great Austrian physicist L. Boltzmann committed suicide after being accused of relying too much on the notion of atoms – the very existence of which was not proven. Just 6 years later, in 1912, M. von Laue's observation (which earned him a Nobel Prize) of diffraction of X-rays by crystals finally proved that the structure of matter is discrete and atoms do exist. Also in 1912, W.H. Bragg and W.L. Bragg performed the first X-ray structure analysis – the first analysed materials were halite (NaCl) and sphalerite (ZnS) – resulting in another Nobel Prize. By 1920 Braggs determined several dozens of crystal structures and proposed the first system of atomic radii. Later W.L. Bragg formulated basic principles of mineral structure. M. Born (Nobel Laureate) and coworkers devised the formalism and methods to predict crystal structures and lattice dynamics. 1927 – L. Pauling (twice Nobel Laureate) formulates his famous 5 rules for ionic structures. His later works laid the foundations of the theory of chemical bonding – widely using quantum mechanics, he formulated such notions as electronegativity, hybridisation, bond valence. Approximately at the same time V.M. Goldschmidt creates one of the most popular systems of ionic radii, and applies them in geochemistry. L.D. Landau (Nobel Laureate) invents a general theory of phase transitions, later developed by K. Wilson (Nobel Laureate). High-pressure crystallography was founded in the pioneering works of P.W. Bridgman (Nobel Laureate). D. Hodgkin (Nobel Laureate) made important contributions by solving structures of biological molecules using X-ray diffraction. Generally speaking, crystallographic methods are widely used in molecular chemistry and biology – solving the structure of molecular crystals (e.g., proteins, DNA, etc.) allows one to extract the molecular structure. In the post-war period, N.V. Belov was prominent in mineralogical crystallography: his studies resulted in dozens of new mineral structures and their deepened understanding. Important contributions to structural chemistry were made by F. Laves, Yu.T. Struchkov, P. Coppens. With time, crystal structure determination ceased to be a challenge – now this is almost a routine task. The breakthrough in the methodology of structure solution was made by J. Karle and H.A. Hauptman (Nobel Laureates), who invented the so called “direct methods”. R.E. Smalley (Nobel Laureate) and co-workers discovered fullerenes, an exotic form of carbon with a number of unique properties (including superconductivity in metal-doped forms) – this was a major boost to studies of unusual materials. W. Kohn (Nobel Laureate) and coworkers opened a new era in quantum mechanics by formulating density functional theory – now even complex crystal structures can be studied theoretically, opening new ways of predicting and understanding the structure of matter. The second half of the XX century witnessed the discovery of a number of new unusual phenomena (stability of incommensurate phases and quasicrystals, hitherto unknown complex magnetic structures, unusual structural and electronic transitions under pressure, etc.). Crystallographers have solved structures of complex biological molecules (proteins, DNA, etc.) and even viruses. Great progress is being continually made in the understanding of chemical bonding. Now we are at the beginning of being able to predict materials properties on the quantum-mechanical basis, with an outlook to materials design.

New powerful methods and new exciting challenges guarantee that crystallography will remain an interesting and practically important science.

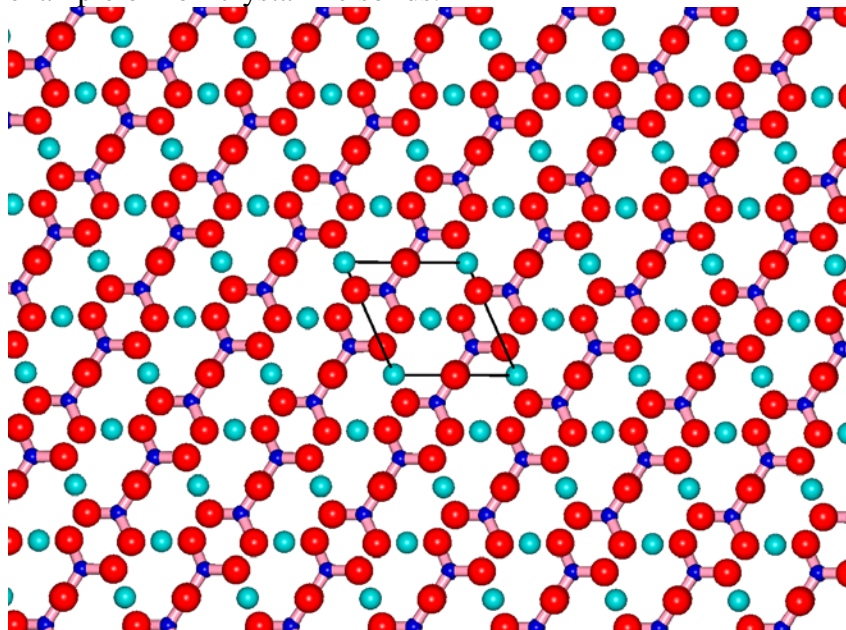


1 – G. Cardano, 2 – J. Kepler, 3 – N. Steno, 4 – R.-J. Hauy, 5 – R. de L'isle, 6 – A. Bravais, 7 – E.S. Fedorov, 8 – M. von Laue, 9 – M. Born, 10 – W.L. Bragg, 11 – V.M. Goldschmidt, 12 – L. Pauling, 13 – L.D. Landau, 14 – P.W. Bridgman, 15 – A.V. Shubnikov, 16 – D. Hodgkin, 17 – N.V. Belov, 18 – J. Karle, 19 – H.A. Hauptman, 20 – K. Wilson, 21 – R.E. Smalley, 22 - W. Kohn.

In this course we will learn some basics about the external shape of crystals and ways of describing and understanding it, about the internal structure of minerals and its relationship with their properties and ways of understanding and predicting it, about chemical bonding in minerals and the dramatic changes in the structure, properties, and bonding in crystals that occur under high pressures and temperatures inside the Earth and other planets.

3. How crystals grow.

By a crystal we understand a solid with a well-defined periodic atomic structure. All minerals are CRYSTALLINE. Often one has a polycrystalline aggregate, where a multitude of tiny crystals are intergrown in random orientations. Glasses are an example of non-crystalline solids.



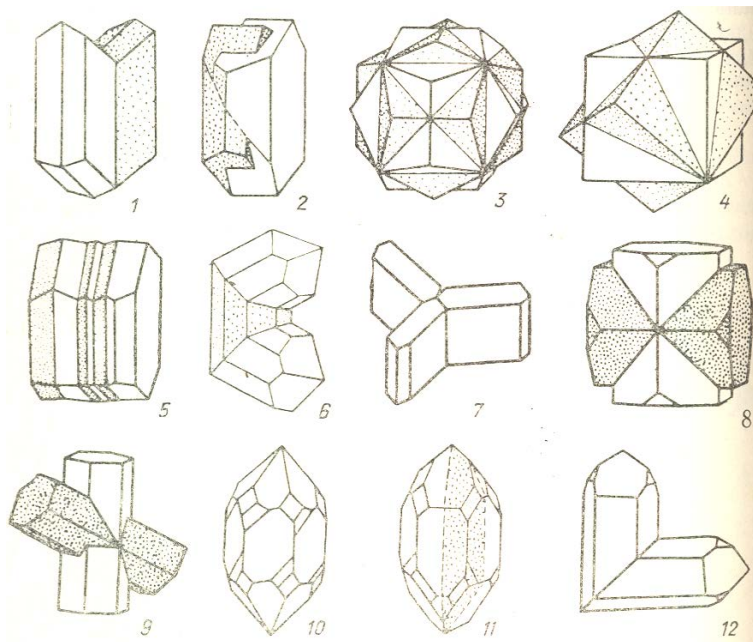
Crystal structure of calcite (CaCO_3) showing periodicity and the unit cell.

Crystals can grow from:

- From the gas phase
- From solution
- From melt
- In the solid phase – recrystallisation
- In a chemical reaction

By growing crystals on a substrate, if the two have similar crystal structure, one can often achieve epitaxy – growth oriented by the substrate. Epitaxial growth is important in technology (computer industry etc.). It can produce new unusual phases as it introduces a strain in the growing crystal.

Twinning. Another type of oriented intergrowth of crystals is twinning – where there is a symmetry relation between two or more intergrown crystals. One distinguishes between simple twins (2 crystals), multiple twins (3 or more crystals) and polysynthetic twins (very large number of crystals). Twins are formed during either crystal growth, phase transition, or mechanical deformation. Twinning can destroy certain physical properties – e.g., pervasive twinning of quartz destroys useful piezoelectric properties (used in quartz watches) of most natural crystals of quartz.



1-“swallow-tail” twin of gypsum, 2- Karlsbad twin of feldspar, 3- twin of pyrite, 4- spinel twin, 5- polysynthetic twin of plagioclase, 6- multiple twin of rutile, 7- triple twin of aragonite, 8,9- twins of staurolite, 10-Dauphine twin of quartz, 11- Brazilian twin of quartz, 12- Japanese twin of quartz. (after Yegorov-Tismenko, 1992).

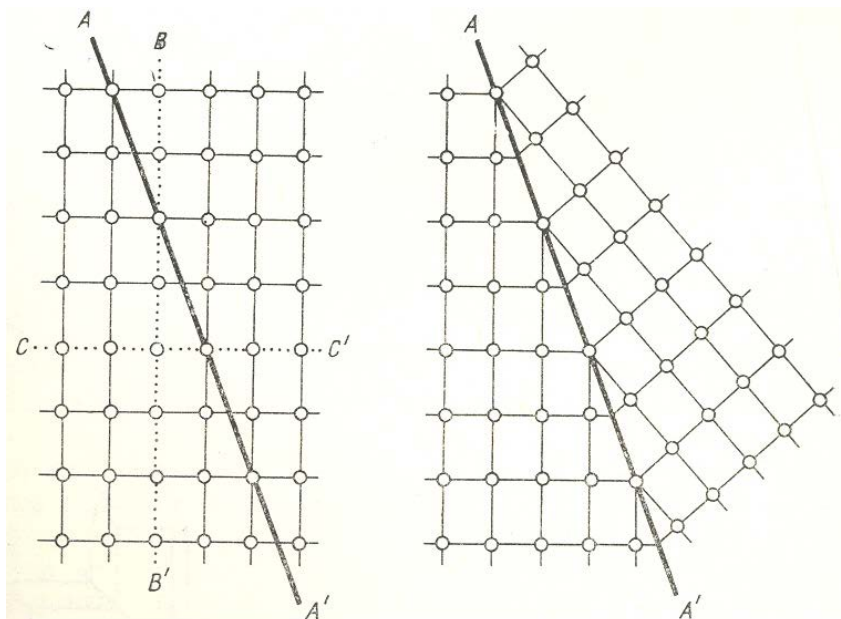


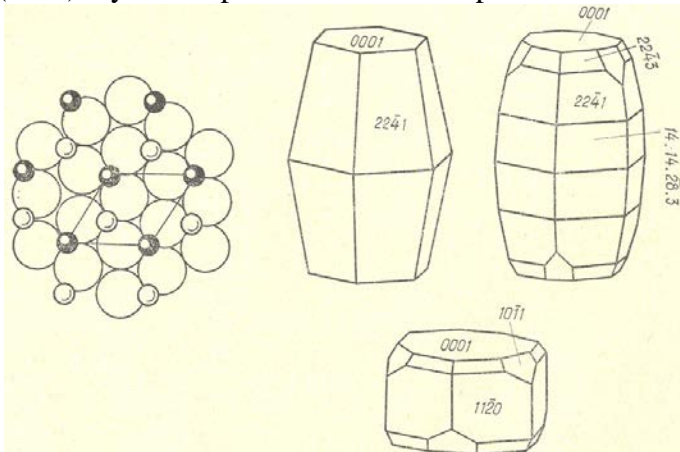
Illustration of the link between crystal structure and twinning (from Yegorov-Tismenko, 1992). Left – untwinned crystal, right – twin.

Genetic significance of crystal morphology. To an experienced mineralogist, crystal morphology can tell a detailed story of how the mineral was formed, grew, and changed. E.g., skeletal forms indicate very rapid non-equilibrium growth.



Skeletal crystals of sal ammoniac (NH_4Cl).

Crystals of corundum (Al_2O_3) grown in alkaline environments are flat, whereas in acidic environments they grow isometric or elongated. For many minerals, e.g. quartz (SiO_2) crystal shape indicates the temperature of formation.



Crystal shapes and structure of corundum Al_2O_3 (from Kostov, 1976).

Factors determining crystal shape.

The first important rule – *geometric*: crystallographic faces with the lowest indices (e.g., $\{100\}$, $\{010\}$, $\{001\}$, $\{110\}$, $\{210\}$) are usually preferred. This rule was confirmed by numerous studies; exceptions are very few – among the most notorious is calcite CaCO_3 , for whose crystals ~700 different faces are known, often involving large indices. However, in accordance with our rule, these faces are usually small. Another exception is calaverite AuTe_2 , whose crystals actually prefer to have faces with huge indices – only a few years ago it was found that calaverite structure is modulated, and this fact is responsible for the weird morphology.

Of course, the crystal shape is entirely due to the crystal structure and the effects of the environment. E.g., crystals of corundum (Al_2O_3) grown in alkaline solutions, always have a tablet shape – i.e. very large basal faces $\{0001\}$. A likely explanation is that during crystal growth the $(\text{OH})^-$ ions are adsorbed on the $\{0001\}$ surfaces forming thin films of gibbsite $\text{Al}(\text{OH})_3$. These thin films are very stable and slow down the growth of the crystal in the direction perpendicular to this surface. As a consequence, $\{0001\}$ faces predominate. Note: generally, the slowest-growing faces are the most common ones. Fast-growing faces are

very small. This is the second important rule that we discover in the field of crystal morphology. It is based on the *kinetics* of crystal growth. Wulff's theorem is the other important rule, but based on *thermodynamics* – i.e. considering crystal growth as a very slow process. These rules complement each other.

Wulff's theorem. Atoms at the surface of a crystal are weaker bound to the rest of the crystal than atoms inside the crystal. There always is an energy cost associated with the formation of a surface. Take, e.g., breaking a piece of glass – new surfaces, introduced by fracturing, cannot be formed unless you spend some energy on this process (e.g., energy of a stone hitting the glass window!) So, there is an energy cost associated with the formation of surfaces. Crystals want to minimise this cost. If crystals were isotropic (like glasses and liquids), they would be bound to have a spherical shape to minimise the surface area. The

anisotropy of crystals means that different surfaces – e.g., $\{100\}$ and $\{1\bar{1}0\}$ have different surface energies. Of course, the crystal would prefer to have the low-energy surfaces rather than the high-energy ones. Minimising the total surface energy, Russian crystallographer G.Wulff has found a remarkable theorem called the Wulff theorem, for a macroscopic crystal in equilibrium:

$$W_1/d_1=W_2/d_2=W_i/d_i=\text{constant},$$

where W_i are the surface energies for particular faces, and d_i the lengths of the normals from the centre of the growing crystal to the face. The shorter the normal, the larger the face. In accordance with our expectations, the lowest-energy faces have the shortest normals and largest areas. Larger-energy faces can also be present – their role is to minimise the total surface area of the crystal, to cut the edges and corners. From Wulff's theorem and the kinetic principle of crystal morphology it can be seen that the speed of growth of a crystallographic face at equilibrium is proportional to its surface energy. As always, there is a close link between kinetics and thermodynamics! This is strictly true for slowly-growing crystals, close to the thermodynamic limit. For fast-growing crystals, the attachment energy (showing how easy it is for particles to settle upon a given surface) that will govern the growth rate and crystal shape.

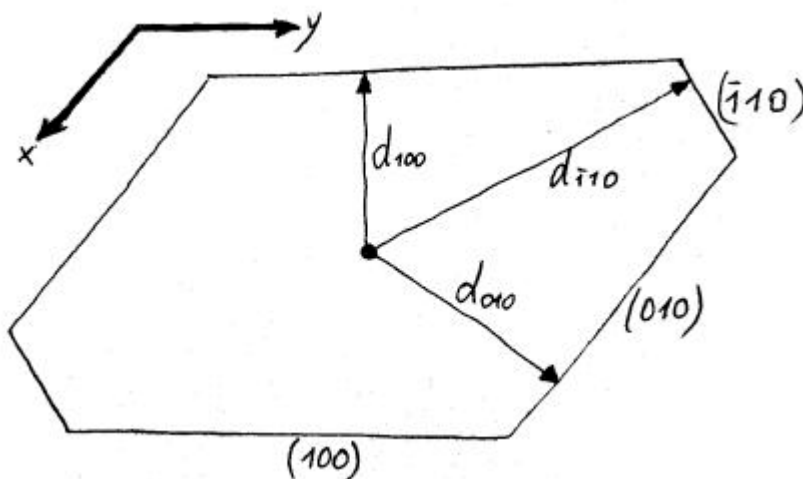
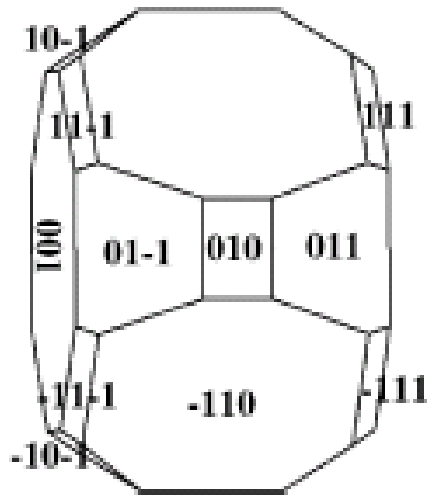
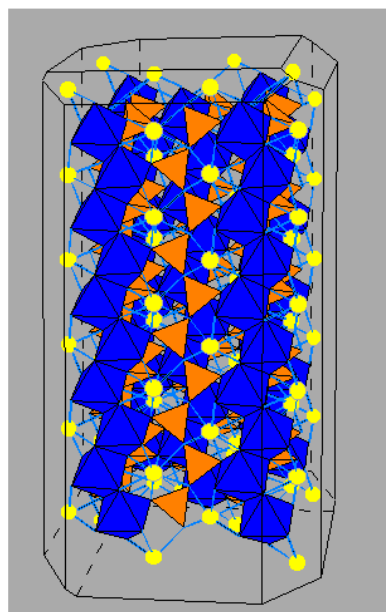


Illustration of the Wulff theorem.



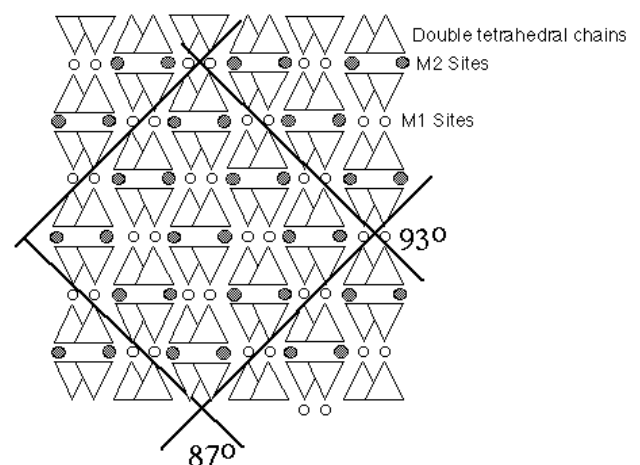
Equilibrium shape of crystals of MgSiO_3 perovskite, predicted with the Wulff theorem (Alfredsson et al., 2005).

Now, what determines the surface energy? The structure of the crystal *and* the environment. The effects of the environment are mainly to neutralise the surface charge, saturate the broken bonds at the surface, and also to put an impurity atom on the surface. The crystal structure can tell you which surfaces will involve the disruption of the strongest bonds and, therefore, would be unfavoured. In the pyroxene structure the strongest bonds are Si-O. SiO_4 tetrahedra form infinite $[\text{SiO}_3]$ chains parallel to the c axis. To create a $\{001\}$ surface means to break an $[\text{SiO}_3]$ chain and bonds within it. On the other hand, creation of surfaces parallel to c can be imagined without breaking any Si-O bonds, and therefore has a lower energy. These faces are clearly preferred – explaining the prismatic habit of the pyroxenes. Note also that in the vacuum the effects of the environment are absent, and crystal structure alone determines the surface energies. Cleavage planes would correspond to the lowest-energy surfaces – hence the relation between the crystal morphology and cleavage geometry (in pyroxenes, also prismatic).



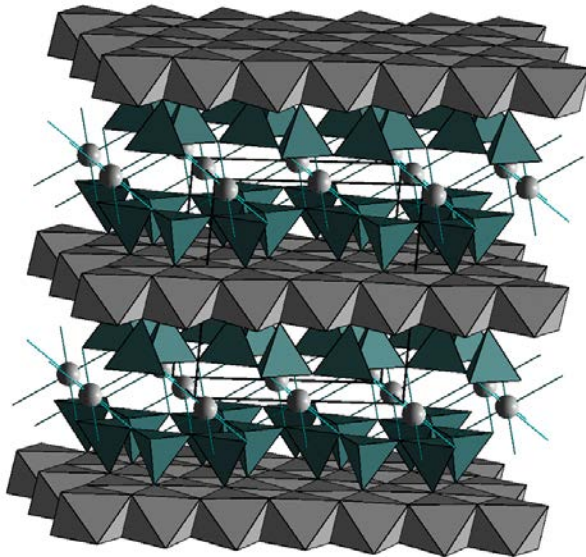
A.

Pyroxene Structure and Cleavage Angles:



B.

Crystal structure of pyroxene diopside ($\text{CaMgSi}_2\text{O}_6$) and morphology of its crystals. SiO_4 tetrahedra red, MgO_6 octahedra blue, Ca atoms yellow. One can see a clear relationship between crystal morphology and structure. B. Cleavage planes in pyroxenes (projection perpendicular to the c axis).



Layered crystal structure of mica – micas have perfect cleavage along the layers of structure, and platy habit.

4. Geometric macrocrystallography.

Crystal morphology.

Not every crystal is perfectly shaped and symmetric, crystals often grow in asymmetric shapes due to asymmetric growth conditions. It was Steno who first observed that the angles between the corresponding faces of a crystal are constant, characteristic for a given mineral. These angles are dictated by the internal structure, not by the conditions of growth (which can only change the relative areas of different faces). Therefore, the relative orientation of crystal faces contains information on the symmetry of the crystal. The macroscopic symmetry of crystals is characterised by a set of symmetry operations called a point group, and there are only 32 possible crystallographic point symmetry groups. We will consider these groups in more detail below, first we focus on symmetry elements possible in crystals.

In a macroscopic crystal, we distinguish the following symmetry elements:

- Mirror plane (m).
- Centre of symmetry (or inversion centre – C).
- Rotation axes: twofold (2), threefold (3), fourfold (4), sixfold (6).
- Rotoinversion axes: only fourfold ($\bar{4}$).

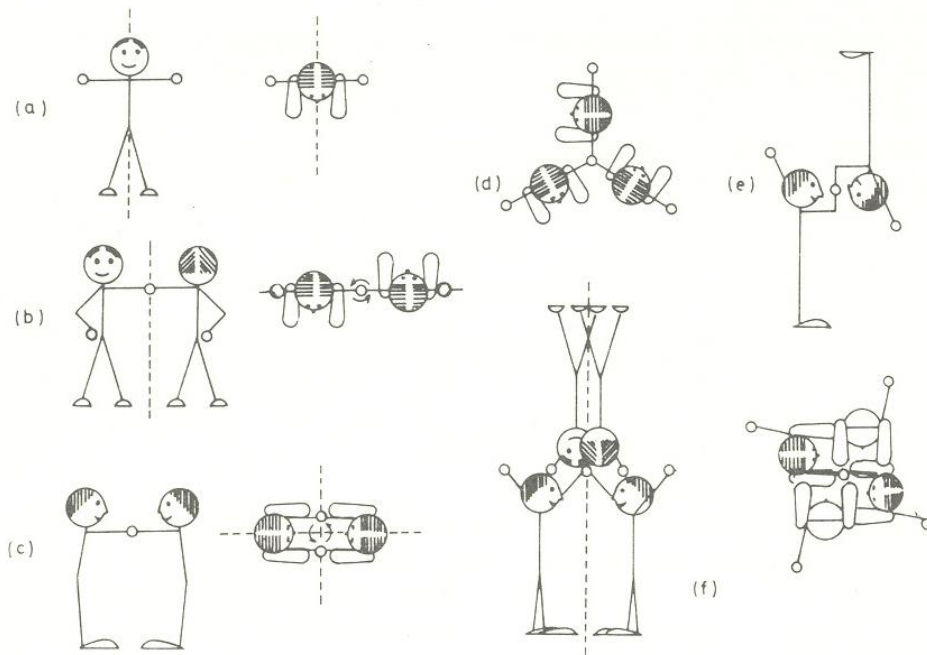
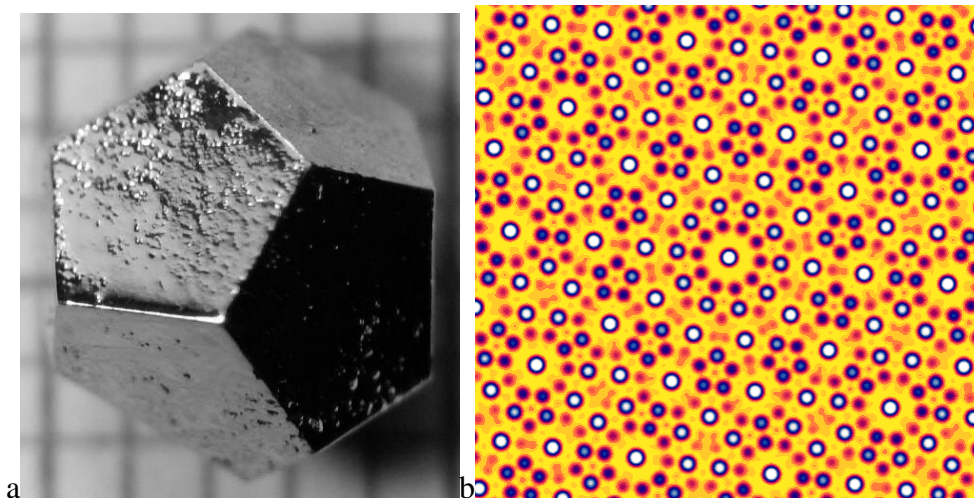
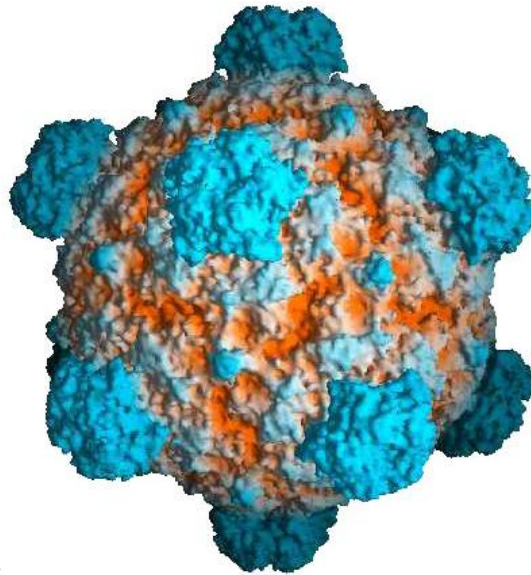


Fig. 1.3. Some symmetry elements, represented by human figures. (a) Mirror plane, shown as dashed line, in elevation and plan. (b) Two-fold axis, lying along broken line in elevation, passing perpendicularly through clasped hands in plan. (c) Combination of two-fold axis with mirror planes; the position of the symmetry elements given only in plan. (d) Three-fold axis, shown in plan only. (e) Centre of symmetry (in centre of clasped hands). (f) Four-fold inversion axis, in elevation and plan, running along the dashed line and through the centre of the clasped hands. (After L. S. Dent Glasser, Chapter 19, *The Chemistry of Cements*: Academic Press, 1964.)

Theorem: 3-dimensional periodicity is incompatible with the presence of 5-fold and greater than 6-fold symmetry axes. These “inconsistent” symmetry axes are called non-crystallographic and can exist in aperiodic systems like quasicrystals, molecules, viruses, etc. (to illustrate this, it is easy to show that it is impossible to fill a plane with regular pentagons). Until recently, quasicrystals were unknown in the nature. However, in 2009 L. Bindi (Italy) and coauthors reported a naturally occurring stable and well-ordered quasicrystal of composition $\text{Al}_{63}\text{Cu}_{24}\text{Fe}_{13}$ (Bindi et al., *Science* 2009), forming micron-size grains.





c

Examples of fivefold symmetry in aperiodic objects. a-Ho-Mg-Zn quasicrystal, b-electron microscopy image of a quasicrystal structure, c – icosahedral virus.

DREHACHSEN		DREHINVERSIONSACHSEN	
Zähligkeit	Symbol in der Zeichnung	Zähligkeit	Symbol in der Zeichnung
1		$\bar{1}$ = Symmetriezentrum	o
2	●	$\bar{2} (= m)$	m : <ul style="list-style-type: none"> — m steht senkrecht auf der Zeichenebene — m liegt in der Zeichenebene
3	▲	$\bar{3} (= 3+\bar{1})$	▲
4	◆	$\bar{4}$	◆
6	●	$\bar{6} (= \frac{3}{m})$	●

Notation of symmetry elements (from Weiss & Witte, 1983).

Crystal categories and systems, coordinate systems: 3-,4-, and 6-fold axes are called major axes. Symmetry axes and normals to mirror planes are called special directions. According to their presence or absence, we distinguish three crystal categories, which are detailed below with a description of the coordinate systems:

- High: more than one major axis present.

Only cubic crystal system. The choice of coordinate' system is obvious.

- Medium: Only one major axis.

Hexagonal (6-fold axis), trigonal (3-fold axis), tetragonal (4-fold axis) systems. Coordinate system: *c* along the major axis, *a* and *b* are in the perpendicular plane and along some special direction.

- Low: No major axes present.

Orthorhombic: three special directions (defining coordinate axes). Monoclinic: one special direction (axis *b*, for historical reasons), axes *a* and *c* are chosen in the perpendicular plane. Triclinic: no special directions, coordinate axes in the general orientation.

This division is based on a mathematical analysis of possible crystal symmetries: e.g., it is not possible to have only two special directions in a crystal, interaction of symmetry elements will necessarily produce the third special direction. Note that often “proper hexagonal” and “trigonal” systems are considered as subsystems of the hexagonal system.

Below is a summary of crystal systems:

Category	Crystal system	Features	Coordinate system	Mineral examples
High	Cubic	Four 3-fold axes	$a=b=c,$ $\alpha=\beta=\gamma=90^\circ$	Native Cu, Fe, diamond (C) Halite (NaCl) Sphalerite (ZnS) Garnets
Medium	Hexagonal	One 6-fold axis	$a=b\neq c,$ $\alpha=\beta=90^\circ, \gamma=120^\circ$	Graphite (C) Wurtzite (ZnS)
	Trigonal	One 3-fold axis	$a=b\neq c,$ $\alpha=\beta=90^\circ, \gamma=120^\circ$	Quartz (SiO ₂) Calcite (CaCO ₃)
	Tetragonal	One 4-fold axis	$a=b\neq c,$ $\alpha=\beta=\gamma=90^\circ$	Stishovite (SiO ₂)
Low	Orthorhombic	3 special directions	$a\neq b\neq c,$ $\alpha=\beta=\gamma=90^\circ$	Aragonite (CaCO ₃)
	Monoclinic	1 special direction	$a\neq b\neq c,$ $\alpha=\gamma=90^\circ\neq\beta$	Some feldspars (orthoclase KA1Si ₃ O ₈)
	Triclinic	No special directions	$a\neq b\neq c,$ $\alpha\neq\beta\neq\gamma\neq90^\circ$	Some feldspars (albite NaAlSi ₃ O ₈)

A bit of mathematics: indices of vectors, edges and faces in crystals.

Notation – [pqr] for vectors, (hkl) for a particular face, {hkl} for a family of symmetrically equivalent faces.

Now that we have a coordinate system definition, we can work on mathematical descriptions of crystal morphology and its main elements — crystal faces and edges. A vector is denoted by three coordinates defined in our (in general, non-Cartesian!) coordinate system — just like in standard geometry. The same definition applies to crystal edges. For faces things are more complex.

We could define coordinates of a plane by its intersections with the coordinate axes, however, there is a problem — for faces running parallel to a coordinate axis, at least one index will be infinite (no intersection with the axis!). To solve this problem, Miller

indices are used, which use the inverse numbers of these intersections — so, for an axis parallel to \mathbf{a} , the first index is not ∞ , but $1/\infty$ - or just 0.

Generally, if we denote the intercepts of the three coordinate axes as l_a , l_b , and l_c , respectively, unit lengths of the coordinate system as $\mathbf{a}, \mathbf{b}, \mathbf{c}$, and indices of the face as h, k, l , we get the following definition of Miller indices:

$$(\mathbf{a}/l_a): (\mathbf{b}/l_b): (\mathbf{c}/l_c) = h:k:l$$

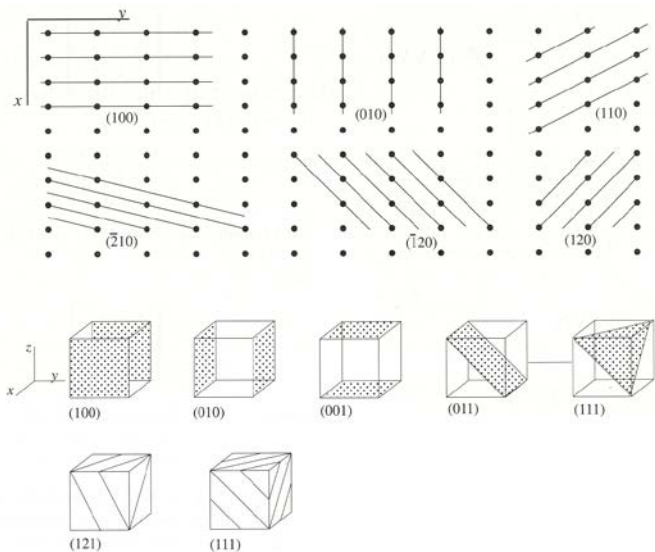
Hauy has found that in crystals $h:k:l$ is always a ratio of small integers (law of rational indices). Note that one takes the smallest integers — for example, (222) should be reduced to (111), (884) will be reduced to (221), etc.

Miller indices have a number of very useful properties often used in structural analysis and theoretical descriptions of crystals.

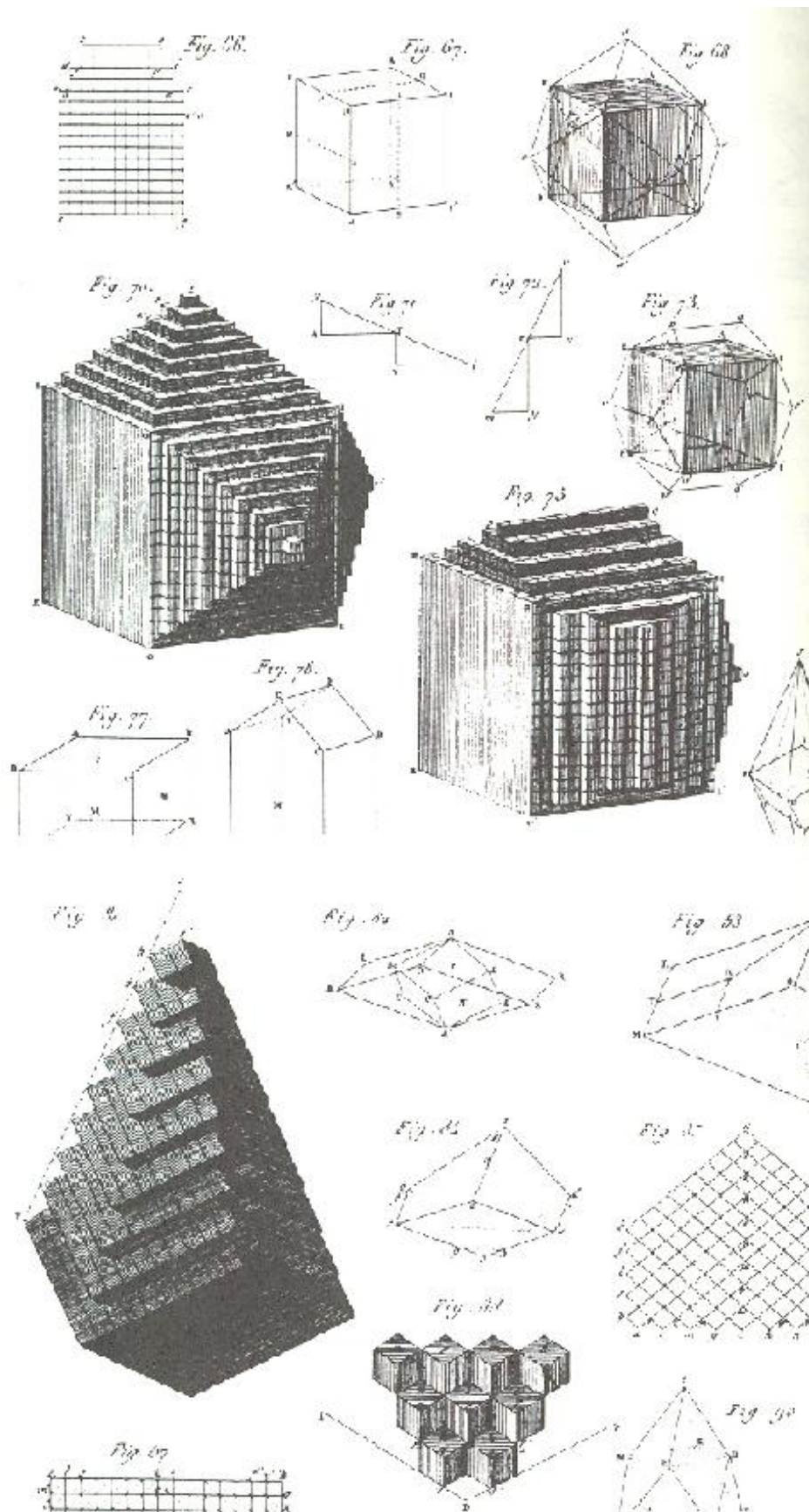
- One interesting property is that a vector $[hkl]$ is perpendicular to the plane $\{hkl\}$.
- Another property is that all faces $\{hkl\}$ parallel to direction $[pqr]$ satisfy the following equation:

$$hp+kq+lr=0$$

Subtlety for hexagonal and trigonal crystals, especially in old literature, four indices were introduced - $\{hkil\}$, since there are three equivalent axes in the a-b plane. However, only three of them are truly independent as $h+k+i=0$ in this case. So, for instance, one can write $\{10\bar{1}0\}$ or simply $\{100\}$ - this means the same.



Examples of Miller indices (from Putnis, 1992).



Hauy's drawings of crystal surfaces: from Hauy's work it followed that for stable crystal faces hkl -indices are small integer numbers. (picture from Hargittai & Hargittai, 1995).

32 point groups. Simple but lengthy mathematical considerations give an important result — there can be only 32 possible crystallographic combinations of symmetry elements.

To list them all, we need a scheme for labelling these classes. Here is the simplest one — we list all the symmetry-independent elements together with their number in the crystal, e.g.:

$22'2''mm'm''C$ — symmetry class of aragonite.

This notation is somewhat lengthy, so it has been replaced by the so-called international, or Hermann-Mauguin, symbols. These symbols contain three positions, which are used as follows:

High category: 1st position for the coordinate direction, 2nd for the threefold axis, 3rd for the diagonal between two coordinate axes.




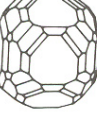

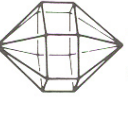
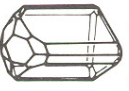

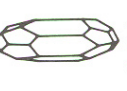



Medium category: 1st position for coordinate direction c , 2nd for direction $a(=b)$, 3rd for the $a-b$ diagonal.

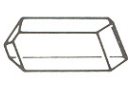



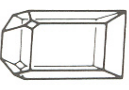
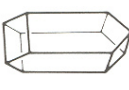

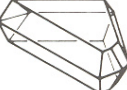
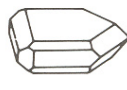

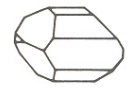
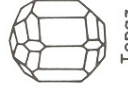

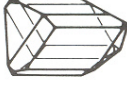

Low category: each position for each coordinate direction in order a,b,c .

Symmetry elements are denoted as $2,3,4,6,\bar{4},m$, and from now on we denote the symmetry centre as $\bar{1}$ (it is equivalent to the 1-fold rotoinversional axis). When there are two elements corresponding to the same direction, e.g. an axis and a normal to a mirror plane, we write, e.g. $4/m$. In Hermann-Mauguin symbols, we write only the necessary and sufficient elements — omitting those that can be generated from this set.

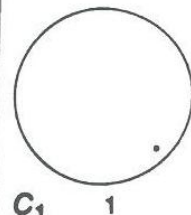
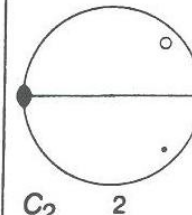
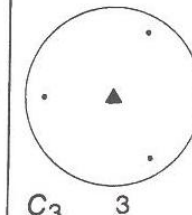
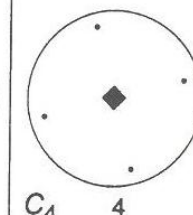
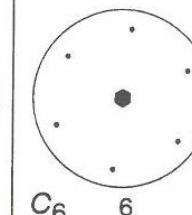
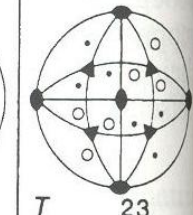
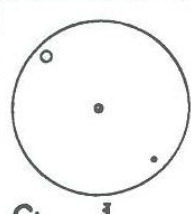
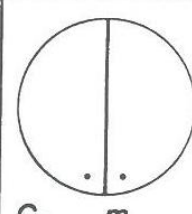
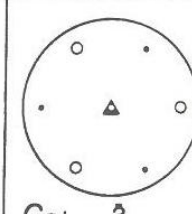
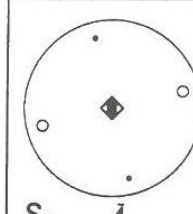
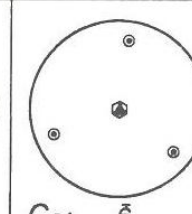
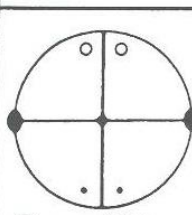
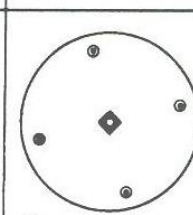
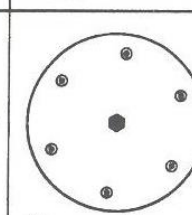
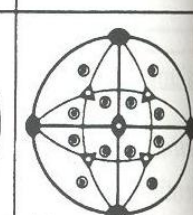
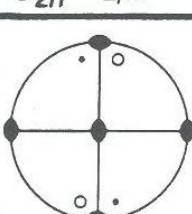
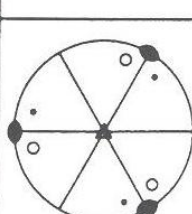
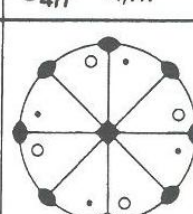
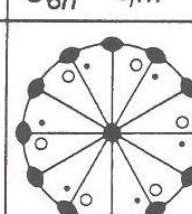
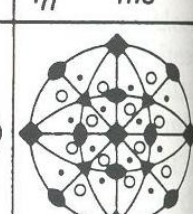
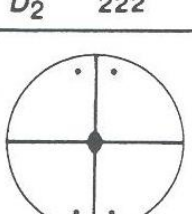
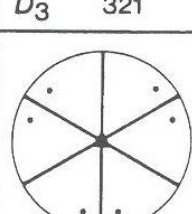
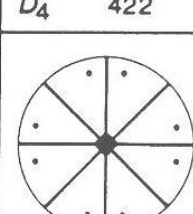
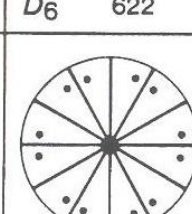
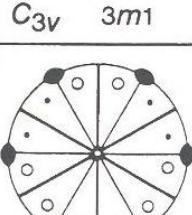
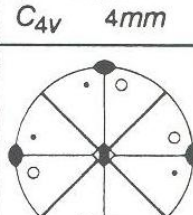
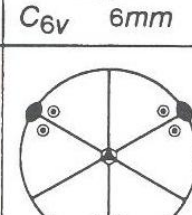
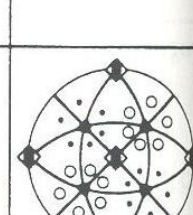
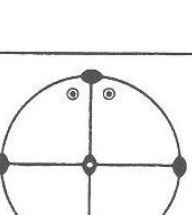
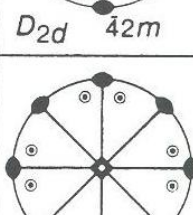
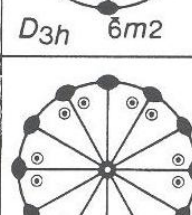
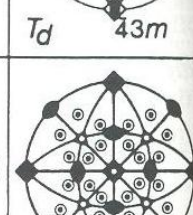
For example, $22'2''mm'm''C = 2/m\ 2/m\ 2/m = mmm$, because all the symmetry elements of this class can be generated from three mutually perpendicular mirror planes.

Below is a table with all crystallographic symmetry classes, with some examples predominantly from the realm of minerals:

Hexagonal		Cubic (Isometric)	
C_3	 NaIO ₄ ·3H ₂ O	C_6	 Nepheline
S_6	 Diopside	$6/m$	 Apatite
D_3	 Quartz	D_6	 Quartz
C_{3v}	 Turmaline	C_{6v}	 Zincite
D_{3d}	 Calcite	D_{6h}	 Beryl
		C_{3h}	 Fluorite
		$\bar{6}$	 Benitoite

Triclinic and Monoclinic		Orthorhombic		Tetragonal	
C_1	 Sr-tartrate tetrahydrate			C_4	 Wulfenite
C_i	 Axinite			C_{4h}	 Scheelite
C_2	 Sucrose	D_2	 Epsomite	D_4	 Nickel sulfide
C_s	 Hilgardite	C_{2v}	 Hemimorphite	C_{4v}	 Diabolite
C_{2h}	 Augite	D_{2h}	 Topaz	D_{4h}	 Cassiterite
				S_4	 Cahnite
				D_{2d}	 Chalcopyrite

Examples of 32 point groups, mainly from minerals (from Hargittai & Hargittai, 1995).

Triclinic	Monoclinic / Orthorhombic	Trigonal	Tetragonal	Hexagonal	Cubic
 C_1 1	 C_2 2	 C_3 3	 C_4 4	 C_6 6	 T 23
 C_i 1	 C_s m	 C_{3i} 3	 S_4 4	 C_{3h} 6	
	 C_{2h} $2/m$		 C_{4h} $4/m$	 C_{6h} $6/m$	 T_h $m\bar{3}$
	 D_2 222	 D_3 321	 D_4 422	 D_6 622	 O 432
	 C_{2v} $mm2$	 C_{3v} $3m1$	 C_{4v} $4mm$	 C_{6v} $6mm$	
		 D_{3d} $3m1$	 D_{2d} $42m$	 D_{3h} $\bar{6}m2$	 T_d $43m$
	 D_{2h} mmm		 D_{4h} $4/mmm$	 D_{6h} $6/mmm$	 O_h $m\bar{3}m$

Symmetry statistics. Quite surprisingly, there is a strong preference of crystals to a small number of point groups. For example, 35% of inorganic and 45% of organic crystals have the point group $2/m$. Though the exact numbers differ between organic and inorganic materials (organic crystals overall have lower symmetry), there is a common trend: lower-symmetry crystal systems are more often adopted, and for each crystal system the highest-symmetry point group is more popular (e.g., $2/m$ among monoclinic groups). The exact explanation for this strange statistics is not known, but much can be explained by the competition between two tendencies: the tendency of structures to adopt the highest possible symmetry, and also by the predominance of chemically complex compounds in statistics (such compounds usually have low symmetries, in contrast to usually highly symmetric chemically simple crystals).

Table 3.2 Population statistics for the 32 crystallographic point groups gathered from more than 280,000 chemical compounds. Inorganic (I) and organic (O) have somewhat different percentages

	I	O		I	O
1	0.67%	1.24%	422	0.40%	0.48%
$\bar{1}$	13.87	19.18	$4mm$	0.30	0.09
2	2.21	6.70	$\bar{4}2m$	0.82	0.34
m	1.30	1.46	$4/mmm$	4.53	0.69
$2/m$	34.63	44.81	6	0.41	0.22
222	3.56	10.13	$\bar{6}$	0.07	0.01
$mm2$	3.32	3.31	$6/m$	0.82	0.17
mmm	12.07	7.84	622	0.24	0.05
3	0.36	0.32	$6mm$	0.45	0.03
$\bar{3}$	1.21	0.58	$\bar{6}m2$	0.41	0.02
32	0.54	0.22	$6/mmm$	2.82	0.05
$3m$	0.74	0.22	23	0.44	0.09
$\bar{3}m$	3.18	0.25	$m3$	0.84	0.15
4	0.19	0.25	432	0.13	0.01
$\bar{4}$	0.25	0.18	$\bar{4}3m$	1.42	0.11
$4/m$	1.17	0.67	$m3m$	6.66	0.12

Symmetry statistics (after Newnham, 2005).

Illustrations of chirality in molecules (glyceraldehyde) and crystals (quartz) (from Hargittai & Hargittai, 1995).

Did you know? Chiral forms of the same molecule have the same physical properties, but VERY DIFFERENT biological activity (and no one really knows why!): right-handed molecule of vitamin C ((+)-ascorbic acid) is a vitamin, whereas left-handed (-)-ascorbic acid is not a vitamin and has no biological activity. (+)glucose is a food, whereas (-)glucose is not. (-)-chloromycetin is a powerful antibiotic, whereas (+)-chloromycetin is not. (-)-adrenaline is many times more active as a hormone than (+)-adrenaline. (+)-form of thalidomide is a safe and effective drug against morning sickness, whereas (-)-thalidomide is an active mutagen (i.e. causes biological mutation and leads to birth defects if taken by pregnant women) [Roberts, 1989].

Did you know? We all know how often table salt (NaCl) particles stick to each other, making it difficult to sprinkle salt on your favourite dish. The reason is that NaCl particles have the shape of a cube, and these cubes (with the help of water molecules from the air) stick to each other along the large surfaces of the cubes. In 2006, a group of Indian scientists patented a way to avoid this, by growing tiny salt crystals from a solution containing small amounts of glycine. Crystals of NaCl grown from such solutions have a different shape, rounder than cube. This rounder shape prevents sticking of salt particles. The reason that this shape appears is that glycine molecules prefer to settle on {210} faces (rather than {100} cubic faces) – and thus slow their growth. Remember that slowly growing faces of a crystal dominate! In the presence of urea, NaCl forms octahedral crystals, but this method is not suitable for culinary purposes!

Curie principle. Unusual morphologies. Pierre Curie has formulated a fundamental principle that only those elements that are common between the object (crystal) and the environment (growth environment) will be preserved in the object. In other words, crystals growing in asymmetric environment, appear to have lower symmetry than what is dictated by crystal structure. It is well known that perfectly symmetric crystals are rare, but sometimes one has truly “deceptive” crystal shapes. E.g., cubic pyrite is known in crystals of trigonal symmetry. Or sal ammoniac, NH_4Cl and cuprite Cu_2O , belonging to non chiral symmetry class $m\bar{3}m$, in natural conditions sometimes have morphological symmetry 432 (i.e. its crystals are chiral, with a distinction between “left” and “right”). The reason for this morphological paradox is in the presence of biological molecules (usually chiral — and predominantly “left” rather than “right”, a paradox still lacking explanation!) in the growth environment — these molecules destroy equivalence between “left” and “right” in the crystal, and we get chiral morphology.

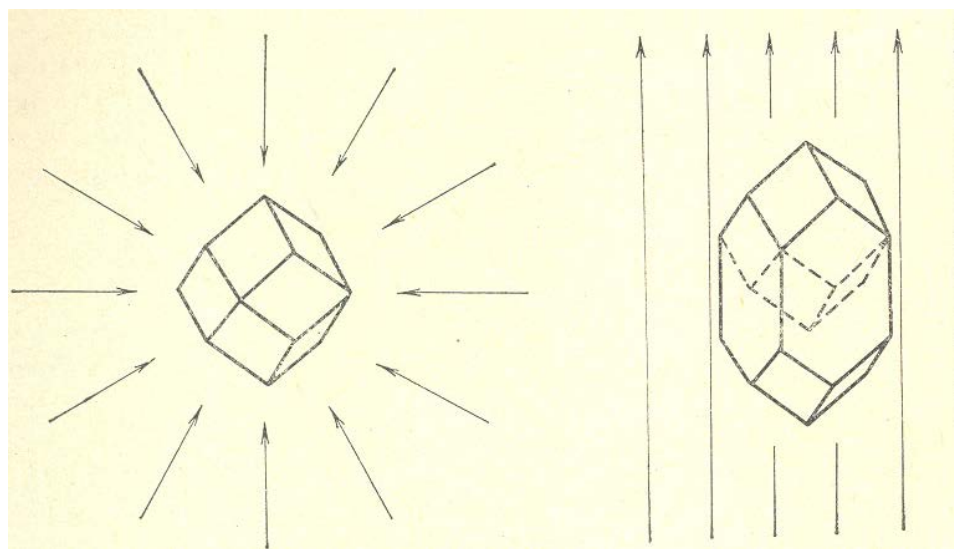


Illustration of the Curie principle. (from Kostov, 1976).

Physical properties and the von Neumann principle. For physical properties, the von Neumann principle is valid: “Physical properties have the same symmetry as the crystal structure, or higher”. For instance, thermal expansion of a cubic crystal has symmetry higher than cubic — spherical.

Generally speaking, many crystal properties are described by the so-called rotation groups (spherical, cylindrical, conical groups). In these, infinite-order rotation axes are present.

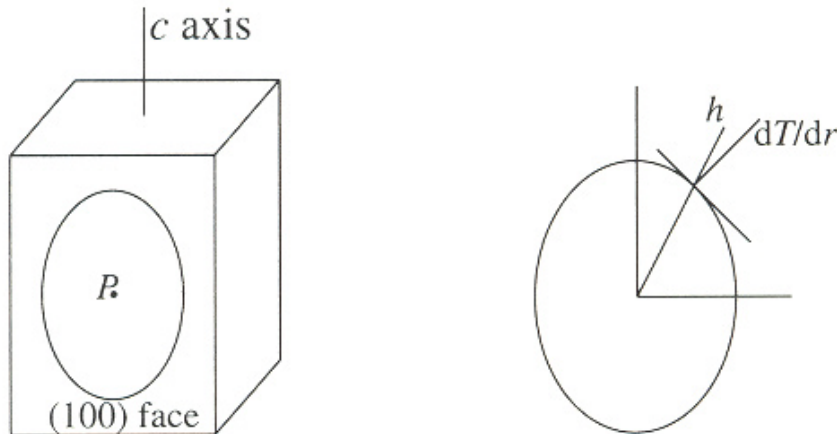


Illustration of the von Neumann principle: symmetry of a physical property (e.g., thermal expansion - right) is higher or equal than symmetry of the crystal (left). (from Putnis, 1992).

5. Space groups.

The symmetry groups considered in the previous chapter are called “point groups” because their symmetry operations leave one point unmoved. These are symmetry groups of finite objects, molecules and clusters, macroscopic crystals. When one considers atomic structure of crystals at the microscopic level, the size of the crystal is so much larger than the size of the atom that it is convenient to consider crystals as infinite objects. These objects have an additional symmetry operation — translation.

Unit cell and Bravais cell. The choice of a unit cell (smallest unit periodically repeated in space) is not unique. The standard choice is a cell with shortest translation vectors.

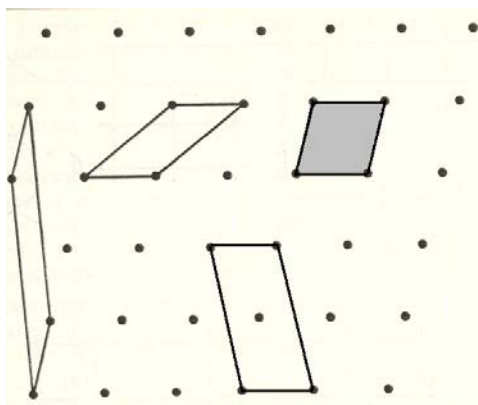


Illustration of non-uniqueness of cell choice. The shaded cell is the standard choice. (modified after Vainstein, 1979).

This smallest unit cell, however, is not always the most convenient one – in some cases its shape will not reflect the symmetry of crystal. By a Bravais cell we understand the smallest periodically repeated crystal fragment, whose shape has the correct point group symmetry of the crystal. Bravais cell and unit cell are identical for primitive (P) lattices, and different for centred lattices.

Different types of cell centering are possible:

Body-centred cells (I-centred)

Face-centred (F-centred)

Base centred (A-, B-, C- centred).

Bravais has demonstrated that only 14 different types of lattices are possible – e.g., cubic lattices can be primitive (P), body-centred (I), or face-centred (F), but not base-centred.

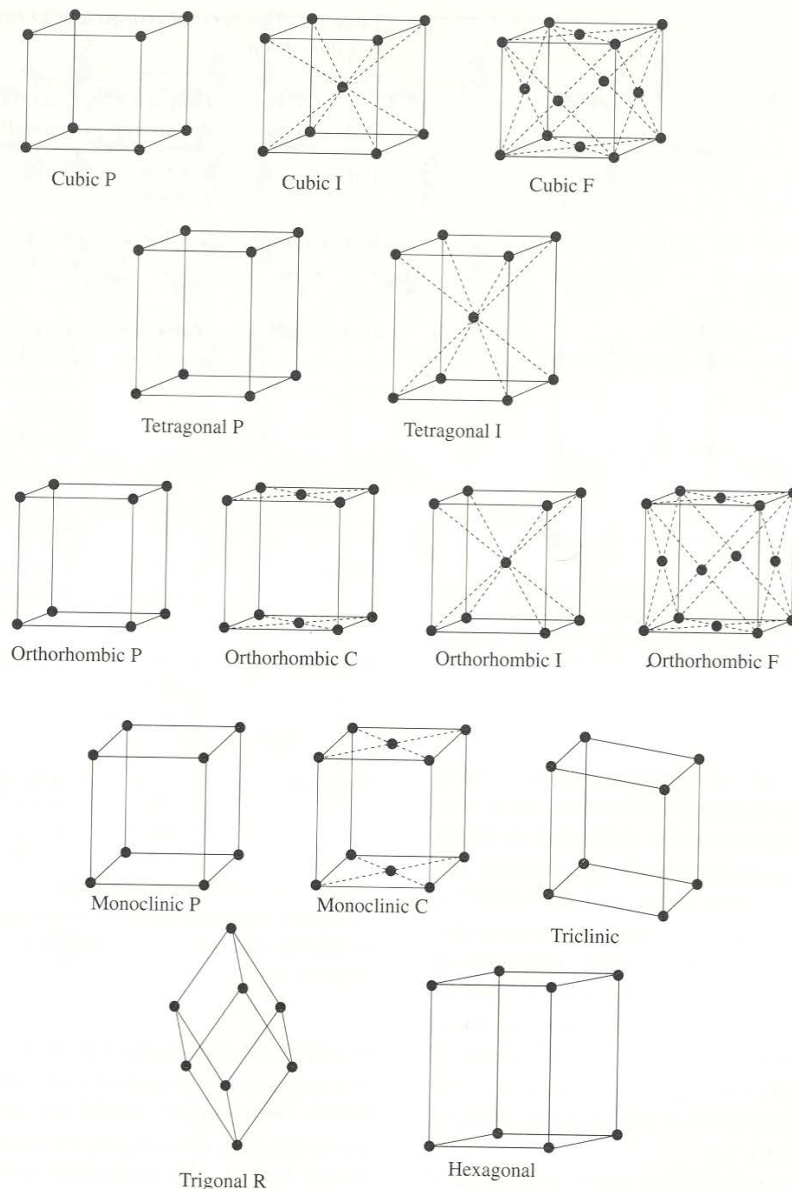


Figure 1.11. The 14 Bravais lattices. All crystalline solids can be described by unit cells which belong to one of these 14 types.

14 Bravais lattices (from Putnis, 1992).

Translational periodicity is the most fundamental feature of crystals. In infinite periodic structures of crystals all the symmetry elements that we discussed before can be present, but there are additional symmetry elements that did not exist in case of finite figures like macroscopic crystals, molecules, etc.:

- Translations (P, I, F, A/B/C, R).
- Screw axes ($2_1, 3_1, 3_2, 4_1, 4_2, 4_3, 6_1, 6_2, 6_3, 6_4, 6_5$) –e.g. 3_1 is called a “left” axis, while 3_2 is “right”. Such axes as $2_1, 4_2$ and 6_3 are neither “left” nor “right”.
- Glide planes (a, b, c, n, d).

Symmetry of infinite 3-dimensional periodic structures is described by 230 space groups listed below.

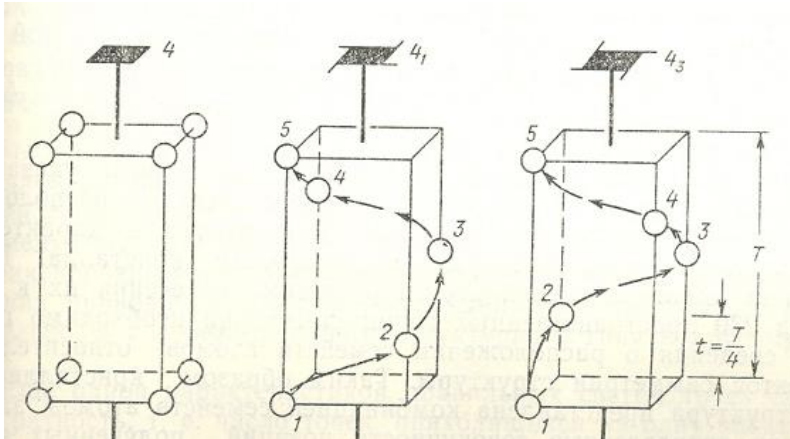
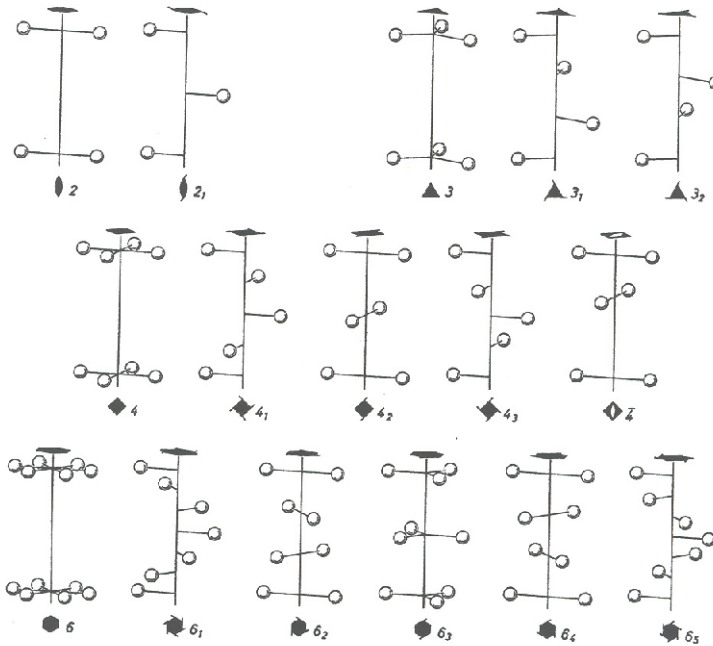


Illustration of fourfold screw axes 4_1 and 4_3 (from Yegorov-Tismenko, 1992).



Screw axes vs rotational axes (from Klockmann, 1978).

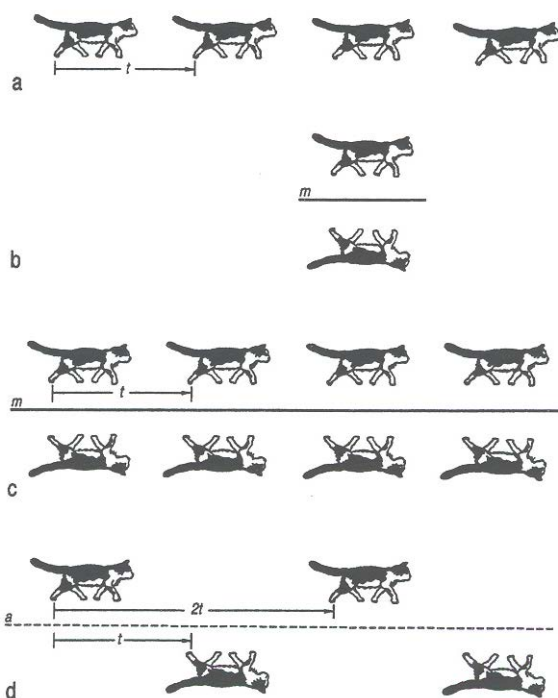


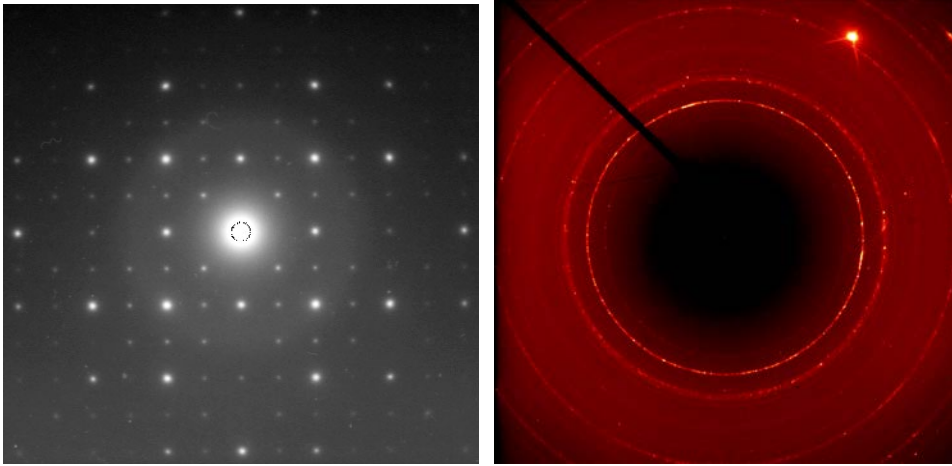
Illustration of a translation (a), mirror plane (b,c) and a glide plane (d) in a periodic structure (from Vainstein, 1979).

The point group of a crystal is easy to find from its space group: just ignore the Bravais lattice type, and replace all translational symmetry elements with their classical counterparts (screw axes are replaced by pure rotational axes, glide planes by mirror planes). For example, the space group $I4_1/amd$ (No. 141) corresponds to point group $4/m\bar{m}m$.

Table. List of 230 space groups.

1	P1	2	P-1	3	P2	4	P2 ₁	5	C2
6	Pm	7	Pc	8	Cm	9	Cc	10	P2/m
11	P2 ₁ /m	12	C2/m	13	P2/c	14	P2 ₁ /c	15	C2/c
16	P222	17	P222 ₁	18	P2 ₁ 2 ₁ 2	19	P2 ₁ 2 ₁ 2 ₁	20	C222 ₁
21	C222	22	F222	23	I222	24	I2 ₁ 2 ₁ 2 ₁	25	Pmm2
26	Pmc2 ₁	27	Pcc2	28	Pma2	29	Pca2 ₁	30	Pnc2
31	Pmn2 ₁	32	Pba2	33	Pna2 ₁	34	Pnn2	35	Cmm2
36	Cmc2 ₁	37	Ccc2	38	Amm2	39	Abm2	40	Ama2
41	Aba2	42	Fmm2	43	Fdd2	44	Imm2	45	Iba2
46	Ima2	47	Pmmm	48	Pnnn	49	Pccm	50	Pban
51	Pmma	52	Pnna	53	Pmna	54	Pcca	55	Pbam
56	Pccn	57	Pbcm	58	Pnnm	59	Pmmn	60	Pbcn
61	Pbca	62	Pnma	63	Cmcm	64	Cmca	65	Cmmm
66	Cccm	67	Cmma	68	Ccca	69	Fmmm	70	Fddd

71	Immm	72	Ibam	73	Ibca	74	Imma	75	P4
76	P4 ₁	77	P4 ₂	78	P4 ₃	79	I4	80	I4 ₁
81	P-4	82	I-4	83	P4/m	84	P4 ₂ /m	85	P4/n
86	P4 ₂ /n	87	I4/m	88	I4 ₁ /a	89	P422	90	P4 ₂ 12
91	P4 ₁ 22	92	P4 ₁ 2 ₁ 2	93	P4 ₂ 22	94	P4 ₂ 2 ₁ 2	95	P4 ₃ 22
96	P4 ₃ 2 ₁ 2	97	I422	98	I4 ₁ 22	99	P4mm	100	P4bm
101	P4 ₂ cm	102	P4 ₂ nm	103	P4cc	104	P4nc	105	P4 ₂ mc
106	P4 ₂ bc	107	I4mm	108	I4cm	109	I4 ₁ md	110	I4 ₁ cd
111	P-42m	112	P-42c	113	P-42 ₁ m	114	P-42 ₁ c	115	P-4m2
116	P-4c2	117	P-4b2	118	P-4n2	119	I-4m2	120	I-4c2
121	I-42m	122	I-42d	123	P4/mmm	124	P4/mcc	125	P4/nbm
126	P4/nnc	127	P4/mbm	128	P4/mnc	129	P4/nmm	130	P4/ncc
131	P4 ₂ /mmc	132	P4 ₂ /mcm	133	P4 ₂ /nbc	134	P4 ₂ /nnm	135	P4 ₂ /mbc
136	P4 ₂ /mnm	137	P4 ₂ /nmc	138	P4 ₂ /ncm	139	I4/mmm	140	I4/mcm
141	I4 ₁ /amd	142	I4 ₁ /acd	143	P3	144	P3 ₁	145	P3 ₂
146	R3	147	P-3	148	R-3	149	P312	150	P321
151	P3 ₁ 12	152	P3 ₁ 21	153	P3 ₂ 12	154	P3 ₂ 21	155	R32
156	P3m1	157	P31m	158	P3c1	159	P31c	160	R3m
161	R3c	162	P-31m	163	P-31c	164	P-3m1	165	P-3c1
166	R-3m	167	R-3c	168	P6	169	P6 ₁	170	P6 ₅
171	P6 ₂	172	P6 ₄	173	P6 ₃	174	P-6	175	P6/m
176	P6 ₃ /m	177	P622	178	P6 ₁ 22	179	P6 ₅ 22	180	P6 ₂ 22
181	P6 ₄ 22	182	P6 ₃ 22	183	P6mm	184	P6cc	185	P6 ₃ cm
186	P6 ₃ mc	187	P-6m2	188	P-6c2	189	P-62m	190	P-62c
191	P6/mmm	192	P6/mcc	193	P6 ₃ /mcm	194	P6 ₃ /mmc	195	P23
196	F23	197	I23	198	P2 ₁ 3	199	I2 ₁ 3	200	Pm-3
201	Pn-3	202	Fm-3	203	Fd-3	204	Im-3	205	Pa-3
206	Ia-3	207	P432	208	P4 ₂ 32	209	F432	210	F4 ₁ 32
211	I432	212	P4 ₃ 32	213	P4 ₁ 32	214	I4 ₁ 32	215	P-43m
216	F-43m	217	I-43m	218	P-43n	219	F-43c	220	I-43d
221	Pm-3m	222	Pn-3n	223	Pm-3n	224	Pn-3m	225	Fm-3m
226	Fm-3c	227	Fd-3m	228	Fd-3c	229	Im-3m	230	Ia-3d



Examples of diffraction from a single crystal (left) and from a powder (right).

Bragg and Wulff, independently, have derived the basic condition of diffraction. In a simple model, one considers diffraction as “reflection” from an atomic plane. Interference between different waves reflected from the same family of planes will be constructive only if phases of reflected waves differ by 2π (or 2π times a whole number), and only in this case diffraction will be observed. Mathematically, this condition is given by the following equation:

$$n\lambda = 2d \sin \theta,$$

where λ is the wavelength of the X-ray, θ is the diffraction angle, d the interlayer spacing, and n is any integer number.

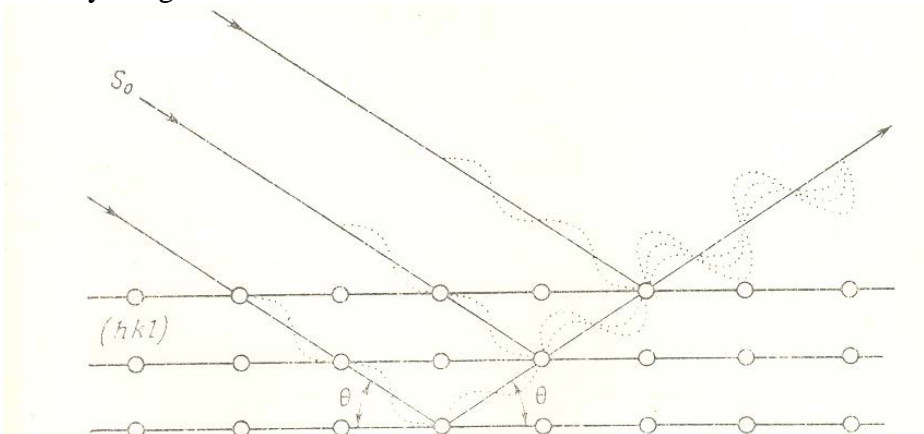
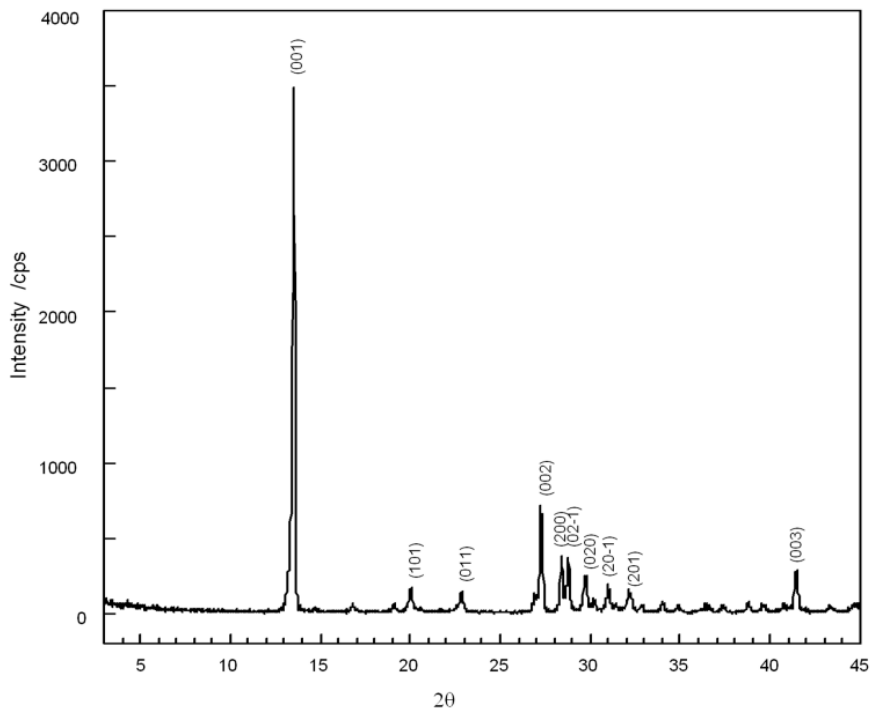


Illustration of the Bragg-Wulff law (from Yegorov-Tismenko, 1992).



Typical X-ray powder diffraction pattern.

Determination of lattice parameters is very simple – positions of diffraction peaks directly give interlayer spacings, from which lattice parameters can be calculated using simple mathematics.

Determination of atomic positions is less simple – information about atomic positions inside the unit cell is contained in the intensities of diffraction peaks. While it is trivial to calculate the diffraction pattern for a given crystal structure, solution of the inverse problem is mathematically very non-trivial. Many methods have been devised for solving this problem, but the most comprehensive solution is given by the so-called direct methods invented by J. Karle and H.A. Hauptman, who were awarded for this a Nobel Prize. Now, with existing methods and computer programs, crystal structure solution is a routine task.

The possibility to solve crystal structures has opened a new era in physics, chemistry, biology, and Earth sciences.

Chemical bonding.

Full theory of chemical bonding is contained in quantum mechanics, but many of its aspects can be understood using simplified classical or semiclassical ideas and models. Main types of bonding: ionic, covalent, metallic, van der Waals. Hydrogen bonds are a special case of ionic/covalent bonding.

Main concepts: radius (ionic, covalent, metallic, van der Waals), atomic charge, electronegativity, polarisability.

- Radii depend on (i) type of bonding, (ii) valence state, (iii) coordination number, (iv) pressure/temperature, (v) spin state for transition metals.

(Coordination number of an atom = the number of its closest neighbours in the structure.)

E.g., for Si: ionic radii are 0.26 Å (fourfold coordination), 0.40 Å (sixfold coordination). Covalent radius: 1.17 Å.

Table of ionic radii (Shannon, 1976). CN = coordination number, IR = ionic radius, HS = high-spin, LS = low-spin.

AC+3	VI	1.12	IV	0.345	IR'	1.032	ION	CH	VI	0.68	IR'	0.665	ION	CH	VI	0.76	IR'	V	0.53						
AG+1	II	0.67	IV	0.49	HS	0.58	LA+3	VI	0.58	VI	0.79	VI	0.6	RB+4	VI	0.88	VI	0.88	VI	0.58					
	IV	1	V	0.49	LS	0.55	VI	VIII	1.1	VIII	0.48	VI	0.6	RH+4	VI	0.845	VIII	VI	0.72						
	IVSQ	1.02	III	0.57	HS	0.645	IX	VIII	1.16	IV	0.48	VI	0.64	RH+5	VI	0.85	VI	0.355	VI	0.46					
	V	1.09	IV	0.26	HS	0.78	IX	VIII	1.27	VI	0.64	VI	0.62	RU+3	VI	0.6	VI	0.54	VI	0.66					
	VI	1.15	VI	0.44	HS	0.85	IX	VIII	1.21	VI	0.69	VI	0.62	RU+4	VI	0.37	VI	0.46	VI	0.66					
	VII	1.22	VI	1.67	VI	0.585	XII	VIII	1.36	VI	0.74	VI	0.565	RU+5	VI	0.56	VI	0.54	VI	0.66					
	VIII	1.28	VII	1.74	IV	0.25	LI+1	IV	0.59	ND+2	VIII	1.29	VI	0.38	TE-2	VI	2.21	VI	0.42	VI	0.66				
AG+2	IVSQ	0.79	VIII	1.78	FR+1	1.8	VI	VI	0.76	IX	1.35	VI	0.36	TE+4	III	0.52	VI	0.62	VI	0.66					
	VI	0.94	IX	1.81	GA+3	0.47	VIII	VI	0.92	ND+3	VI	0.963	IV	0.36	TE+4	III	0.52	VI	0.62	VI	0.66				
AG+3	IVSQ	0.67	X	1.85	V	0.55	LU+3	VI	0.861	VIII	1.109	VI	0.73	S+4	VI	0.97	VI	0.51	VI	0.66					
	VI	0.75	XII	1.88	GD+3	0.62	VIII	VI	0.977	IX	1.163	VI	0.62	S+6	VI	0.97	VI	0.51	VI	0.66					
AL+3	IV	0.39	IV	0.46	1	MG+2	IV	0.57	NI+2	XII	1.27	VI	0.12	TE+6	IV	0.43	VI	0.6	VI	0.66					
	V	0.48	V	0.77	1.053	V	VIII	IVSQ	0.66	IV	0.55	II	0.29	TE+6	IV	0.43	VI	0.6	VI	0.66					
	VI	0.535	VI	0.57	1.107	VI	IX	V	0.72	V	0.63	VI	0.76	TH+4	VI	0.94	VI	0.48	VI	0.66					
AM+2	VII	1.21	VII	0.57	0.73	VIII	VI	VI	0.89	VI	0.63	VI	0.76	TH+4	VI	0.94	VI	0.48	VI	0.66					
	VIII	1.26	VIII	0.65	0.39	MN+2	IV	HS	0.86	NH+3	VI	0.56	VI	0.65	S+2	VI	0.56	VI	0.66	VI	0.66				
AM+3	VI	0.975	VI	0.73	0.53	VI	HS	0.75	VI	HS	0.6	PM+3	VI	0.97	VIII	0.87	VI	1.02	VI	0.66					
	IX	1.31	XII	1.31	VI	LS	0.67	NH+4	VI	LS	0.48	VIII	1.093	SE-2	VI	0.86	VI	1.08	VI	0.66					
	VIII	1.09	VII	-0.1	II	HS	0.83	NO+2	VI	1.1	1.1	IX	1.144	SE+4	VI	0.67	VIII	1.14	VI	0.66					
AM+4	VI	0.85	VIII	1.07	HS	0.58	VII	HS	0.9	NP+2	VI	1.1	PO+4	VI	0.94	SE+6	VI	0.868	VI	0.66					
	VIII	0.95	IX	1.13	VI	0.71	VIII	VI	0.96	NP+3	VI	1.01	VIII	1.08	VI	0.51	VII	0.925	VI	0.66					
AS+3	VI	0.58	X	1.19	0.76	MN+3	V	0.58	NP+4	VI	0.87	PO+6	VI	0.67	SH+4	VI	0.805	VIII	0.965	VI	0.66				
AS+5	IV	0.335	XII	0.912	0.83	VI	VIII	VI	0.58	NP+5	VI	0.98	PR+3	VI	0.99	VI	0.74	IX	1.042	VI	0.66				
	VI	0.46	VI	0.97	0.97	VI	VI	HS	0.645	NP+5	VI	0.75	VIII	1.126	SM+2	VI	0.4	VIII	1.042	VI	0.66				
AT+7	VI	0.62	VIII	1.027	1.19	MN+4	IV	HS	0.645	NP+5	VI	0.72	IX	1.179	SM+2	VI	1.22	TL+1	VI	1.5	ZN+2	IV	0.6	VI	0.66
AU+1	VI	1.37	IX	1.083	0.89	VI	VI	HS	0.53	NP+7	VI	0.71	PR+4	VI	0.85	IX	1.32	XII	1.7	VI	0.74	VI	0.66		
AU+3	IVSQ	0.68	XII	1.14	0.89	VI	IV	0.96	0.33	O-2	II	1.35	VIII	0.96	SM+3	VI	0.959	TL+3	VI	0.75	VIII	0.9	VI	0.66	
	VI	0.85	VI	0.945	1.02	MN+6	IV	0.255	III	0.25	III	1.36	PT-2	IVSQ	0.6	0.8	VIII	1.02	VI	0.885	ZR+4	IV	0.59	VI	0.66
AU+5	VI	0.87	VIII	1.004	1.14	MN+7	IV	0.25	IV	0.25	IV	1.38	PT-2	IVSQ	0.6	0.8	VIII	1.079	VIII	0.98	VI	0.66	VI	0.66	
B+3	III	0.01	VIII	1.062	0.92	VI	VIII	VI	0.46	VI	1.4	PT+4	VI	0.625	IX	1.132	TM+2	VI	1.03	VI	0.72	VI	0.66		
	IV	0.11	VI	1.17	1.015	MO+3	VI	0.69	VI	0.69	VIII	1.42	PT+5	VI	0.57	XII	1.24	VI	1.09	VI	0.78	VI	0.66		
	V	0.27	VII	1.2	1.072	MO+4	VI	0.65	OH-1	II	1.32	PU+3	VI	1	SN+4	IV	0.55	TM+3	VI	0.88	VIII	0.84	VI	0.66	
BA+2	VI	1.35	IV	1.25	1.12	MO+5	IV	0.46	VI	0.46	III	1.34	PU+4	VI	0.86	V	0.62	VIII	0.994	IX	0.89	VI	0.66		
	VII	1.38	IX	1.3	2.2	VI	IV	0.61	IV	0.61	IV	1.35	PU+4	VI	0.96	VIII	0.69	IX	1.052	VI	0.66	VI	0.66		
	VIII	1.42	X	1.35	0.44	MO+6	IV	0.41	VI	0.41	VI	1.37	PU+5	VI	0.74	VII	0.75	U+3	VI	1.025	VI	0.66	VI	0.66	
	IX	1.47	VI	0.947	0.95	VI	III	0.68	VI	0.68	VI	0.63	PU+6	VI	0.71	VIII	0.81	U+4	VI	0.89	VI	0.66	VI	0.66	
	X	1.52	VII	1.01	0.42	VI	VI	0.59	OS+5	VI	0.575	RA+2	VIII	1.48	SR+2	VI	1.18	U+6	VI	0.45	VI	0.66	VI	0.66	
	XI	1.57	IV	1.066	0.53	VII	VIII	0.73	OS+6	V	0.49	XII	1.7	VI	1.21	VIII	1	VI	0.95	VI	0.66	VI	0.66		
BE+2	III	0.16	VI	1.12	0.82	N-3	IV	1.46	VI	1.46	VI	0.545	RB+1	VI	1.52	VIII	1.26	IX	1.05	VI	0.66	VI	0.66		
	IV	0.27	VI	1.285	0.92	N+3	VI	0.16	OS+7	VI	0.525	VII	1.56	IX	1.31	XII	1.31	XII	1.17	VI	0.66	VI	0.66		
	V	0.45	VIII	1.3	0.68	N+5	III	-0.1	OS+8	IV	0.39	VIII	1.61	IX	1.36	U+5	VI	0.76	VI	0.66	VI	0.66	VI	0.66	
BR+3	V	0.96	VI	1.33	0.68	VI	VI	0.13	P+3	VI	0.44	IX	1.63	XII	1.44	VI	0.84	VI	0.66	VI	0.66	VI	0.66	VI	0.66
	VI	1.03	VI	1.33	0.68	VI	VI	0.99	P+5	IV	0.17	X	1.66	TA+3	VI	0.72	U+6	VI	0.45	VI	0.66	VI	0.66	VI	0.66
	VII	1.17	IV	1.33	0.68	VI	VI	1	VI	1	0.29	XI	1.69	TA+4	VI	0.68	IV	0.52	VI	0.66	VI	0.66	VI	0.66	
	VIII	1.17	IV	1.33	0.68	VI	VI	1.02	VI	1.02	0.38	XII	1.72	TA+5	VI	0.64	VI	0.73	VI	0.66	VI	0.66	VI	0.66	
BR+5	VI	0.76	VI	1.33	0.68	VI	VIII	1.12	PA+3	VI	1.04	XIV	1.83	VI	0.69	VI	0.81	VI	0.66	VI	0.66	VI	0.66	VI	0.66
BR+3	VI	0.96	VI	1.33	0.68	VI	VIII	1.18	PA+4	VI	0.9	RE+4	VI	0.63	VIII	0.74	VI	0.86	VI	0.66	VI	0.66	VI	0.66	
	VIII	0.83	VI	1.33	0.68	VI	VIII	1.24	IX	1.24	1.01	RE+5	VI	0.58	VI	0.923	V+2	VI	0.79	VI	0.66	VI	0.66	VI	0.66
	VIII	0.93	VI	1.33	0.68	VI	IX	1.55	XII	1.55	0.78	RE+6	VI	0.55	VII	0.98	V+3	VI	0.64	VI	0.66	VI	0.66	VI	0.66
BR-1	VI	1.96	IV	1.43	1.59	NB+3	VI	0.72	VI	0.72	0.91	RE+7	IV	0.38	VIII	1.04	VI	0.64	VI	0.66	VI	0.66	VI	0.66	
BR+3	IVSQ	0.59	VI	1.43	1.59	NB+3	VI	1.64	IX	1.64	0.95	VI	0.95	IX	1.095	VI	0.64	VI	0.66	VI	0.66	VI	0.66	VI	0.66

Pauling's electronegativity scale.

H																
2.1																
Li	Be											B	C	N	O	F
1.0	1.5											2.0	2.5	3.0	3.5	4.0
Na	Mg											Al	Si	P	S	Cl
0.9	1.2											1.5	1.8	2.1	2.5	3.0
K	Ca	Sc	Ti	V	Cr	Mn	Fe	Co	Ni	Cu	Zn	Ga	Ge	As	Se	Br
0.8	1.0	1.3	1.5	1.6	1.6	1.5	1.8	1.8	1.8	1.9	1.6	1.6	1.8	2.0	2.4	2.8
Rb	Sr	Y	Zr	Nb	Mo	Tc	Ru	Rh	Pd	Ag	Cd	In	Sn	Sb	Te	J
0.8	1.0	1.2	1.4	1.6	1.8	1.9	2.2	2.2	2.2	1.9	1.7	1.7	1.8	1.9	2.1	2.5
Cs	Ba	La	Hf	Ta	W	Re	Os	Ir	Pt	Au	Hg	Tl	Pb	Bi	Po	At
0.7	0.9	1.1	1.3	1.5	1.7	1.9	2.2	2.2	2.2	2.4	1.9	1.8	1.8	1.9	2.0	2.2
Fr	Ra	Ac														
0.7	0.9	1.1														
Lanthanides and Actinides																
Ce-Lu		Th	Pa	U	Np-No											
1.1-1.2		1.3	1.5	1.7	1.3											

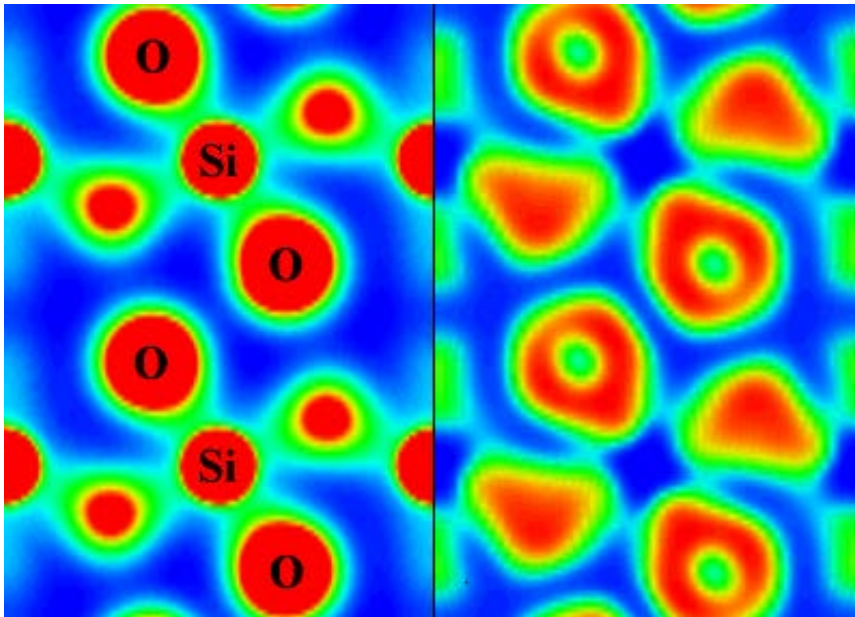
Atomic charge: there are many definitions of atomic charges (from electron density distribution, from lattice dynamics, from dipole moments, from electronegativity differences, ...) which give very different values of charges.

Bader volumes and Bader charges (in parentheses – dynamical charges) of high-pressure forms of SiO₂ (from Oganov et al., 2005).

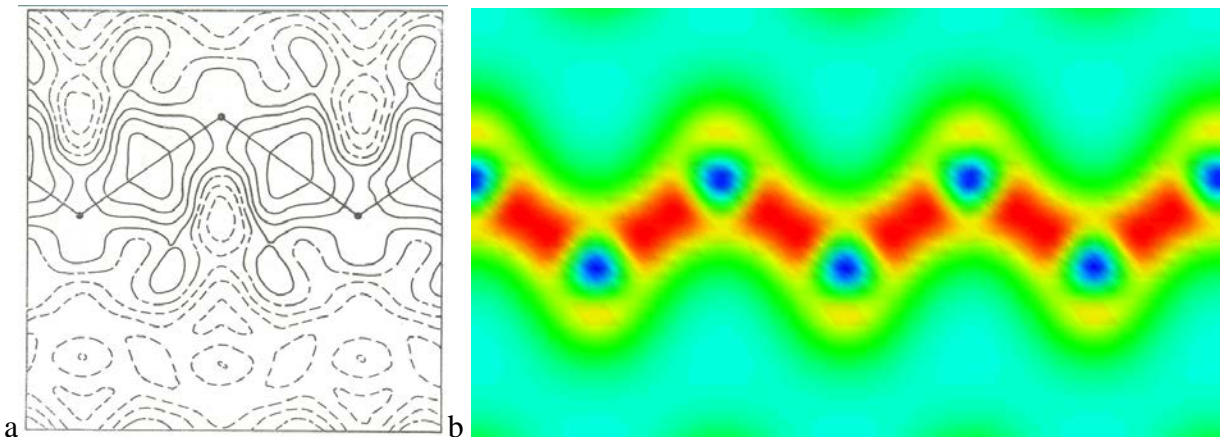
Phase	Z _{Si} , e	V _{Si} , Å ³	Z _O , e	V _O , Å ³
Stishovite	3.2 (3.9) ^a	2.70	-1.6 (-1.9) ^a	10.24
α-PbO ₂	3.2 (3.9) ^a	2.78	-1.6 (-2.0) ^a	10.00
Pa $\bar{3}$	3.2 (4.0) ^a	2.95	-1.6 (-2.0) ^a	9.40

- Polarisability – measure of polarisation of an atom by an electric field. Polarisability defines the strength of van der Waals bonding. Highly polarisable atoms and ions (heavy elements, large cations and anions) often prefer layered structures, which are stabilised by van der Waals interactions.

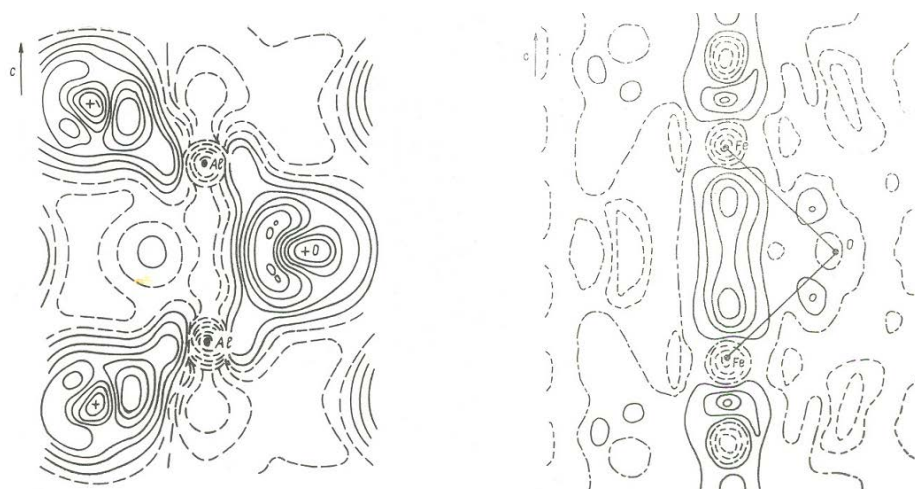
Chemical bonding can be studied experimentally (X-ray studies of electron density distribution) and theoretically (quantum-mechanical calculations). Thanks to such studies, now we have a good understanding of chemical bonding in many compounds. Classical pictures of ionic, covalent, and metallic bonding are largely confirmed by such studies (van der Waals bonding is not well visible on electron density maps).



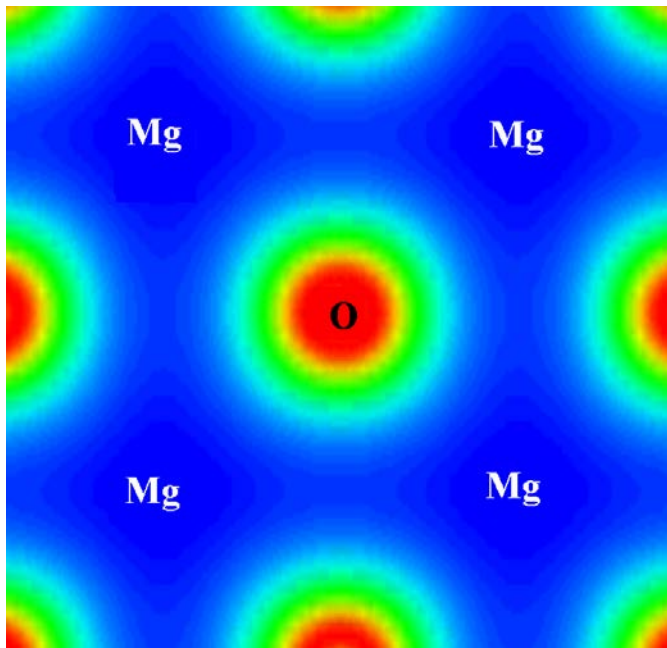
Theoretical electron density (left) and electron localisation function (right) for a high-pressure form of SiO_2 . High density – red, low density – blue. One can see predominantly ionic bonding, but with significant covalency of Si-O bonds. From Oganov et al. (2005).



Covalent bonding: a- experimental deformation density (crystal – sum of atoms) of diamond (C) (from Tsirelson et al., 1986), b- theoretical valence electron density of Si. In (a) solid contours correspond to positive values, dashed – to negative.



Ionic-covalent bonding: Deformation density of corundum (Al_2O_3) – left, and hematite (Fe_2O_3) – right (from Tsirelson et al., 1986).



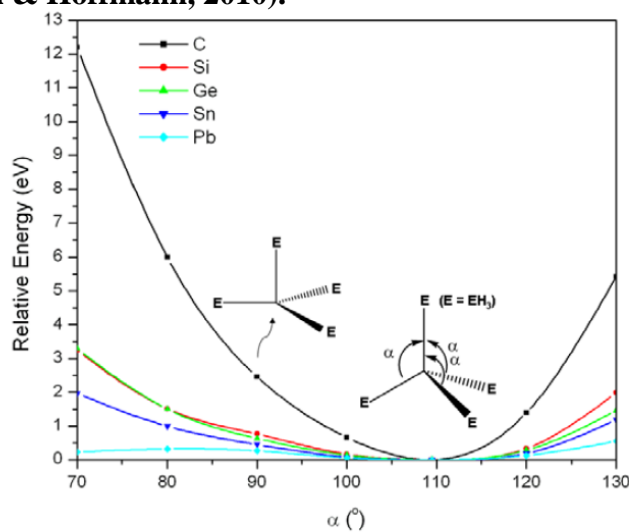
Ionic bonding: theoretical valence electron density of MgO.

Crystals with directional (covalent) bonding tend to have higher melting points (see Table below) and higher hardnesses. As one goes down the Periodic Table, directionality diminishes: while carbon and silicon form strongly directional covalent bonds, tin has two polymorphs (one metallic and one covalent semiconductor), and lead is a typical metal. The decrease of directionality is obvious from the Figure below.

The m.p. (K), b.p. (K) and E-E bond energies (eV) of group 14 elements

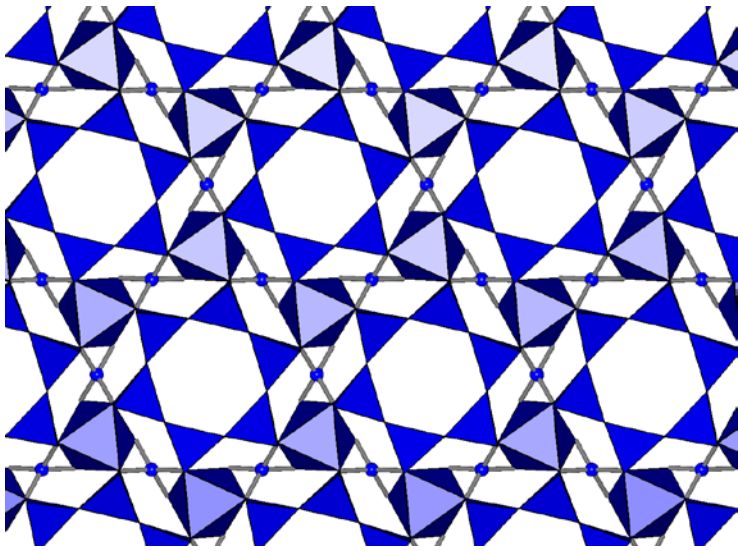
Properties	C	Si	Ge	Sn	Pb
m.p. /K	4373	1693	1218	505	600
b.p. /K	—	~3550	3123	2896	2024
E-E bond energies /eV	3.69	2.35	1.95	1.57	1.02

Melting and boiling points of C, Si, Sn, Pb solids, and their bond energies (from Wen, Cahill & Hoffmann, 2010).

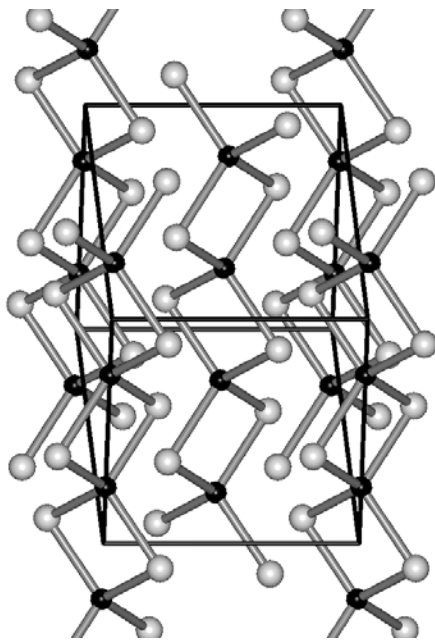


The potential energy surface of the transformation from a perfect tetrahedron T_d to a distorted C_{3v} tetrahedron for $E(EH_3)_4$, where $E = C, Si, Ge, Sn$ or Pb .

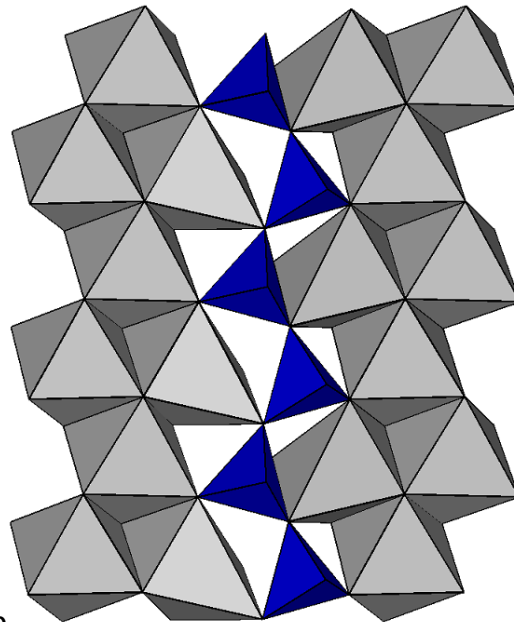
Energy variation as a function of angle, showing little or no directionality in bonds formed by Pb atoms (from Wen, Cahill & Hoffmann, 2010).



Beryl: structure with 6-member rings of silicate tetrahedra.

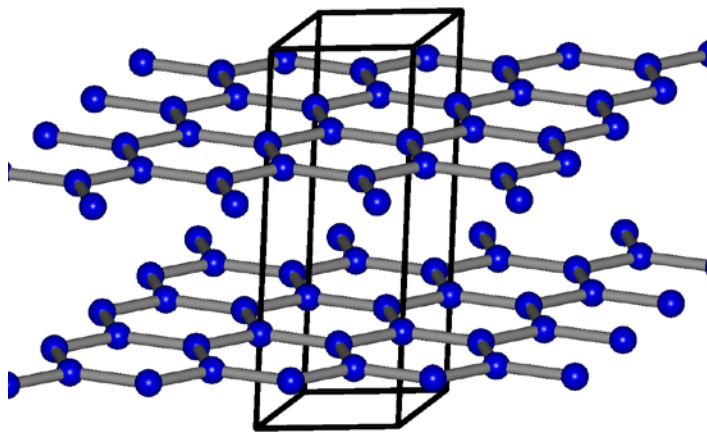


a

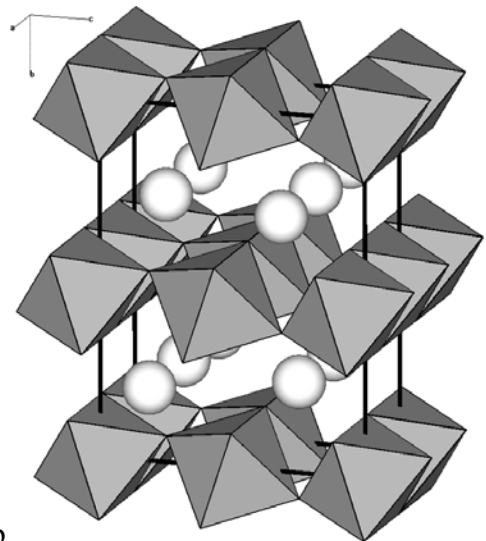


b

Chain structures: a) SiS_2 , b) enstatite.

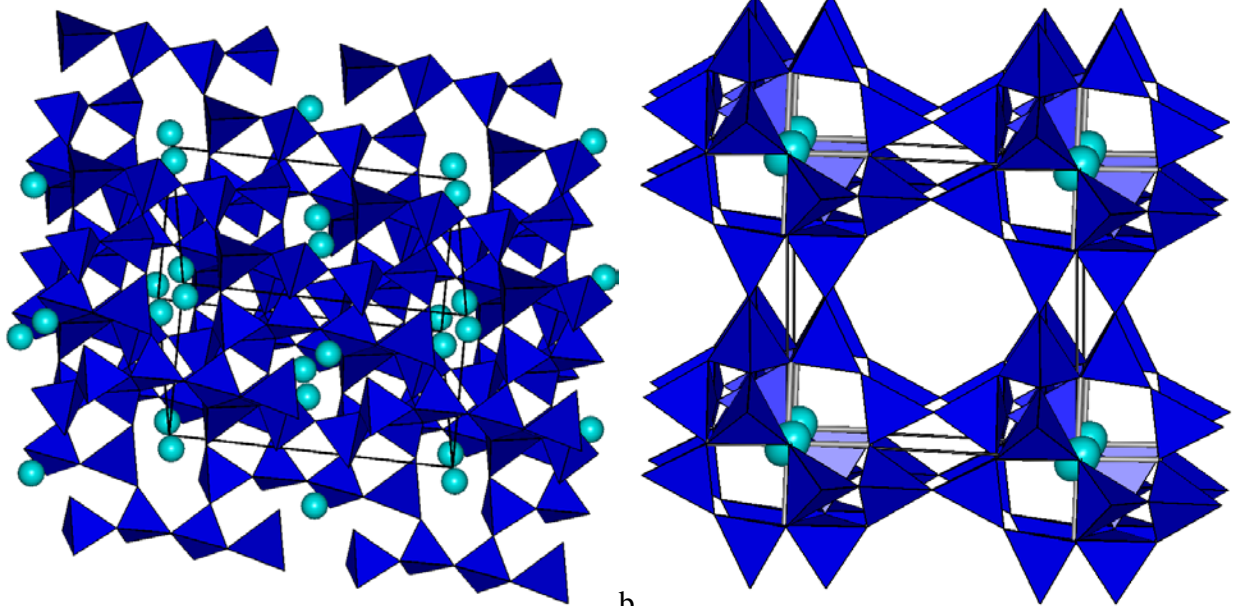


a



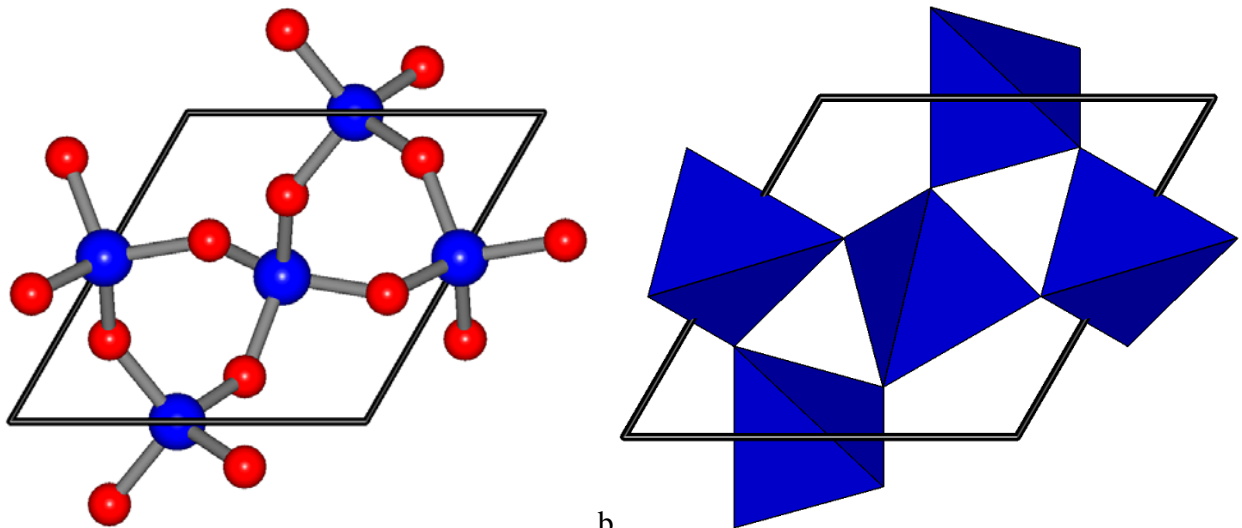
b

Sheet structures: a) graphite, b) post-perovskite form of MgSiO_3 .



a
Framework structures – a) albite, b) chabazite.

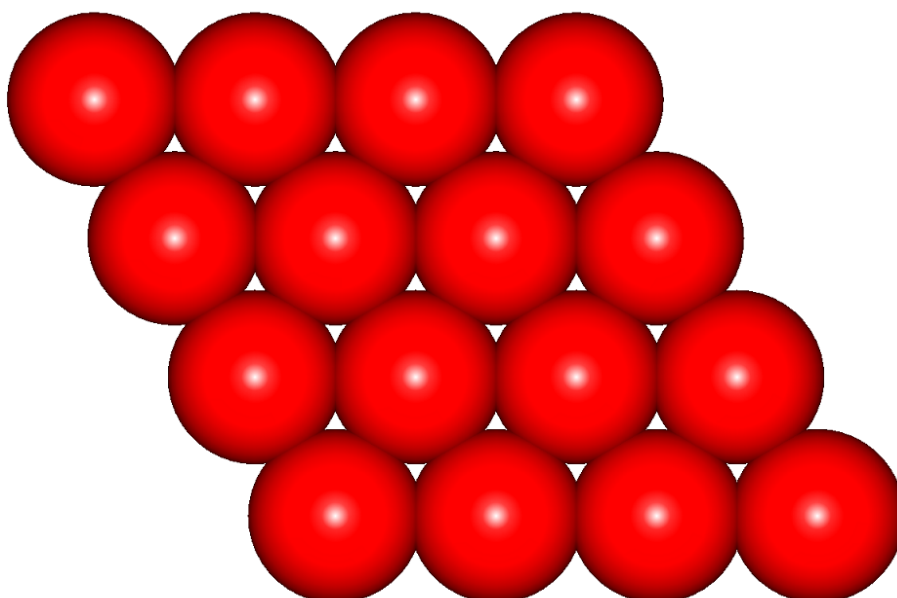
When describing crystal structures, we often use (and have already used many times in illustrations to this course) polyhedral representation of structures. In many cases this description is clearer than the standard ball-and-stick representation.



a
Ball-and-stick (left) and polyhedral (right) representations of the structure of quartz.

Close packing of spheres. It turns out that very many mineral crystal structures can be described on the basis of close packing (usually of anions, since they are usually larger than cations). Theory of close packing of spheres, initially developed by mathematicians, is therefore widely used in crystallography.

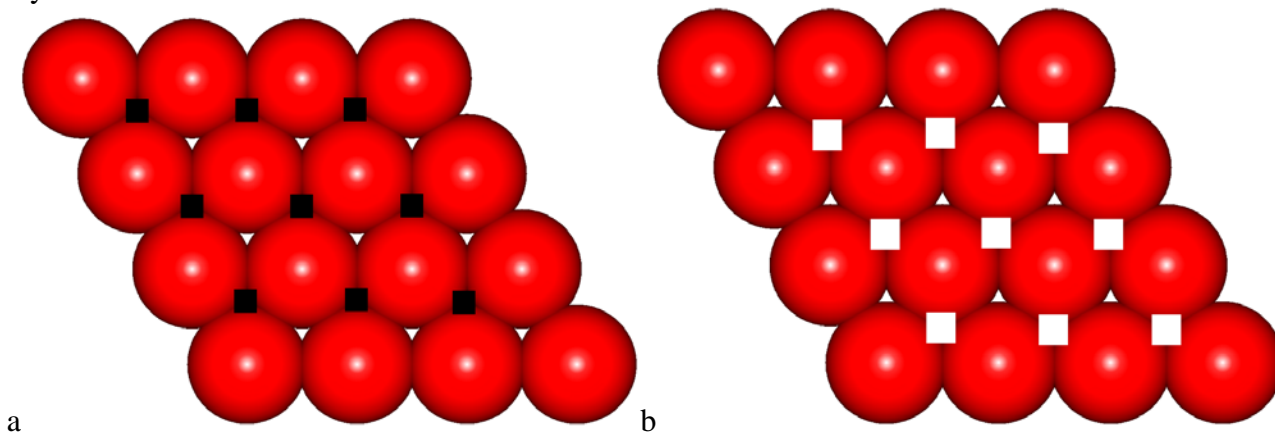
In two dimensions, there is only one way to arrange spheres so as to produce the densest filling:



2-dimensional close packing.

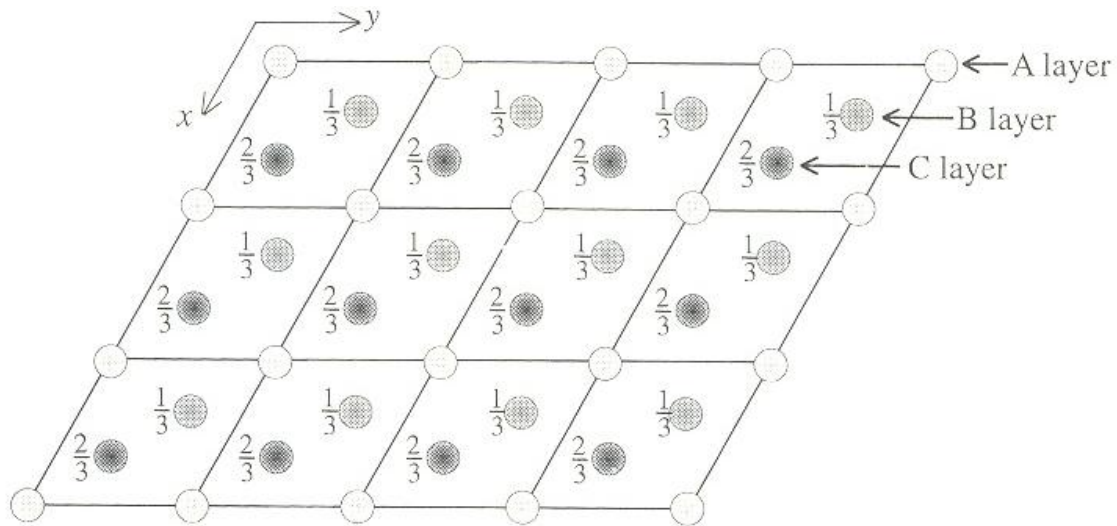
In three dimensions, there are many ways to produce the densest packing of spheres (which we call close packings), but all of them are based on the densely packed layer illustrated above. Different stackings of such layers produce a whole family of different packings having identical density of space filling: in all of them, the spheres fill 74.05% of the total volume. In all of these 3D close packings each sphere touches 12 other close-packed spheres¹.

Indeed, there are two ways of putting the next close-packed layer: if we denote the original layer “A”, these two possibilities for the next layer can be denoted “B” and “C”, respectively. Note that two layers of the same type can never be neighbours in a close packed structure (this arrangement will not be dense – for greater density, atoms have to be on top of empty space, not on top of atoms). Still, there is a great number of possibilities to combine “A”, “B”, and “C” – e.g., “|AB|ABABAB...”, “|ABC|ABCABC...”, “|ABAC|ABACABAC...”, or even disordered or long-period packings. Note that “A”, “B”, and “C” layers have identical geometry – their distinction is arbitrary and done only for convenience of labelling different *stackings* of, in principle, identical layers.



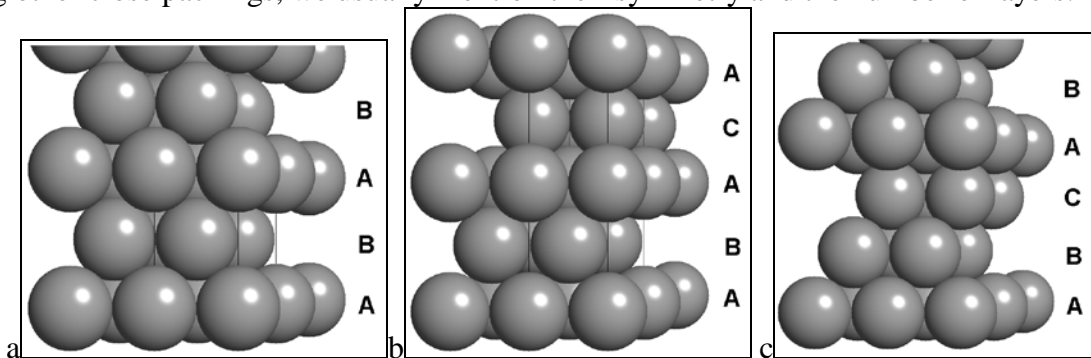
Alternative ways of stacking the next close-packed layer on top of a close-packed layer: a) layer “B” (positions of atoms in this layer are indicated by black squares), c) layer “C” (positions of atoms in this layer - white squares).

¹ The number of touching spheres in close packings in mathematics is called „kissing number“ k , which for space dimensionalities between 1 and 8 equals 2, 6, 12, 24, 40, 72, 126, 240. The value for 24-dimensional space (196560) is also known.



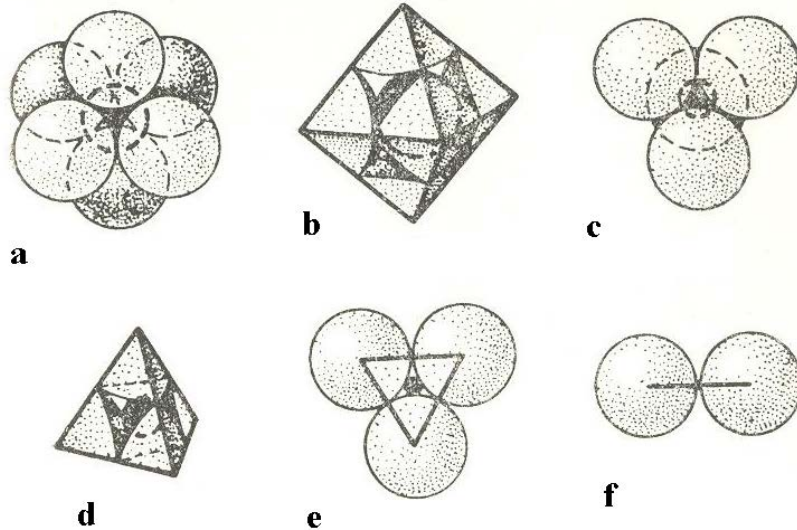
Stacking of close-packed layers (from Putnis, 1992).

All close packings have a hexagonal or trigonal symmetry. Only one packing - |ABC| - has a higher symmetry: it is easy to see that this actually is a face-centred cubic structure; this packing is therefore called “cubic close packing” (structure type of Cu). The |AB| stacking is called “hexagonal close packing” (structure type of Mg), |ABAC| is often called “double hexagonal close packing”, describing other close packings, we usually mention their symmetry and the number of layers.

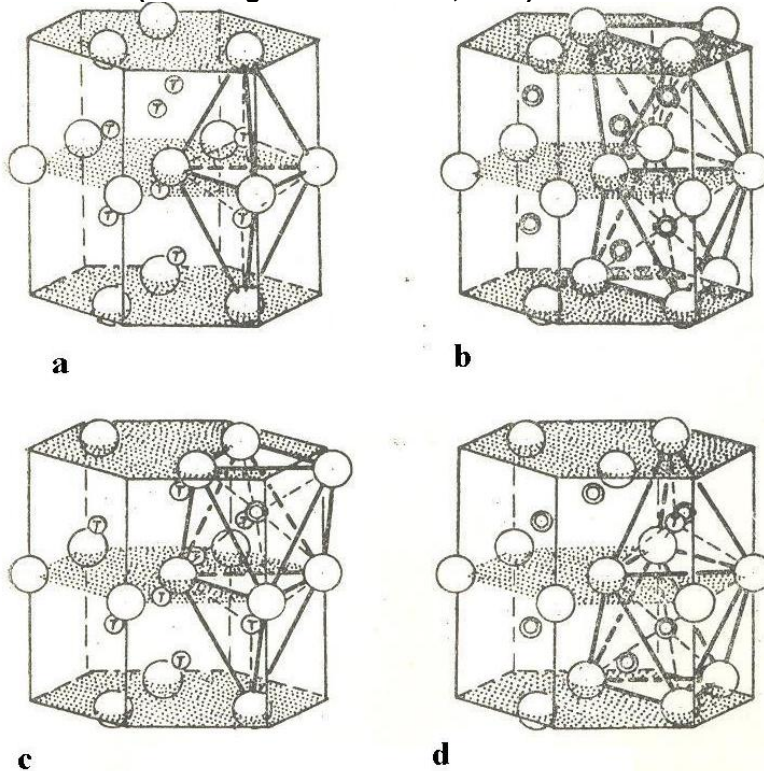


Examples of close packings –a) Hexagonal, b) Double hexagonal, c) Cubic.

If anions make up the close packing, it is important to know which cavities in this packing are available for cations. There are “trivial” 2- and 3-coordinate sites, but also 4-coordinate (tetrahedral) and 6-coordinate (octahedral) cavities. There are 2 tetrahedral voids and 1 octahedral void per anion. In hexagonal close packing both tetrahedral and octahedral voids are “on top” of each other and share a polyhedral face – this is unfavourable if cations are highly charged (because the distance between the centres of adjacent voids is relatively small, and Coulombic repulsion will be high).



Voids in close-packed structures: a-b)Octahedral, c-d)Tetrahedral, e)Three-coordinate, f)Two-coordinate. (from Yegorov-Tismenko, 1992)



Location of tetrahedral and octahedral voids in a-b) hexagonal, c-d) cubic close packing (from Yegorov-Tismenko, 1992).

Structures based on close packed atomic arrangements are very common among materials with non-directional bonding: metals, ionic crystals, noble gases. Many mineral structures are based on close packing as well. Since close packing is the densest possible arrangement of spheres of identical size, one expects close-packed structures to be particularly stable at high pressure. Often this is the case, but there are many exceptions. For example, close-packed Mg transforms into a body-centred cubic structure at ~ 50 GPa. This and many other examples should caution against absolutisation of the close packing principle: because atoms are not hard spheres, close packing often is a purely geometrical, rather than physical, concept.

Pauling's rules. In 1927, Linus Pauling (then, only 26-years old!) formulated his famous 5 rules of stability of ionic crystals.

1st rule: ‘A coordinated polyhedron of anions is formed about each cation, the cation-anion distance being determined by the radius sum and the coordination number of the cation by the radius ratio’. This rule allows one to predict bond distances on the basis of ionic radii tables. Also it allows one to understand why in silicates Si atoms have a fourfold coordination (because Si⁴⁺ ions are small), Al atoms 6-fold coordination (Al³⁺ ions are larger), and Mg atoms 6-8-fold coordination (Mg²⁺ ions are even larger).

The basic point is that cations occupying structural cavities, should be large enough to “touch” or even “push out” the surrounding anions. Based on this, one arrives at the so-called Magnus-Goldschmidt rule summarised by the following table:

Cation coordination number	Minimum r_+/r_-
12	1
8	0.732
6	0.414
4	0.215
3	0.155

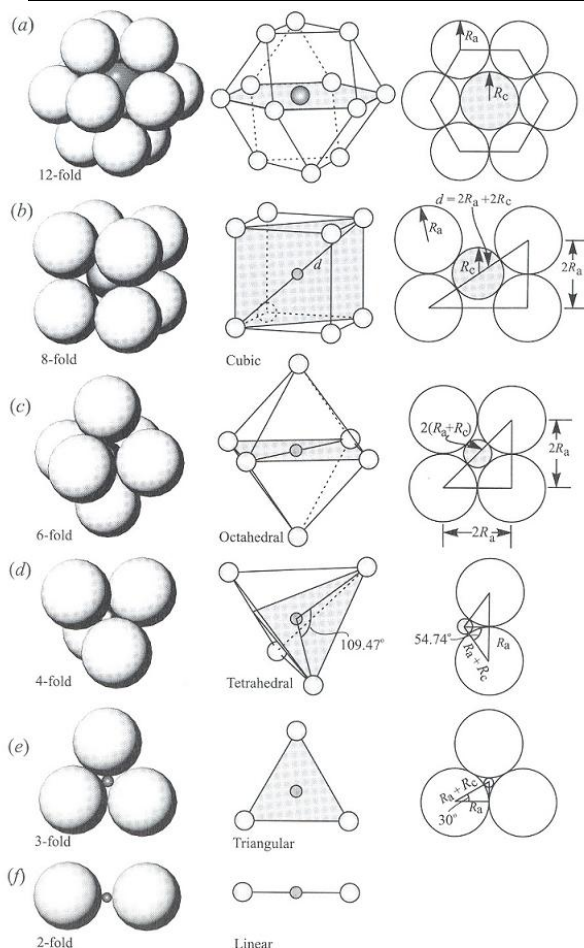


Illustration of some common coordination environments (from Nesse, 2000)

2nd rule: ‘In a stable co-ordinated structure the total strength of the valency bonds which reach an anion from all the neighboring cations is equal to the charge of the anion’ (Pauling, 1929). The bond strength according to Pauling is calculated in a simple way: the valence of the cation divided by its coordination number. And according to the rule, the sum of such strengths on each anion is equal to the anion’s charge. E.g., in silicates the strength of each Si-O bond is = (valence of Si)/CN_{Si} = 4/4 = 1. When there are 2 Si-O bonds on one O atom, the total bond strength is 2 – equal to the (absolute value of the) charge of O ion, 2. On the other hand, 3 silicate tetrahedra

having a common O-atom are forbidden by this rule – such configurations are never observed. When we have, e.g., sulphates, two sulphate tetrahedra having a common O-atom would imply the total bond strength on the bridging oxygen of $2 \cdot 6/4 = 3$. This is too different from the needed value of 2, and sulphate tetrahedra polymerise only in exceptional circumstances, and never in minerals. This simple rule is a very powerful means to understand crystal structures of minerals. Deviations from it are known (e.g., andalusite and sillimanite, Al_2SiO_5), but they never exceed 25%.

3rd rule: ‘The existence of edges and particularly faces, common to two anion polyhedra in a coordinated structure decreases its stability; this effect is large for cations with high valency and small coordination number, and is especially large when the radius ratio approaches the lower limit of the stability of the polyhedra’. In accordance with this rule, silicate tetrahedra never share faces, extremely seldom share edges (e.g., in the metastable fibrous silica SiO_2), and prefer either to remain single, or share only corners. The rule is not so strict for larger cations – e.g., MgO_6 -octahedra in pyroxenes share edges.

4th rule: ‘In a crystal containing different cations, those of high valency and small coordination number tend not to share polyhedra elements with each other’.

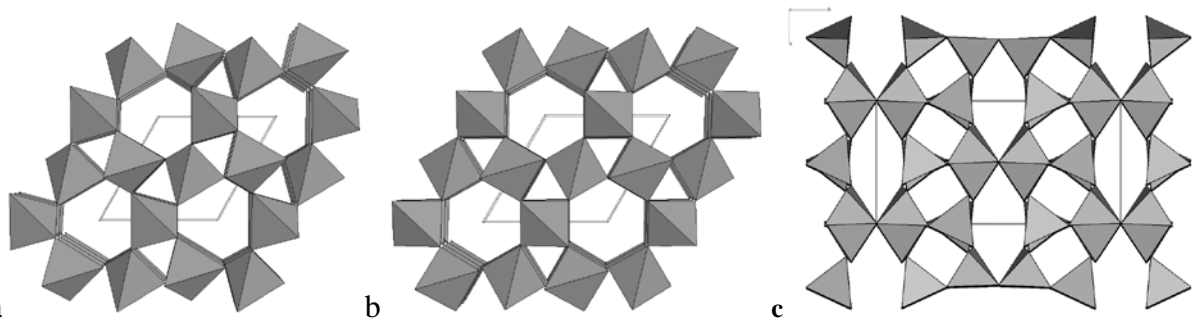
5th rule: ‘The number of essentially different kinds of constituent in a crystal tends to be small’. In other words, nature prefers simplicity. Many silicate structures are very complicated, but the simplest ones are often the most stable ones.

Pauling’s rules were originally formulated for ionic crystals (because for ionics they have a more or less transparent explanation), but afterwards it was realised that they are perfectly valid for significantly covalent crystals as well. Metallic and almost entirely covalent crystals require different approaches for the explanation of their structures.

8. Crystal Chemistry: Part III. Polymorphism, polytypism. Morphotropy. Solid solutions.

Polymorphism – phenomenon of the existence of several distinct crystalline modifications of the same compound. E.g.: graphite and diamond (C), calcite and aragonite (CaCO_3), pyrite and marcasite (FeS_2), etc. Most compounds have many polymorphs at different pressure-temperature conditions. Polymorphs can be stable or metastable, depending on whether they have the lowest free energy at given P - T conditions or not. Since structures of different polymorphs are different, their properties can be very different too. By definition, polymorphs have identical compositions.

When one polymorph transforms into another, we talk about a phase transition. Phase transformations can be reversible or irreversible. Often one has reversible phase transitions with a hysteresis. Phase transitions can be first-order (jumps in volume and entropy) or second-order (jumps in thermal expansion, heat capacities, elastic constants). In some cases (e.g., cubic-tetragonal transition in BaTiO_3) the same transition can be first- or second-order at different P - T conditions. Landau has shown that for a second-order transition the two phases must be structurally related, and their symmetry groups must conform to certain group-subgroup relations. An interesting case are structural transitions involving no changes in crystal symmetry: these are first-order at low temperatures, but on increasing temperature the first-order discontinuity gradually decreases and can disappear completely producing a fully continuous transition at high temperatures. Such isosymmetrical transitions are known for Ce, SmS, KTiOPO_4 , and other compounds. On increasing temperature, one usually obtains higher-symmetry phases, and on increasing pressure symmetry also usually increases, but there are more exceptions.

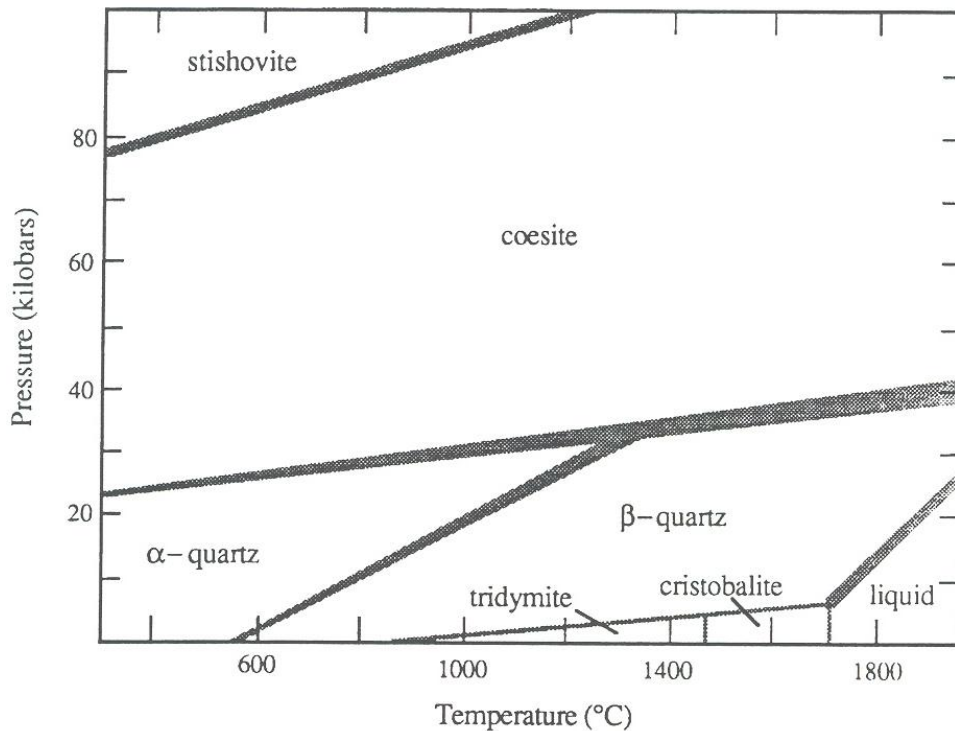


Displacive transition: α -quartz (a) to β -quartz (b) at 846 K and a reconstructive transition from quartz to coesite (c) at 2.5 GPa.

Thermodynamics of first order transitions are based on the Clapeyron relation:

$$\frac{dP}{dT} = \frac{\Delta S}{\Delta V}, \quad (1)$$

where ΔS and ΔV are the entropy and volume differences between the phases. This relation is valid only for first-order transitions, because for continuous transitions both ΔV and ΔS are equal to zero. Using (1) it becomes possible to determine the slopes of the equilibrium lines on the P - T phase diagram.



Druck-/Temperatur-Phasendiagramm für SiO₂ (Griffen, 1992, 1-1)

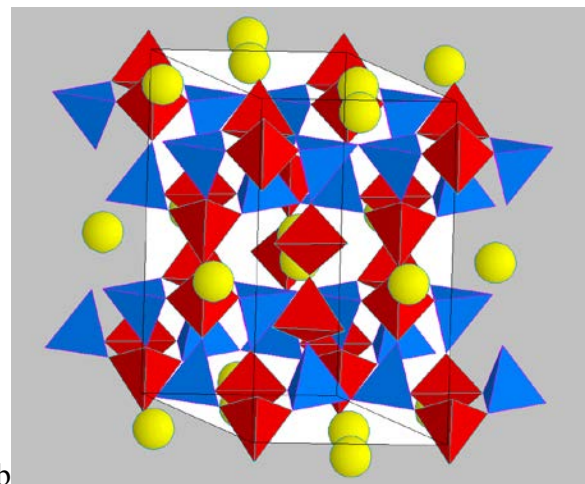
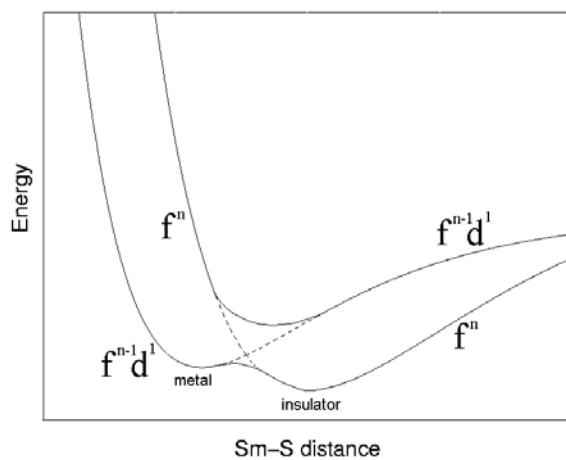
A relation, analogous to (1), for second-order transitions was derived by Ehrenfest:

$$\frac{dP}{dT} = \frac{\Delta C_p}{TV\Delta\alpha}, \quad (2)$$

where ΔC_p and $\Delta\alpha$ are the jumps of the heat capacity and thermal expansion at the transition. However, precise experiments, computer simulations, and modern theories indicate a qualitatively different behaviour of the heat capacity – instead of having a finite jump, it logarithmically diverges to infinity on both sides of the transition. This ‘ λ -behaviour’ invalidates the Ehrenfest relation.

M.J.Buerger (1962) distinguished two main types of phase transitions – those with and without changes of the first coordination number. Each of these types was further classified into

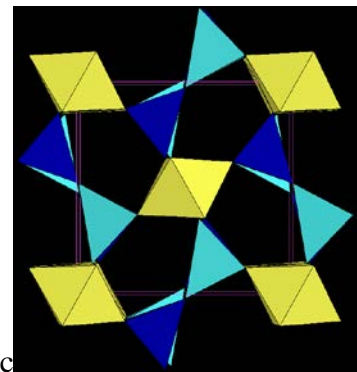
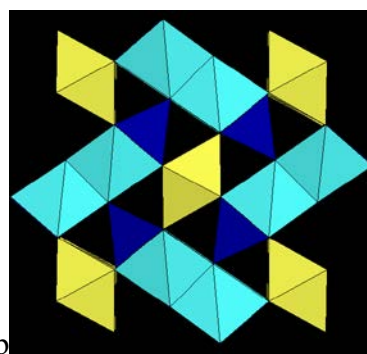
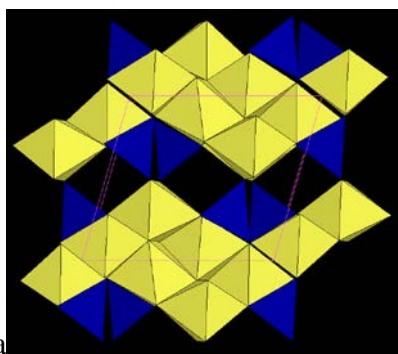
reconstructive (i.e., requiring formation/breaking of bonds), displacive, order-disorder, electronic, etc. transitions. *Displacive* phase transitions are accompanied by small atomic displacements (hence the name), which usually destroy some elements of symmetry. These displacement patterns are determined by the eigenvectors of one or more normal modes – the so-called soft modes. *Order-disorder* transitions occur between a low-temperature structurally ordered (e.g., having positional order in cation distribution – e.g., microcline KAlSi_3O_8 , and orientational order of atomic groups – e.g., NH_4Cl) and a high-temperature disordered phase (e.g., positional disorder – sanidine $\text{K}(\text{Al},\text{Si})_4\text{O}_8$, or orientational disorder – e.g., high-T “CsCl-like” phase of NH_4Cl , where due to almost free rotation the NH_4^+ -group behaves as a spherical ion). *Electronic* transitions are accompanied by a change of the electronic or magnetic structure and/or valence state of atoms in the structure; the structure type may or may not change in this process. *Reconstructive* phase transitions, by Buerger’s definition, involve breaking/formation of at least some bonds. These transitions are always first order, involve a latent heat, and require activation for bond breaking. Order-disorder and displacive transitions can in principle be of any order.



a

b

Phase transitions: (a) isosymmetric electronic transition in SmS, (b) order-disorder transition in feldspars.



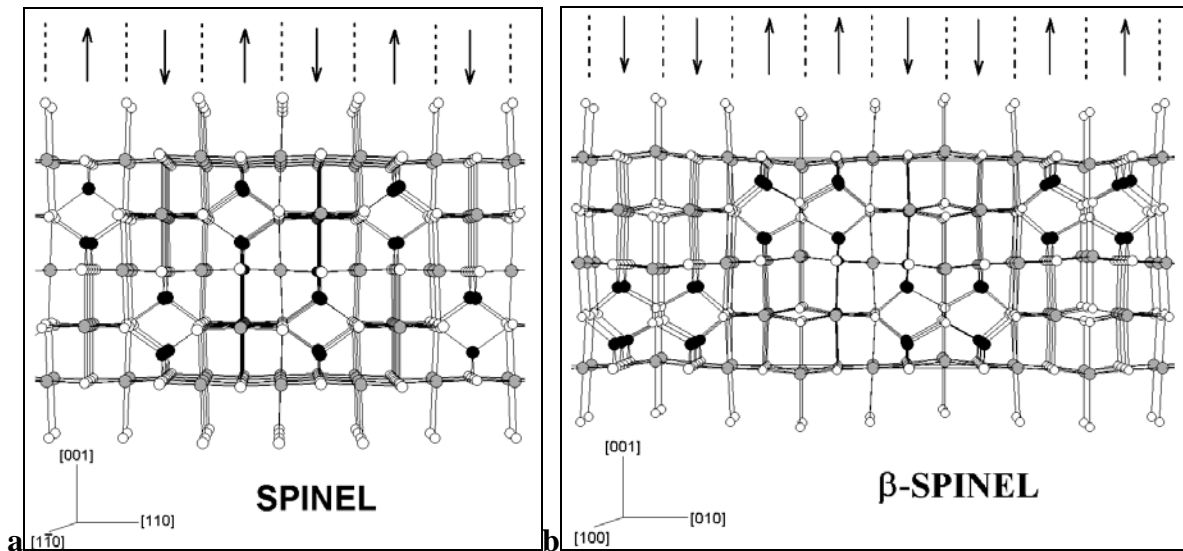
a

b

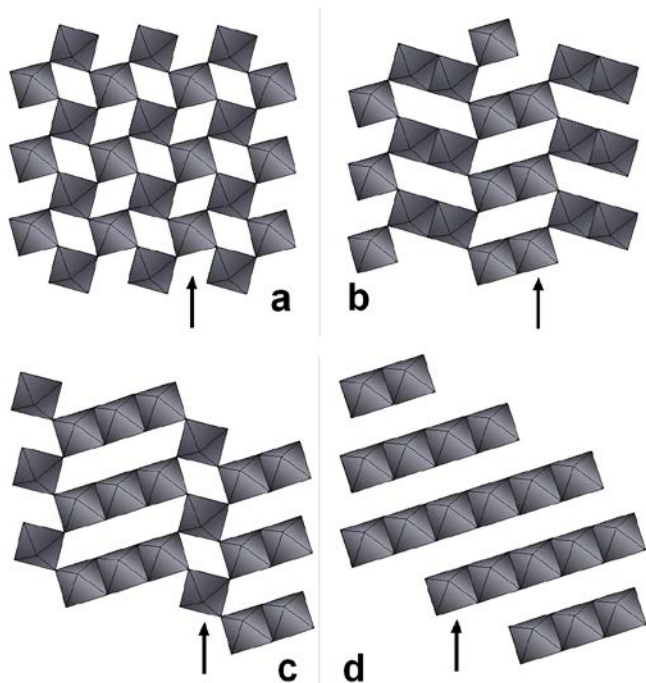
c

Polymorphs of Al_2SiO_5 : a) kyanite, b) andalusite, c) sillimanite. All transitions between these structures are reconstructive and involve changes in coordination numbers.

Polytypism: existence of two or more modifications with structures consisting of the same layers, but in different stacking. This is a special case of polymorphism. Since energy difference between polytypes usually are very small, often several polytypes coexist in the same sample. Most of polytypes in such situations are metastable. Polytypism is extremely common in layered structures (micas, graphite, molybdenite,...), but many non-layered structures can also be described as polytypic: close-packed structure, Earth-forming spinelloids, etc. The most famous example of polytypism is SiC – the “king of polytypes” - which has over 60 polytypes structurally characterised already by 1980!



Structures of ringwoodite (a) and wadsleyite (b) – polymorphs/polytypes of Mg_2SiO_4 .



Structures of $MgSiO_3$ polymorphs/polytypes: perovskite (a), post-perovskite (d), two intermediate polytypes (b,c). Only SiO_6 octahedra shown, Mg atoms are omitted for clarity. $MgSiO_3$ perovskite is the main mineral of the Earth's lower mantle and post-perovskite is the main mineral of the core-mantle boundary. Arrows show the layers, the displacement of which produces all the polytypes.

Morphotropy – sudden change of structure type in a series of compounds having the same ratio of structural units. E.g., sphalerite ZnS , troilite FeS and oldhamite CaS have the same ratio of cations and anions – yet, they belong to three different structure types: sphalerite, nickeline, and sodium chloride structure types.

Many interesting examples of morphotropy can be found by looking at compounds formed by atoms from the same column of the Periodic Table, e.g. MCO_3 carbonates:

$MgCO_3$: calcite structure, Mg in octahedra

$CaCO_3$: calcite structure, Ca in octahedra ;

$CaCO_3$: aragonite structure, Ca in 9-fold coordination

SrCO_3 : aragonite structure, Sr in 9-fold coordination

BaCO_3 : aragonite structure, Ba in 9-fold coordination

Ca^{2+} ion appears to have a radius in between those needed for 6-fold (octahedral) and 9-fold coordinations.

Solid solutions, or mixed crystals – crystals of variable composition, which can be considered as “solution” of one pure end-member in the other pure end-member. For example, olivines $(\text{Mg,Fe})_2\text{SiO}_4$ are solid solutions between pure end-members forsterite Mg_2SiO_4 and fayalite Fe_2SiO_4 . Mg and Fe atoms in this structure occupy the same structural position, with a statistical distribution of Mg and Fe.

Chemically pure minerals do not exist, and most minerals are in fact solid solutions. Understanding solid solutions is crucial also for geochemistry – suitability of an atom as an impurity in major minerals determines the geochemical fate of many, especially rare, elements. In mantle geochemistry, there is a special term “incompatible element”, indicating that a particular element is not concentrated in mantle-forming minerals (e.g., large cations like Na^+ , K^+ are incompatible in the mantle and are concentrated in melts – the source of magma – rather than in mantle minerals, mainly silicates of Mg).

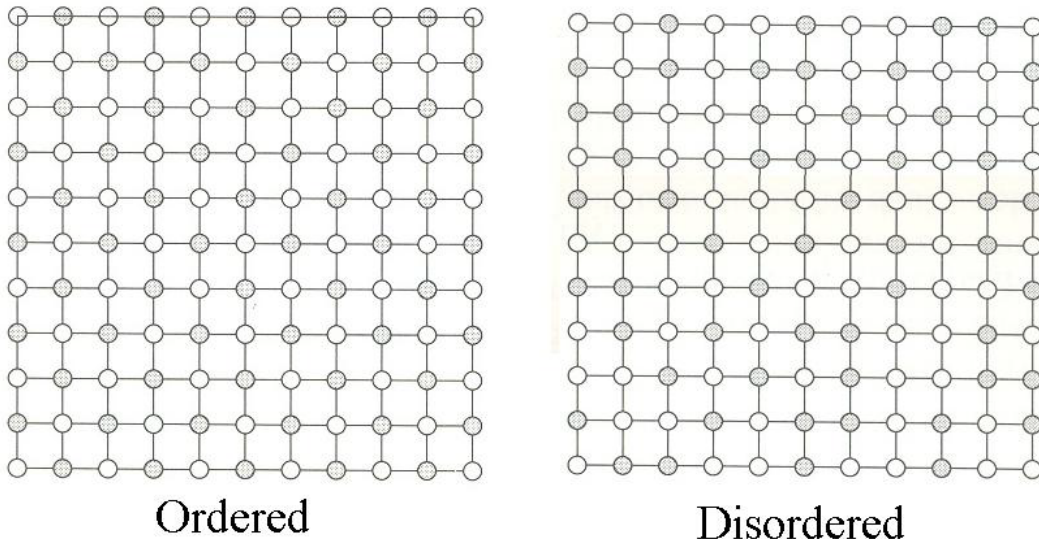


Illustration of ordered and disordered distributions of two sorts of atoms over positions in a simple cubic structure (from Putnis, 1992).

Solid solutions can be isovalent (the substituting atoms have the same valence – e.g., Mg^{2+} and Fe^{2+} in olivines) or heterovalent (their valences are different, and therefore some charge compensation is required – e.g., coupled $\text{Na}^+\text{Si}^{4+}$ - $\text{Ca}^{2+}\text{Al}^{3+}$ substitution in feldspars).

Energetically, solid solutions are always unfavourable – insertion of a foreign atom always causes distortions of the lattice. The enthalpy ($H=E+PV$) of a solid solution is always higher than the enthalpy of an isochemical mixture of pure end-members – in other words, the enthalpy of mixing ΔH_{mix} is always positive (see below).

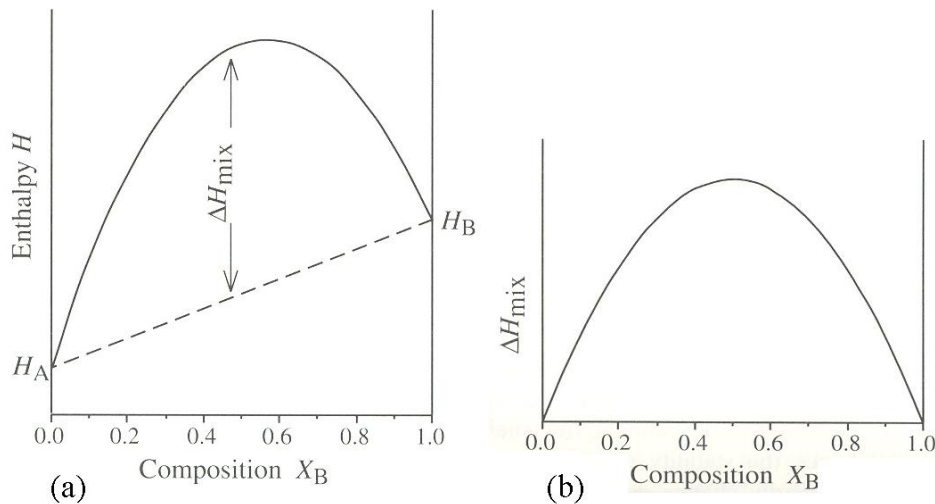


Illustration of the enthalpy of mixing for a solid solution (from Putnis, 1992).

Nevertheless, solid solutions are stable at high temperatures – due to the entropy associated with atomic disorder. Gibbs free energy ($G=H-TS$) of mixing can be negative, if the entropy factor (TS) outweighs the enthalpy, and this of course happens at high temperatures. On decreasing temperature, solid solubility decreases. The line on T - x (temperature-composition) phase diagram, below which solid solutions decompose, is called solvus (see below). Solid solubility is small when the differences in the sizes (e.g., ionic radii) of the substituting atoms are large (typically $> 15\%$) or when chemical bonding in the end members is very different (e.g., almost purely ionic NaCl and significantly covalent AgCl form very limited solid solution series, although radii of Na^+ and Ag^+ are very similar).

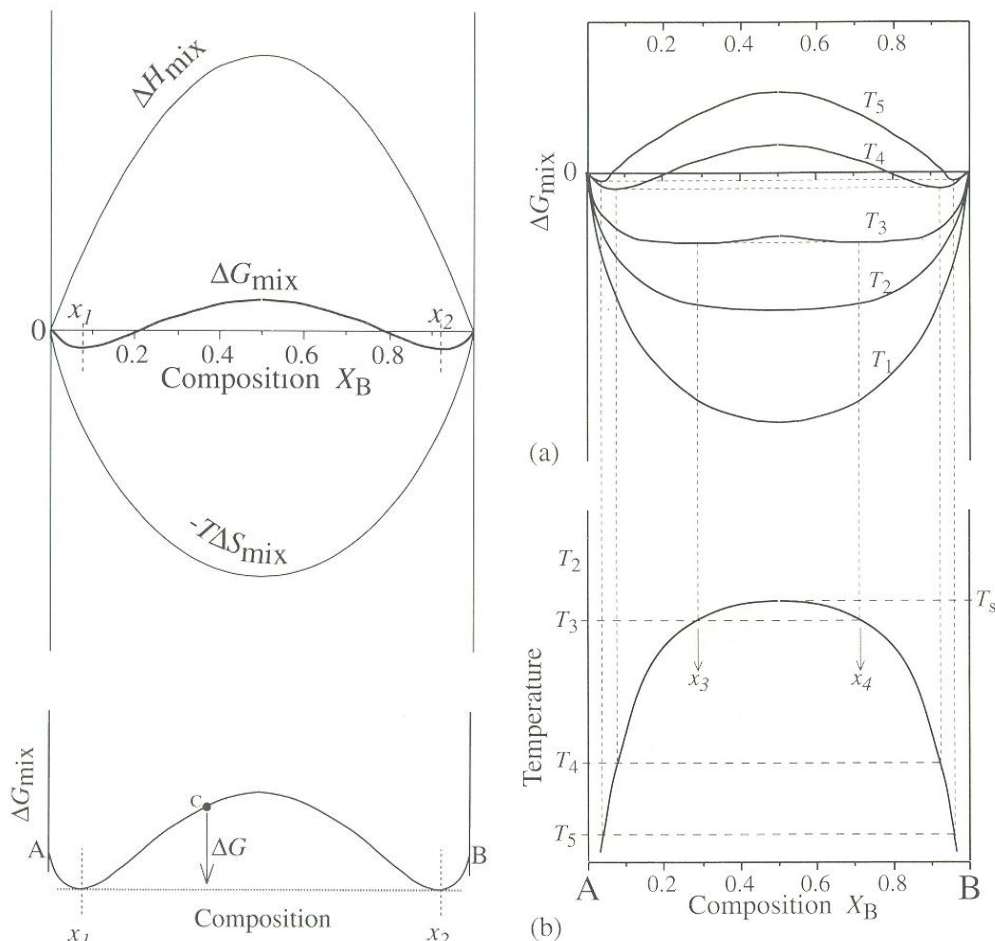
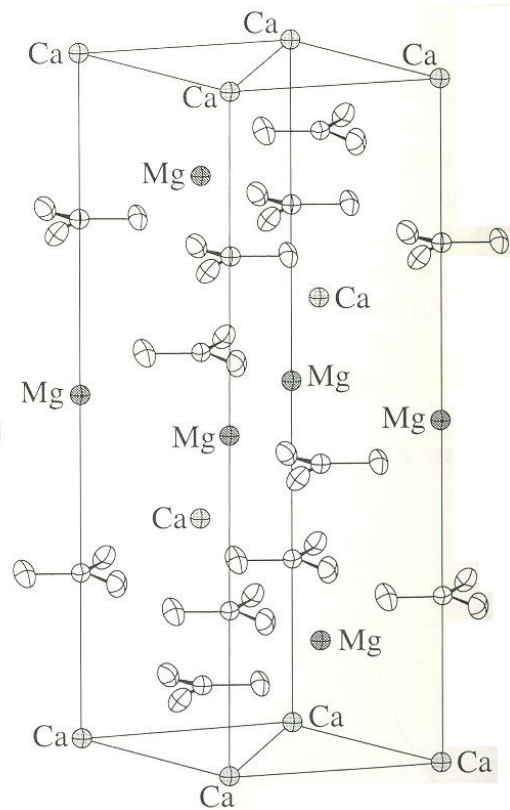
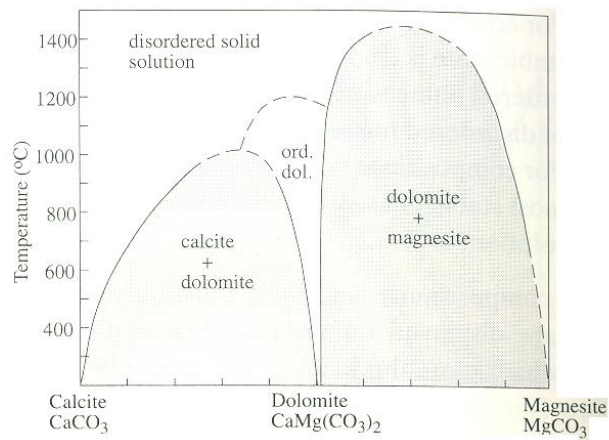


Illustration of the Gibbs free energy of mixing (left), its evolution with temperature and solvus line (from Putnis, 1992).

Sometimes, especially when the differences between the substituting atoms are too large, an intermediate ordered compound may exist. In this case, one has a more complicated phase diagram – as in the case of CaCO_3 - MgCO_3 system with an intermediate phase, dolomite $\text{CaMg}(\text{CO}_3)_2$.



Phase diagram of the calcite-magnesite system and the ordered structure of dolomite. (from Putnis, 1992).

9. Structure types of minerals.

Structure of the elements. Elemental solids, in spite of simple chemical composition, are often structurally complex. We can distinguish several situations:

- metallic elements (these usually have fcc-, hcp-, bcc- structures – but there are exceptions such as Mn, Ga, Hg, rare earth elements, actinides)
- noble gases (fcc-structures, but He crystallises in the hcp-structure)
- molecular solids (H₂, halogens, N₂, O₂, some forms of phosphorus – P₄, and sulphur – S₈), chain structures (S, Se, Te) and sheet structures (P, As, Sb, Bi) with a gradual transition to 3D-structures on increasing degree of metallization (Bi is a semiconductor, but Po is a metal with a unique simple cubic structure)
- non-molecular covalent crystals (B, C, Si, Ge) gradually losing directionality of bonds upon increasing degree of metallicity down the column of the Periodic Table (C-Si-Ge-Pb).

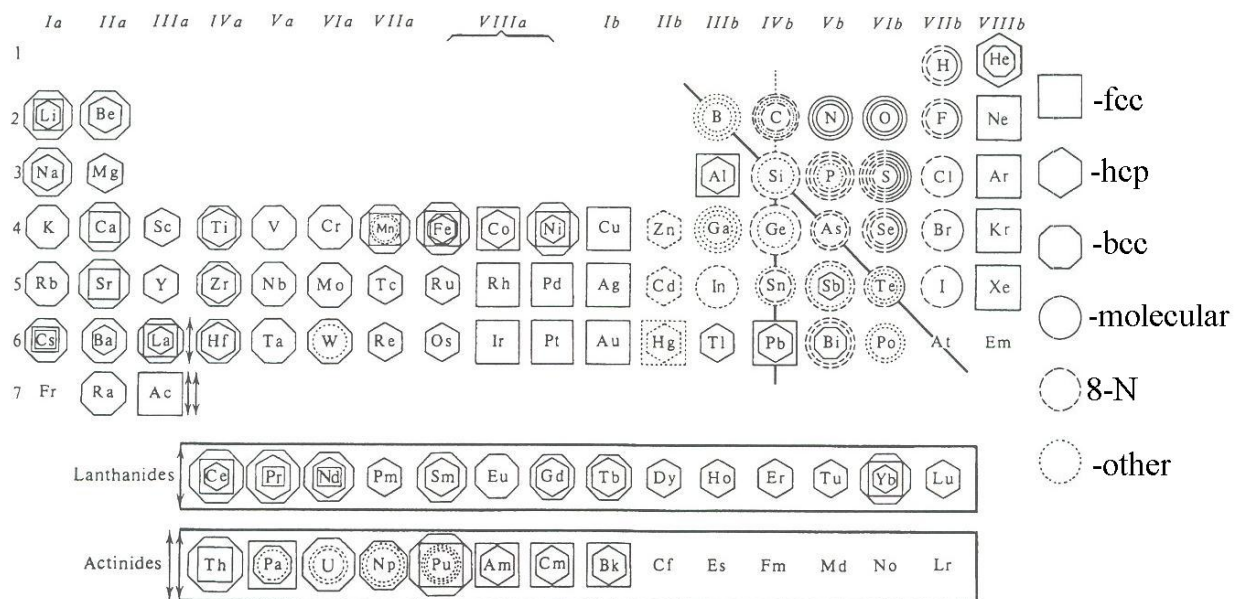


Abb. 3.4.1-3 Polymorphie der Elemente symbolisch dargestellt: 1 kubisch, 2 hexagonal dichte Packung, 3 innenzentriert kubisch, 4 Molekülstruktur, 5 Struktur mit KZ=8-N, 6 andere Struktur. Der Übergang von einem äusseren zu einem inneren Symbol bedeutet einen Phasenübergang von einer Hoch- zu einer Tieftemperaturphase, und schliesslich zu einer Hochdruckmodifikation. Die Zintl-Linie verläuft von B über Si, As, Te nach At (Vainshtein, 1995, 2-1).

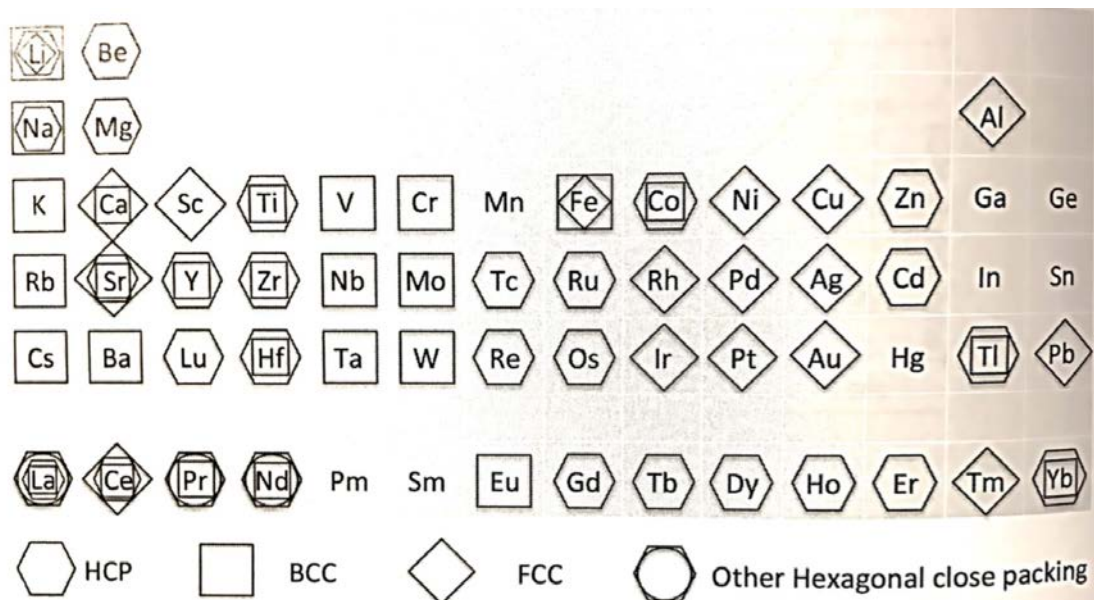
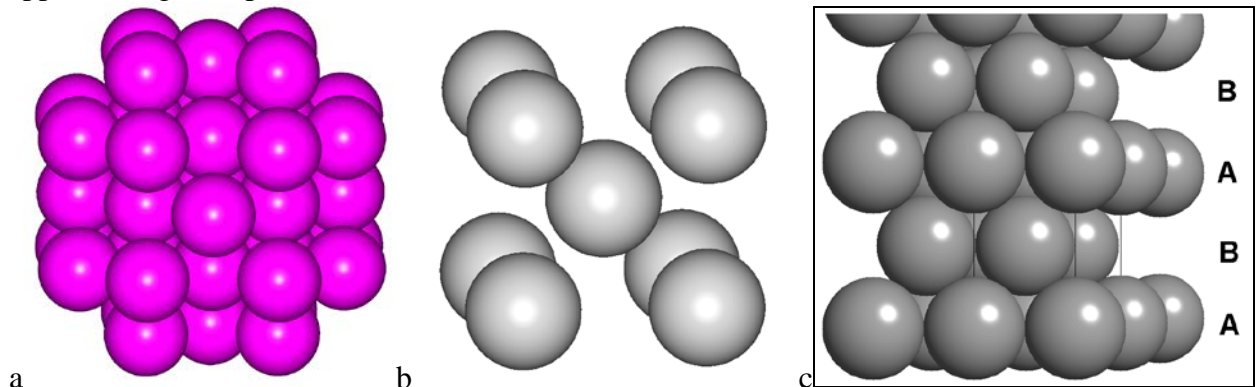


Fig. 10.7 Crystal structures adopted by elemental metals. The largest symbol denotes the room temperature structure. “Other hexagonal close packing” refers to stacking sequences such as ABAC, as was shown in Fig. 10.6. From data in: C. Barrett and T. B. Massalski, *Structure of Metals*, 3rd Rev. Edn, Pergamon Press, New York (1980).

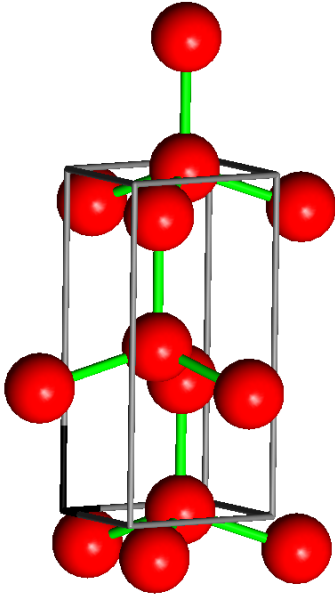
Many covalent structures of the elements follow the so-called “8-N” rule that the number of nearest neighbours for atoms in such structures is equal to 8 minus the number of the column of the element in the Periodic Table. E.g., in chain structures of S, Se, Te (VI group) each atom has 2 neighbours, at the same time $8-6 = 2$. Such “8-N” structures are formed if all atoms are connected by ordinary covalent bonds – in this case, taking into account the electrons shared in covalent bonds, they guarantee the stable 8-electron configuration for atoms. Other examples of such structures are P, As, Sb, Bi (V group) with 3 neighbours for each atom, C (diamond), Si and Ge (IV group) with 4 neighbours for each atom. If there are multiple covalent bonds, the number of neighbours is smaller – e.g., 1 in crystalline oxygen, or 3 in graphite (C).

Some elements have remarkably complex structures (B, Mn, Ga, actinides). However, most elements that can be found as minerals have rather simple structures – fcc, hcp, bcc, diamond, graphite. E.g., Fe has bcc, fcc, hcp structures at different P-T conditions. Cu, Ag, Au, Al, Pb have the fcc structure. Distorted simple cubic structure is found for As, Sb, Bi. Sulphur (S) has many modifications, some consisting of cyclic molecules S_n ($n=7,8,9,10,12,18,20$), others consisting of S_∞ chains. At room temperature the most stable phase is orthorhombic, containing S_8 molecules. Above 95.4°C , a monoclinic phase is stable – this one consists of the same S_8 molecules, but one third of them have random configurations (which increases the entropy, thus enabling this phase to appear at high temperatures).

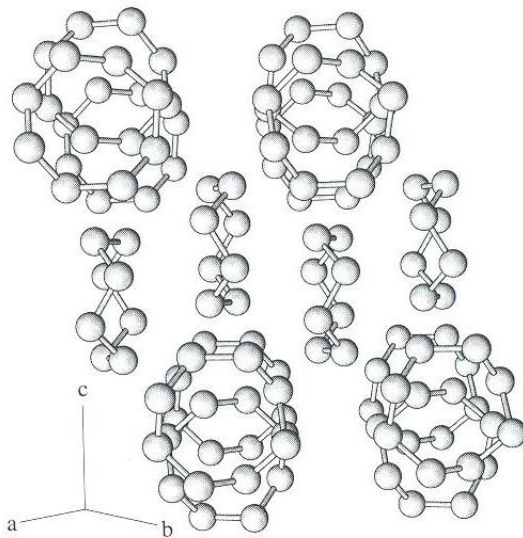


Simple metal structures: a) fcc (Cu, Ag, Au, Al, noble gases except He; Fe at high temperature), b) bcc (Fe at normal conditions, Na, K, Rb, Cs, V, Cr), c) hcp (Fe at high pressure, He, Mg, Zn).

For carbon, there is an interesting form called lonsdaleite, whose structure can be considered as a hexagonal polytype of diamond. This mineral, like diamond, exists at high pressures (often as thin lamellae within diamond).

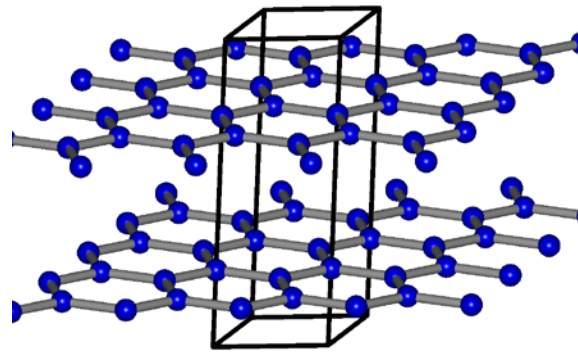


Crystal structure of lonsdaleite.



a

a) Molecular structure of sulphur, with S_8 ring molecules. Within the molecules, bonding is covalent, between them - van der Waals bonding (from Nesse, 2000).



b

b) Layered structure of graphite with covalent bonding within the layers, and van der Waals between them.

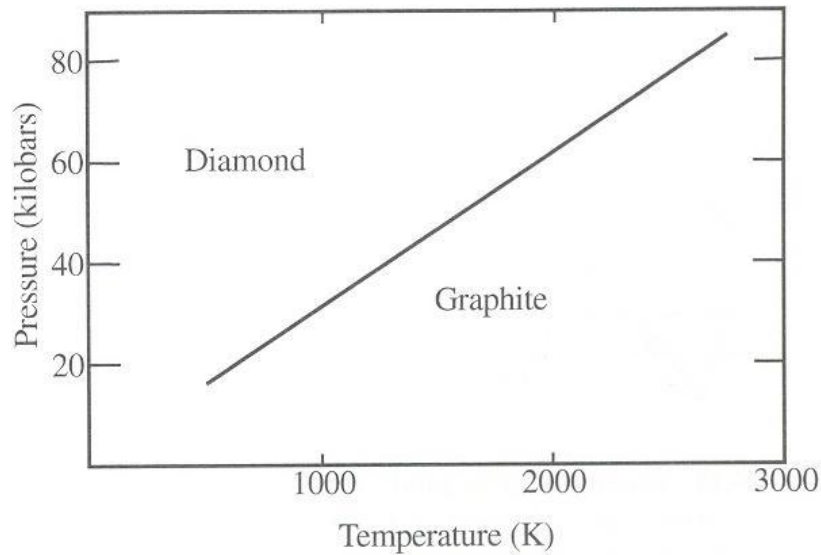
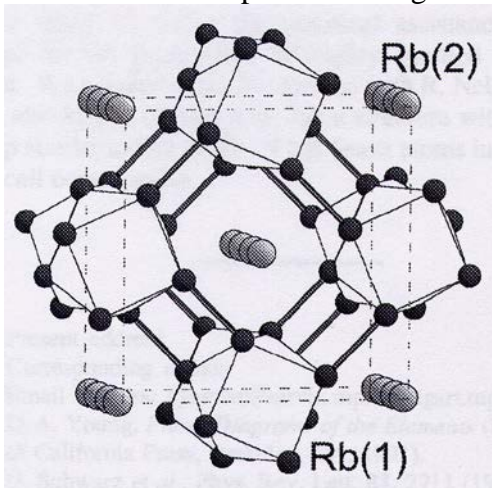


Figure 4.10 Diamond–graphite stability fields. Diamond is stable at pressures normally found only in the Earth’s mantle.

Structural stability of diamond and graphite (from Nesse, 2000).

An interesting observation has been made by K. Syassen and W. Holzapfel (Germany) and R. Nelmes and M. McMahon (U.K.): many elements with simple structures and apparently well-understood chemical bonding transform into extremely complex crystal structures at high pressure – e.g., Li, K, Rb, Cs, Ba, Bi, Sb, etc. This is usually associated with appearance of d-electrons in these elements at high pressure, i.e. great changes in chemistry under high pressure. This could have interesting geochemical consequences (e.g., K becomes a transition metal at high pressure and could be incorporated in larger amounts into the Fe-rich Earth’s core).



Complex “self-hosting” high-pressure structure of Rb(IV) – Schwarz et al. (1999).

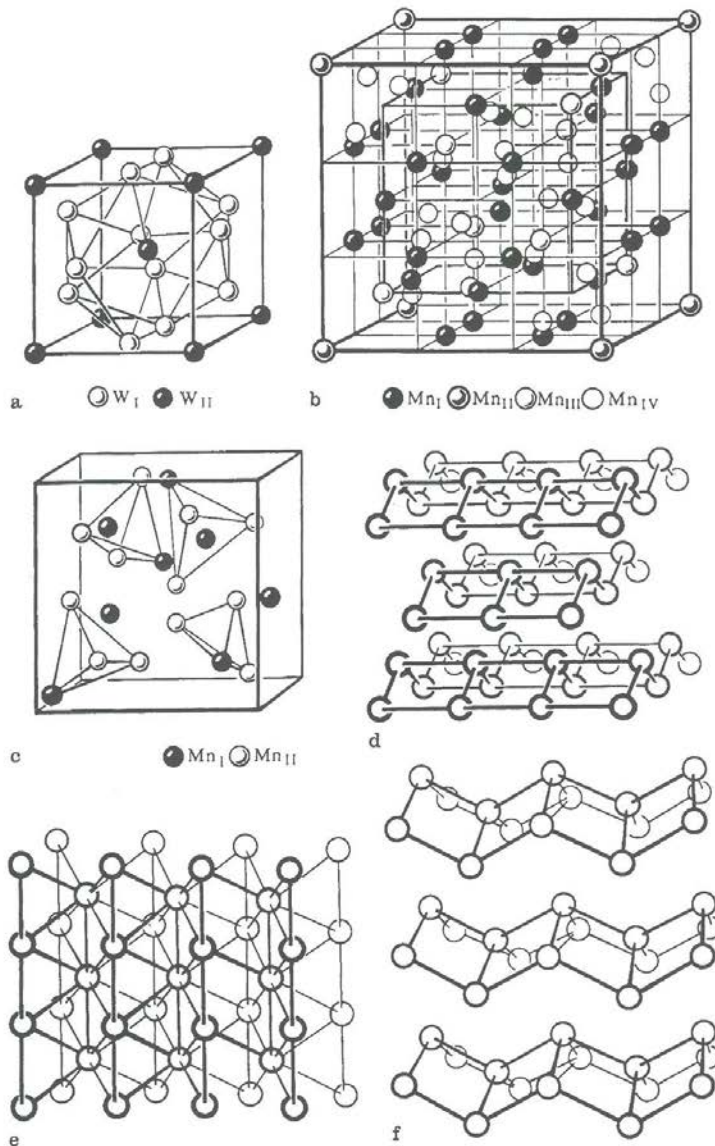
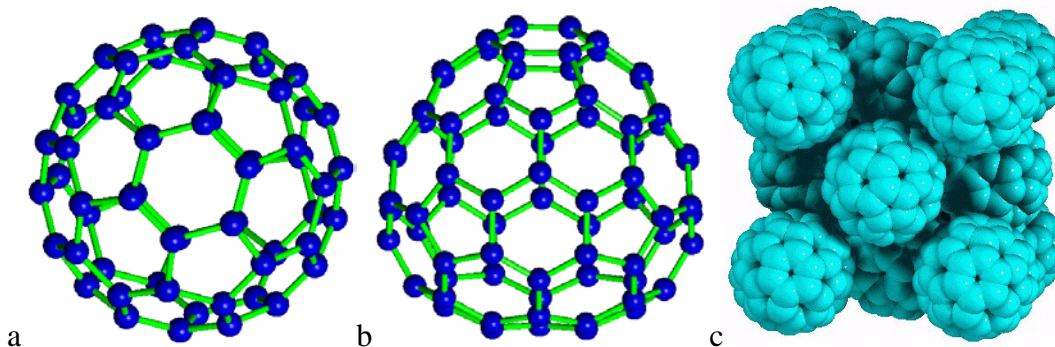


Abb. 3.4.1-4 Beispiele einiger metallischer Elementstrukturen: (a) β -Wolfram, Mangan, (c) β -Mangan, (d) α -Uran, (e) β -Neptunium (Vainshtein, 1995, 2-3).

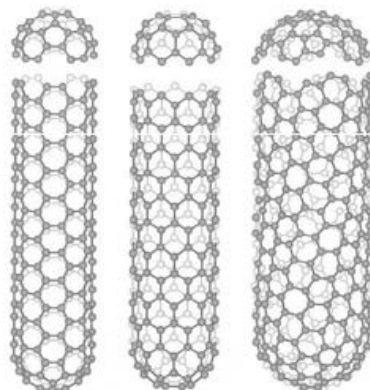
Illustration of complex structures of some elements at normal pressure.

Another class of rather complex elemental structures is fullerenes, metastable molecular forms of carbon, with centres of large C_n molecules (the most stable molecule is C_{60}) occupying positions of an fcc-structure. Fullerenes can be easily doped with metal atoms (e.g., K, Rb, Cs) – such doped forms are superconductors with relatively high $T_c \approx 30$ K. Fullerene discovery in 1985 by H. Kroto, R. Curl and R. Smalley earned them a 1996 Nobel Prize in Chemistry.



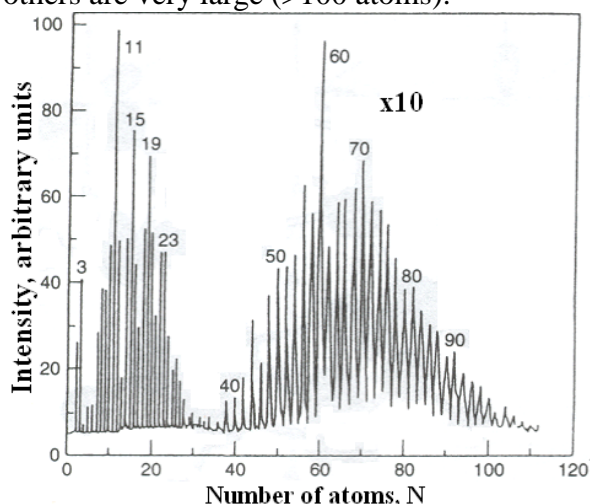
Fullerenes: a) C₆₀, b) C₇₄, c) packing of fullerene molecules in the solid.

Fullerenes can be imagined as a spherical “convolution” of a graphite sheet. One can also imagine extended tubular “convolutions” called carbon nanotubes, which have been experimentally observed and found to possess very interesting physical properties. Carbon nanotubes were discovered in 1952 by Russian scientists L.V. Radushkevich and V.M. Lukyanovich, although many “outsiders” to this field believe that the discovery was made in 1991 by S. Iijima. Unique electronic properties are also possessed by single sheets of graphite – the so-called graphene, experimentally separated in 2004 by A.Geim and K.Novoselov. Curiously, the motion of the electrons in graphene obeys the laws of relativistic quantum mechanics.



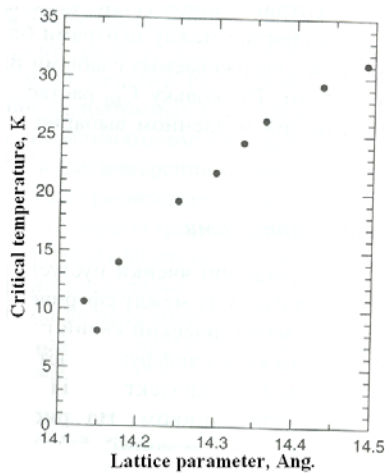
Carbon nanotubes.

Many different types of fullerene clusters have been synthesised. Figure below shows a mass-spectrum of such clusters, from which it is clear that the most stable fullerenes contain 60 and 70 atoms. Some fullerenes are rather small, e.g. C₂₀ or C₂₂, others are very large (>100 atoms).



Mass-spectrum of carbon clusters (from Poole & Owens, 2003).

In the structure of fullerenes, there are large voids between the fullerene cages, and these voids can be occupied by large alkali metal atoms. Such intercalation compounds are superconductors, and there is a clear increase of the critical superconductivity temperature with the size of the intercalating atom.



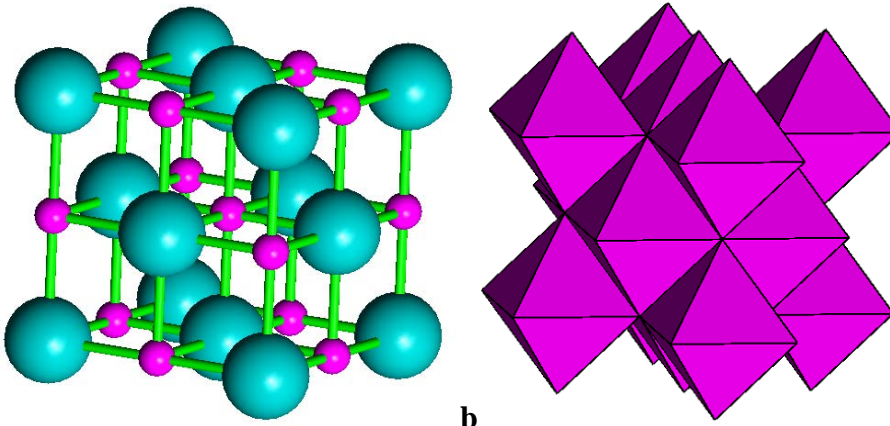
Critical temperature of cubic A_3C_{60} intercalated fullerenes (A=alkali atom) as a function of the lattice parameter (from Poole & Owens, 2003).

Structures of some sulphides, oxides, halides. Here, there are several dominant structure types:

I. AX types.

NaCl-type – cubic close packing of anions (B) with all octahedral voids filled by cations (A). Cation octahedra share the edges and the corners. This structure is enormously common among ionic, covalent, metallic compounds. Space group $Fm\bar{3}m$.

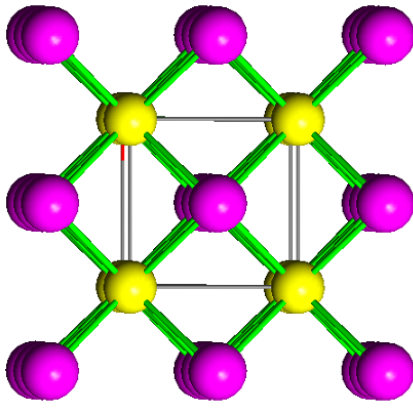
Examples: Galena PbS, periclase MgO, wüstite FeO (at low pressures Fe-deficient), halite NaCl, silvite KCl, also oldhamite CaS, non-minerals CaO, MnO, LiF, RbCl, NaBr, NaI,...



a Structure of NaCl in a)ball-and-stick and b)polyhedral representations.

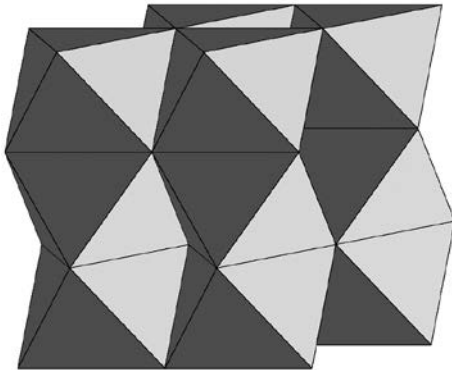
CsCl-type – simple cubic structure formed by the anions (B) with cations (A) occupying the centres of all cubes. These cation cubes share the faces, edges, and corners. Space group $Pm\bar{3}m$.

Examples: Sal ammoniac NH_4Cl , many alloys, high-pressure phases of NaCl-type materials (NaCl, KCl, ...), some metallic alloys.

**CsCl structure**

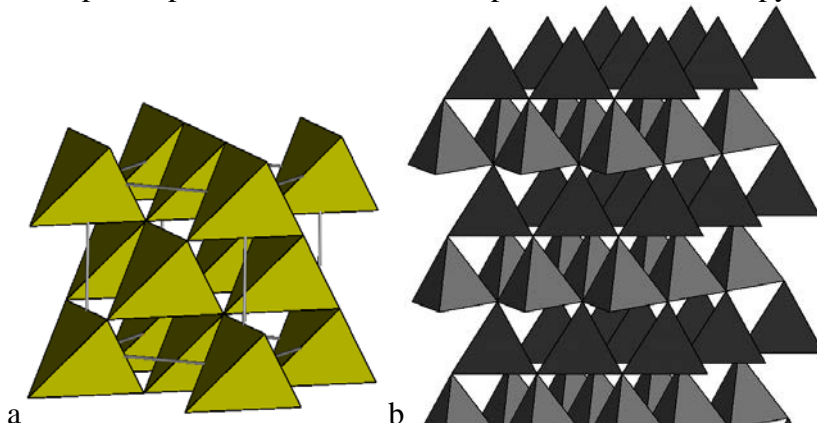
NiAs-type – hexagonal close packing of anions (B) with all octahedral voids filled by cations (A). Cation octahedra share the faces and the edges and the corners. Face-sharing is disfavoured in ionic crystals, so this structure is adopted only by covalent and metallic crystals. Face-sharing is favourable in cases where is a cation-cation bond across the shared face (as it happens in troilite FeS and nickeline NiAs). Formally, NaCl- and NiAs-type structures can be considered as polytypes, but because of different chemical bonding types needed for these two structures they almost never exist for the same compound. Space group $P6_3/mmc$.

Examples: Nickeline NiAs, troilite FeS (usually Fe-deficient), many sulphides, phosphides, arsenides, ...

**NiAs structure, with octahedral drawn around Ni atoms.**

Zincblende- (sphalerite-)type – cubic close packing of the anions (B) with half of the tetrahedral voids occupied by the cations (A). Cation tetrahedra share only the corners. Common structure for covalent crystals. Space group $F\bar{4}3m$.

Examples: Sphalerite ZnS, ordered superstructure – chalcopyrite CuFeS₂, ...

**Structures of a) sphalerite, b) wurtzite.**

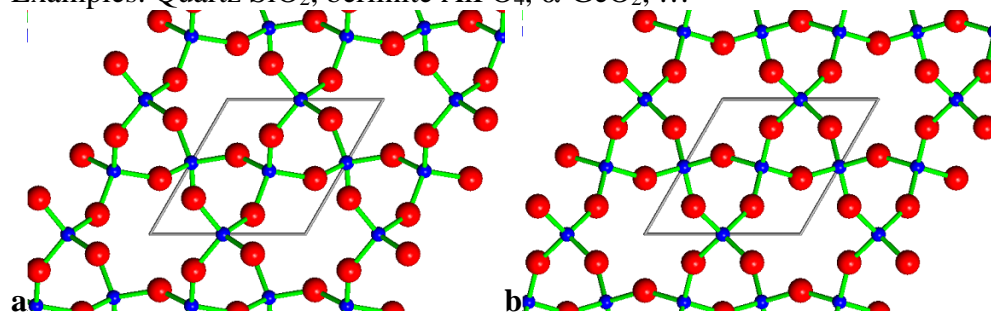
Wurtzite-type – hexagonal close packing of the anions (B) with half of the tetrahedral voids occupied by the cations (A). Cation tetrahedral share only the corners. Common structure for covalent crystals. Energetically similar to sphalerite, these two structures can be considered as polytypes. $P6_3mc$. Wurtzite-type crystals can have interesting piezoelectric properties. Under pressure sphalerite- and wurtzite-structured crystals often adopt the NaCl-type structure. Wurtzite structure is derived from the lonsdaleite structure, whereas sphalerite structure is derived from the diamond structure.

Wurtzite ZnS, greenockite CdS, zincite ZnO, ...

II. AB_2 types.

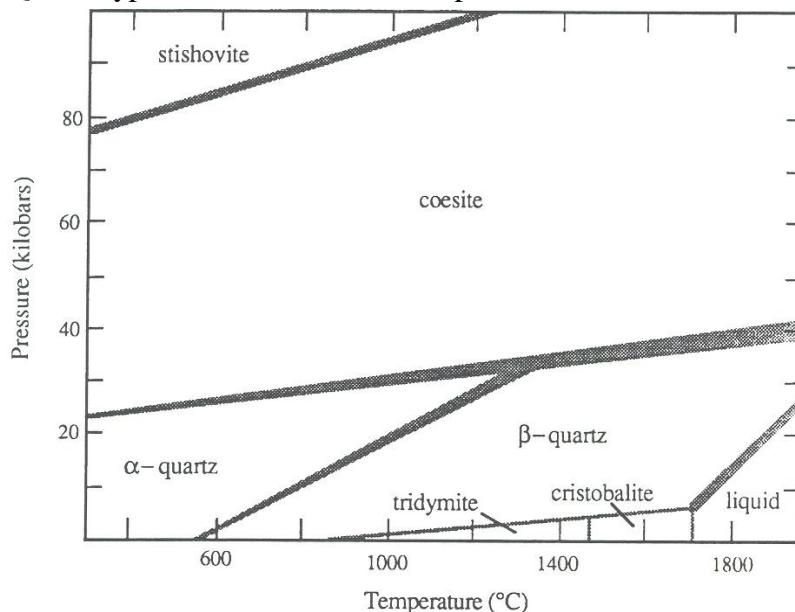
Quartz-type – Three-dimensional framework of corner-sharing SiO_4 -tetrahedra. This structure is not very dense and easily transforms into denser structures (coesite, stishovite, ...) under pressure.

Examples: Quartz SiO_2 , berlinite $AlPO_4$, α - GeO_2 , ...



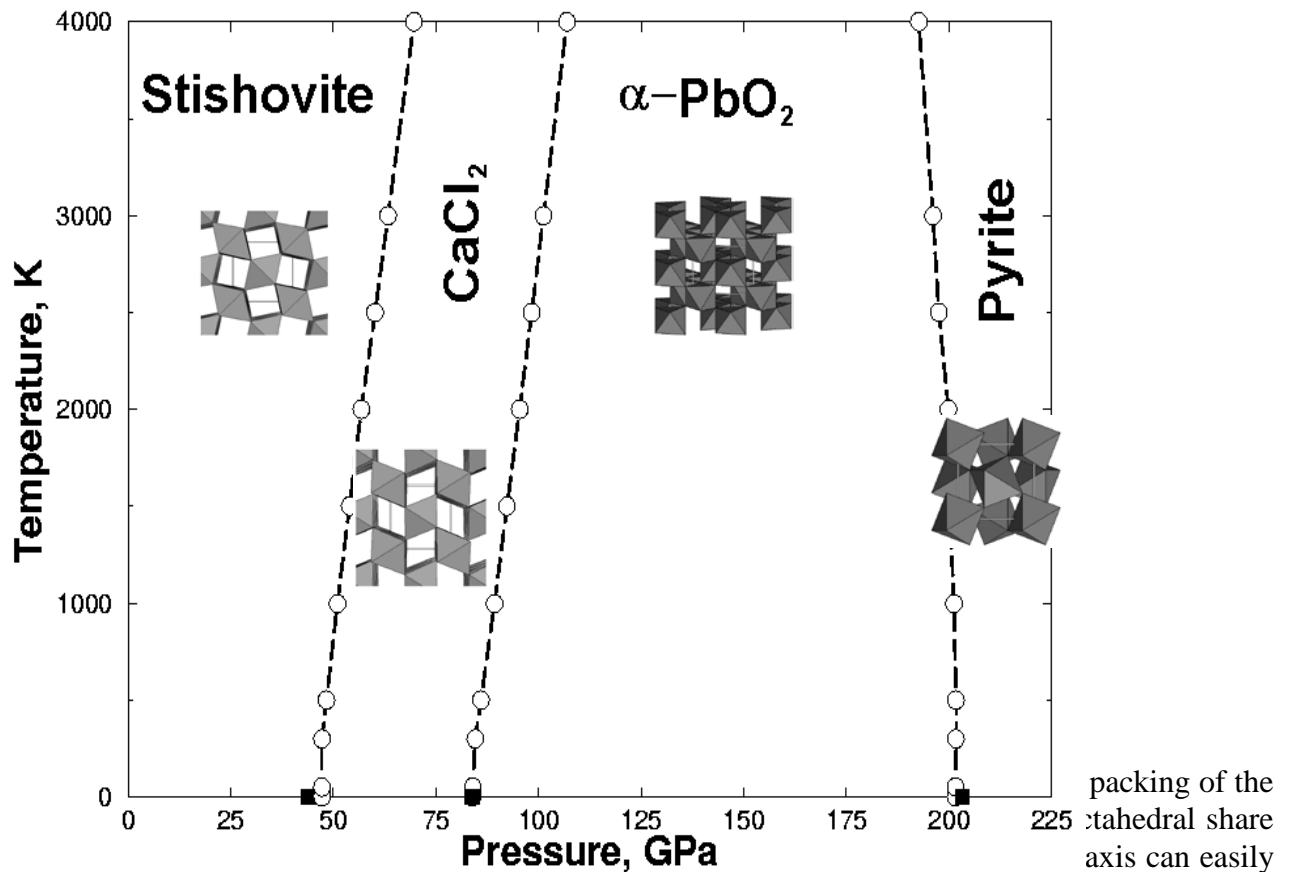
Structure of quartz: a) low-temperature trigonal α -quartz, b) high-temperature hexagonal β -quartz (stable above 573 °C).

Quartz-type materials are valuable piezoelectric materials used, e.g. in watch manufacturing.



Druck-/Temperatur-Phasendiagramm für SiO_2 (Griffen, 1992, 1-1)

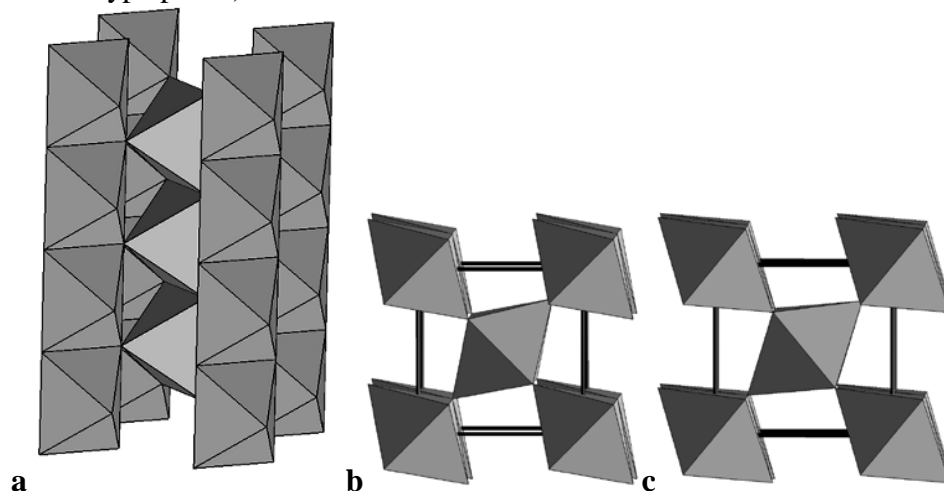
Low-pressure phase diagram of SiO_2 .



be seen in this structure; these columns define anisotropy of many properties of rutile-structured materials.

Examples: Rutile TiO_2 , pyrolusite MnO_2 , stishovite SiO_2 , sellaite MgF_2 , ...

Distorted orthorhombic variants – marcasite FeS_2 , CaCl_2 . In marcasite, one has molecular S_2 -ions, while the CaCl_2 structure is a distortion towards more regular close packing of anions (hence more stable under high pressure – e.g., rutile-structured stishovite SiO_2 at ~ 50 GPa transforms into a CaCl_2 -type phase).



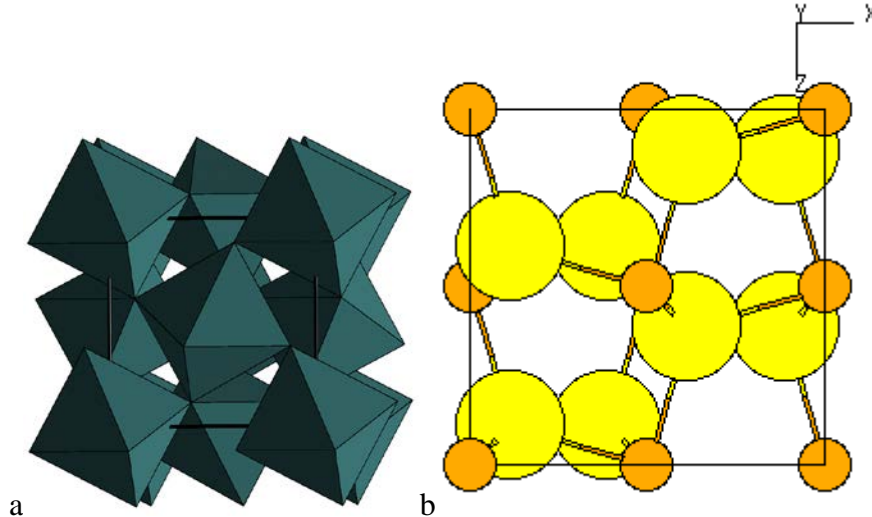
Rutile structure: a) showing octahedral columns running along c-axis, b) view perpendicular to c-axis, c) the same view for the orthorhombic CaCl_2 structure.

Pyrite-type: the structure of pyrite (FeS_2) has Fe atoms and S_2 groups occupying positions of Na and Cl, respectively, in the rocksalt structure. Since the symmetry of persulphide group S_2 is lower than the spherical symmetry of the Cl ion, pyrite has a lower symmetry – $\overline{Pa}3$ instead of $\overline{Fm}3m$. Persulphide-ion creates a strong crystal field (stronger than sulphide-ion S^{2-}), therefore pyrite

contains Fe^{2+} in the non-magnetic low-spin state, whereas pyrrhotine FeS has Fe^{2+} in the high-spin state, which determines the magnetic properties of pyrrhotine.

When the distance between the anions (e.g., S-S) is too large to describe it as a chemical bond, one has the PdF_2 -subtype. The high-pressure form of SiO_2 belongs to this sub-type, i.e. has no O-O bonds (Oganov et al., 2005). In pyrite- and PdF_2 -type crystals, the cations are octahedrally coordinated by the anions.

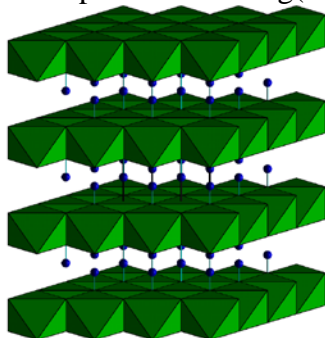
Examples: Pyrite FeS_2 , MnS_2 , CoS_2 , PdF_2 , high-pressure form of SiO_2 ...



Pyrite structure: a) polyhedral, b) ball-and-stick representations.

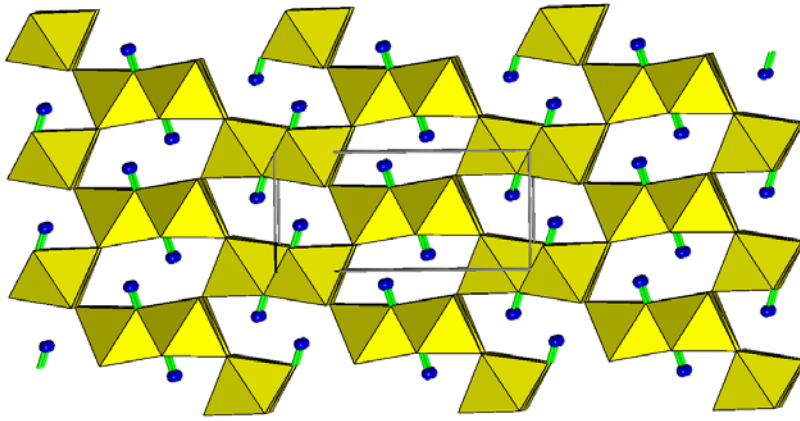
CdI_2 -type – can be described as close packing of the anions where $\frac{1}{2}$ of the octahedral voids are occupied (in alternating layers) by the cations. Layered structures are usually favoured in materials with highly polarisable anions, such as I^- , OH^- , S^{2-} , etc. Different polytypes with very close energies exist for this structure type. Brucite-type layers exist in many other structures, e.g. chlorites.

Examples: Brucite $\text{Mg}(\text{OH})_2$, ...



Structure of brucite, showing Mg-centred octahedra.

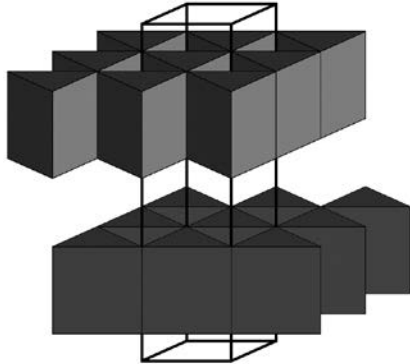
Another structure type of hydroxide minerals, that of goethite $\text{FeO}(\text{OH})$, is shown below. This structure can be derived from the rutile type (like the hollandite structure, see below). It has Fe^{3+} in the octahedral coordination, and the structure is characterised by the presence of hydrogen bonds:



Structure of goethite, showing Fe-centred octahedra.

Molybdenite-type – unusual layered structure that has Mo atoms in the trigonal prismatic (6-fold) coordination.

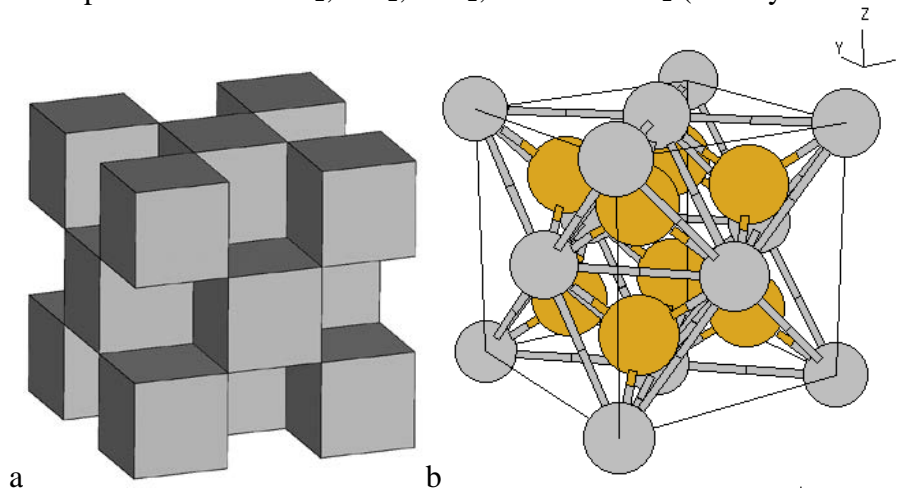
Examples: Molybdenite MoS_2 ,...



Structure of molybdenite. Polyhedra (trigonal prisms) are drawn around Mo atoms.

Fluorite-type – This structure can be described as cubic close packing of the cations with the anions filling all the tetrahedral voids in it. The coordination number of the anions is then 4 (tetrahedral coordination), of the cations – 8 (cubic coordination). Alternatively, the structure can be described as a checker-board arrangement of cation-centred cubes.

Examples: Fluorite CaF_2 , SrF_2 , BaF_2 , uraninite UO_2 (usually U-deficient),...



Fluorite structure in the a) polyhedral and b) ball-and-stick representations.

Hollandite-type – This structure is derived from rutile, but is different in that here there are double octahedral chains running parallel to c -axis, and the channels are much larger and can now

incorporate large cations (Ba^{2+} , Pb^{2+} , ...) making such minerals interesting as sources of these elements, as possible materials for radioactive waste disposal, and as possible hosts of such elements in the Earth's lower mantle – at high pressures corresponding to the lower mantle, microcline KAlSi_3O_8 transforms into a hollandite-type phase that could be an important mantle mineral (Madon et al., 1989).

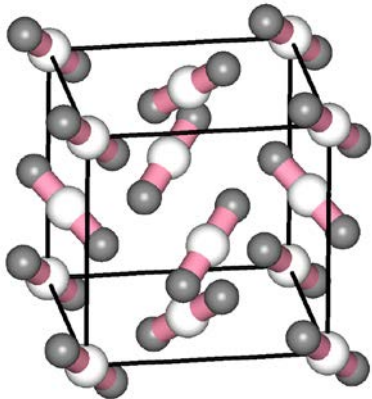
Cation-stuffed forms of MnO_2 (hollandite $\text{Ba}(\text{Mn}^{4+}, \text{Mn}^{2+})_8\text{O}_{16}$), high-pressure KAlSi_3O_8 , ...



Structure of hollandite, showing Mn-centred octahedra.

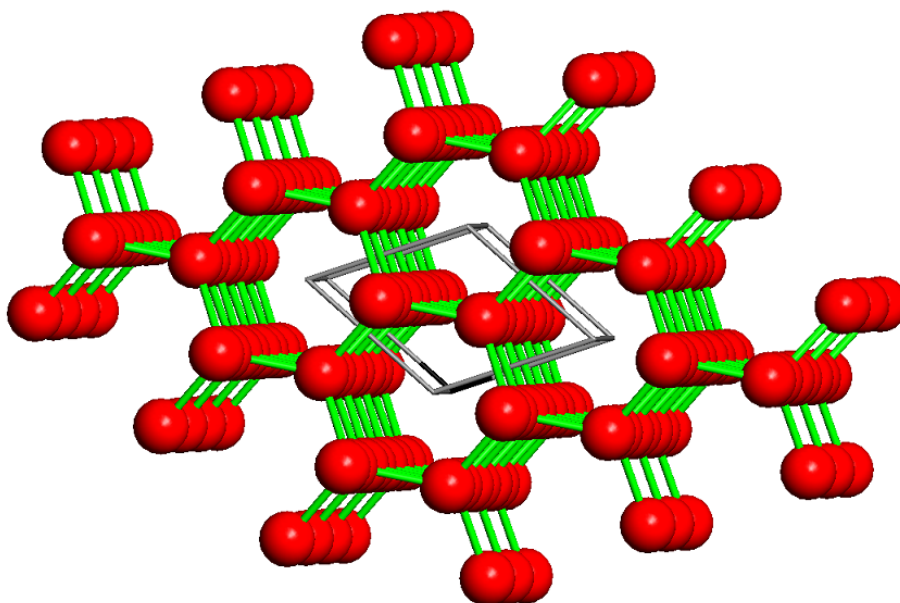
CO₂-type – molecular structure with centres of the CO₂ molecules occupying positions of an fcc lattice. Geometrically, this structure type is related to the pyrite and fluorite structure types: all

these structures have the space group $P\bar{a}3$ with the cations occupying positions of an fcc-lattice, and the only difference is in the oxygen atom coordinate x_{O} : ~ 0.1 in the CO₂-type, 0.25 in the fluorite type, ~ 0.34 -0.36 in the PdF₂ sub-type, and 0.37-0.41 in the pyrite type.



Structure of CO₂.

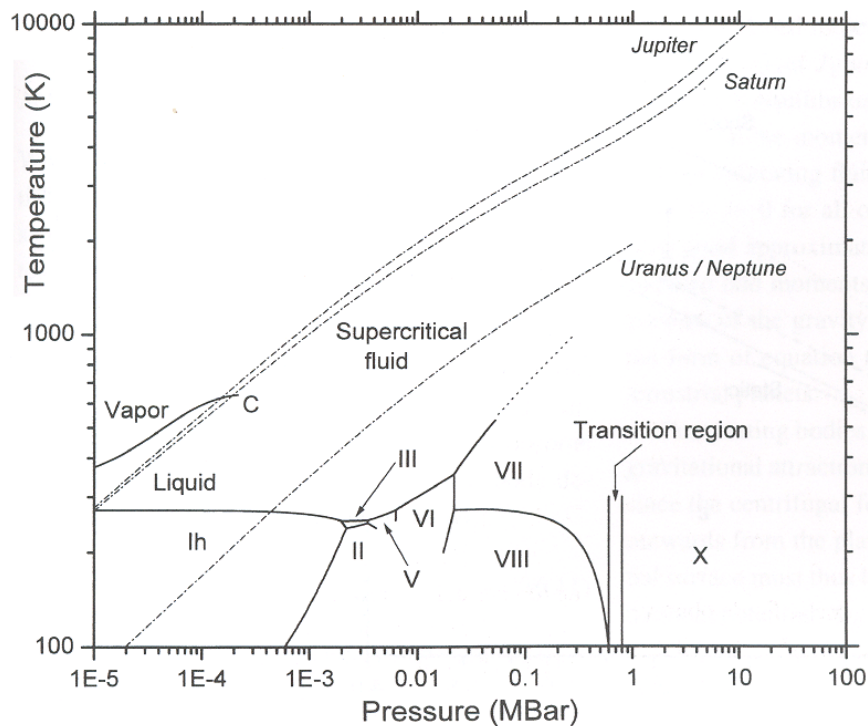
Ice and water. At low pressures and temperatures, ice Ih has the structure, where O occupy the same positions as C atoms in the structure of lonsdaleite, with H atoms in between and forming hydrogen bonds. This structure has large empty hexagonal channels, and therefore has a low density. When ice melts, these channels are destroyed, and as a result water has a slightly greater density than ice (which is unusual, since in most other cases solids are denser than liquids) – hence, ice can float on water.



Structure of ice Ih. Only the positions of oxygen atoms are shown (red spheres). This structure belongs to the structure type of lonsdaleite (“hexagonal diamond”), there is also another structure (ice Ic) belonging to the cubic structure type of diamond.

Did you know how clouds are dispelled? The method for doing so (first invented by Irving Langmuir, and the modern version of the method created by Bernard Vonnegut (brother of novelist Kurt Vonnegut)) is based on the fact that clouds contain supercooled water vapor (i.e. vapor below the freezing temperature, but unable to crystallize due to difficulties of nucleation of the crystalline phase) and involves incorporation of “seeds” into clouds. B.Vonnegut proposed to seed clouds with AgI – which has the same (lonsdaleite or wurtzite) structure as ice Ih, and very similar lattice parameters. This enables ice crystals to grow on AgI substrate (phenomenon known as *epitaxy*), leading to an avalanche-like crystallization of ice and dissolution of clouds. AgI is used mainly for hail suppression, while other techniques are used for enhancement of rainfall. Crystallography of ice I figured in Kurt Vonnegut's novel *Cat's Cradle*.

On increasing pressure, a large number of other, denser structures are formed. Ice X is the highest-pressure phase known and has very strong symmetrical hydrogen bonds (in most cases, except for the strongest hydrogen bonds F-H...F, hydrogen bonds are very asymmetric and relatively weak). Water, together with NH₃ and CH₄, is a very important component of the giant planets Uranus and Neptune.

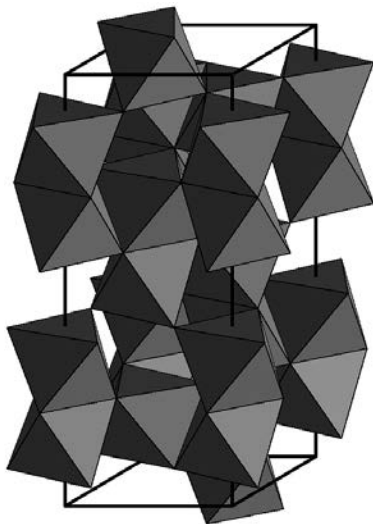


Phase diagram of H_2O (from de Pater and Lissauer, 2001).

III. A_2X_3 types.

Corundum-type – in corundum Al_2O_3 , one has hexagonal close packing of the O atoms, with $2/3$ of the octahedral voids occupied by the Al atoms. Al-centred octahedra share faces, edges and corners. Ilmenite (FeTiO_3) structure is a superstructure of the corundum structure with doubling of the c parameter: Fe and Ti occupy octahedral positions in alternating layers.

Corundum Al_2O_3 , hematite Fe_2O_3 , escholaite Cr_2O_3 , ilmenite FeTiO_3 , akimotoite MgSiO_3 ...



Structure of corundum, showing Al-centred octahedra.

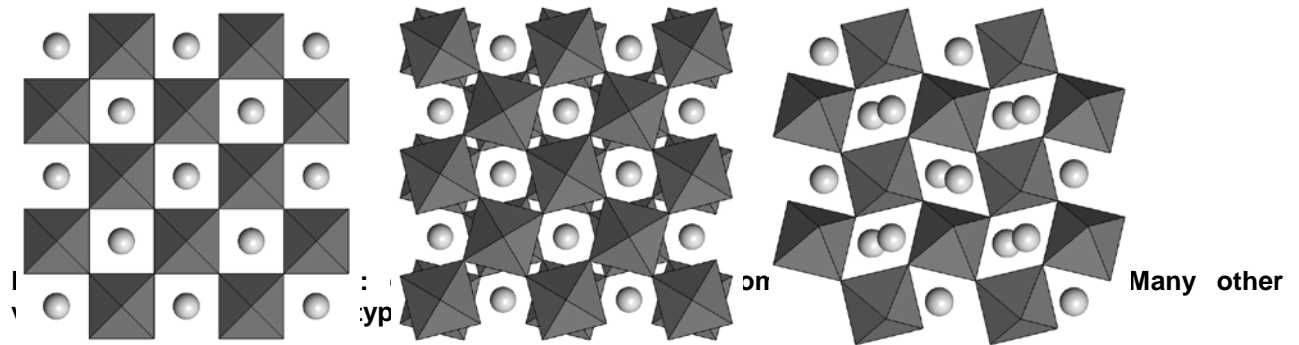
IV. ABO_3 types.

Perovskite-type – in perovskite CaTiO_3 , one has corner-sharing Ti-centred octahedral, with Ca atoms occupying large cages formed by the octahedra. Ideal perovskite structure is cubic (below, left: SrTiO_3 at room temperature, CaSiO_3 at mantle conditions), but for most compounds the structure is distorted to tetragonal (SrTiO_3 at low temperatures, CaSiO_3 at room temperature), orthorhombic (below, right: MgSiO_3 in the lower mantle), or one of many other variants.

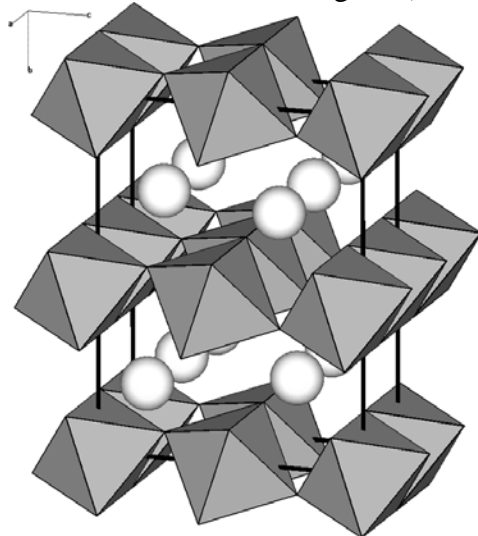
MgSiO_3 perovskite makes up ~ 75 vol.% of the Earth's lower mantle (equivalent to ~ 40 vol.% of the entire Earth (!), this is the most abundant mineral in the Earth), and CaSiO_3 perovskite makes

~5 vol.% of the lower mantle. Some perovskites (e.g., NaMgF_3) are good ionic conductors of electricity. In fact, the same could be true for MgSiO_3 perovskite in the mantle, and this was put forward as a possible explanation for the high electrical conductivity of the lower mantle inferred by geophysicists (Constable & Constable, 2004). Most high-temperature superconductors contain layers of perovskite structure. Finally, many perovskites, due to the proximity of numerous phase transitions, possess enormous dielectric constants and are good ferroelectric materials (e.g., BaTiO_3).

Perovskite CaTiO_3 , lueshite NaNbO_3 , perovskite-type MgSiO_3 and CaSiO_3 , SrTiO_3 , BaTiO_3 , NaMgF_3 ,...



CaIrO₃-type – unusual layered structure with Ir-centred octahedra forming layers, between which Ca atoms (in 8-fold coordination) are sandwiched. Until recently, this structure was known only for a handful of synthetic compounds, but recently it was found (Ono et al., 2004; Oganov & Ono, 2004, 2005; Murakami et al., 2004) at high pressure in several important systems (high-pressure forms of Fe_2O_3 , Al_2O_3 , MgSiO_3)

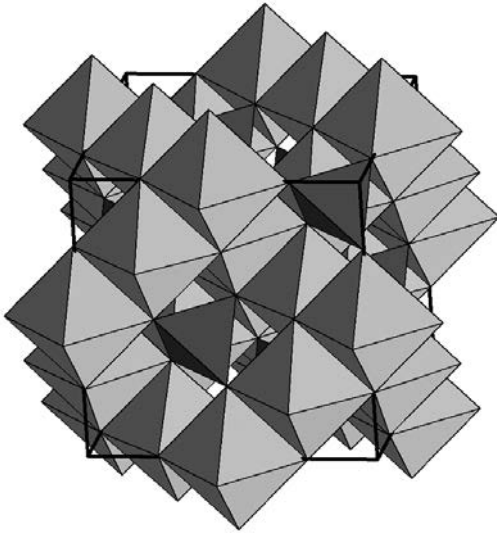


Structure of MgSiO_3 post-perovskite (structure type CaIrO_3), showing layers of Si-centred octahedra.

V. AB_2X_4 types.

Spinel-type – in spinel MgAl_2O_4 , O atoms form cubic close packing, Mg atoms occupy 1/8 of the tetrahedral sites, and Al atoms – 1/2 of the octahedral ones. This structure is adopted by many minerals and compounds. From the technological point of view, many spinels are interesting magnetic materials (ferrites) and are used in magnetic tapes. Ringwoodite Mg_2SiO_4 is the main mineral of the Earth at depths 520-670 km.

Spinel MgAl_2O_4 , magnetite Fe_3O_4 , chromite FeCr_2O_4 , ringwoodite Mg_2SiO_4 ,...



Structure of spinel, showing Al-centred octahedra and Mg-centred tetrahedra.

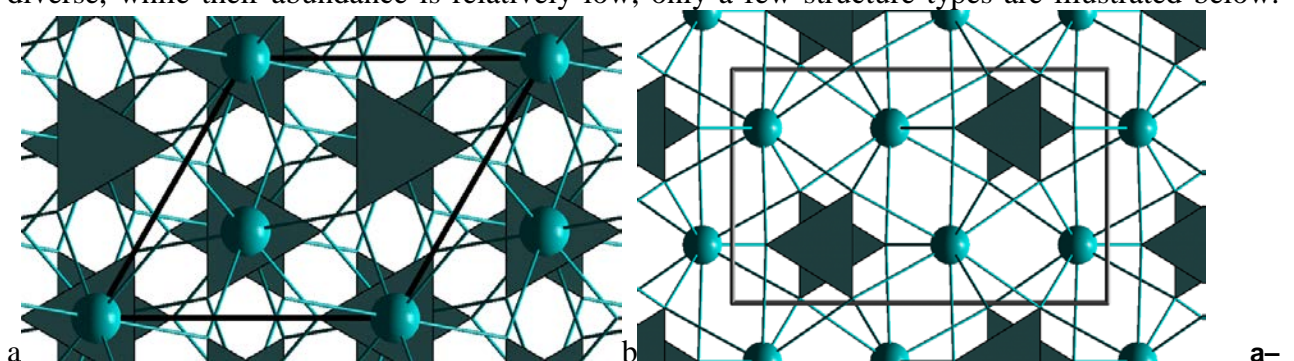
Structures of some borates, carbonates, phosphates, sulphates. The main features are:

- Carbon only trigonal CO_3 -groups in carbonates.
- Phosphates and sulphates have tetrahedral PO_4^{3-} and SO_4^{2-} ions, respectively.
- In carbonates, phosphates, sulphates, anion groups are isolated, i.e. do not share even corners with each other.
- Borates are more complicated: they can have both BO_3^{3-} and BO_4^{5-} anions, and these very often share corners forming complex polymeric anions.
- This ability/inability to polymerise can be understood from the II Pauling's rule, e.g.:

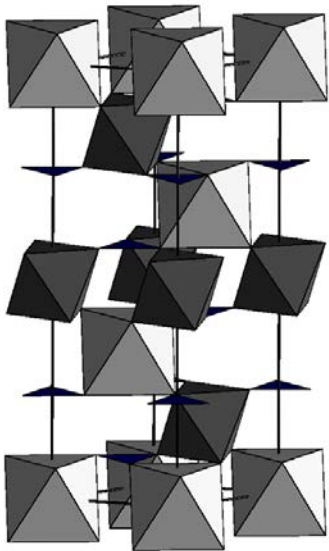
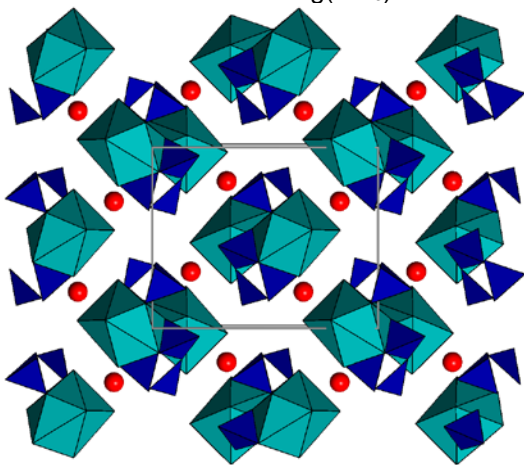
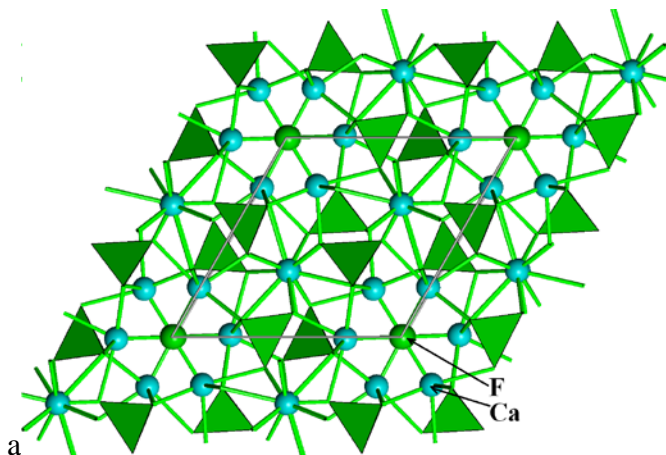
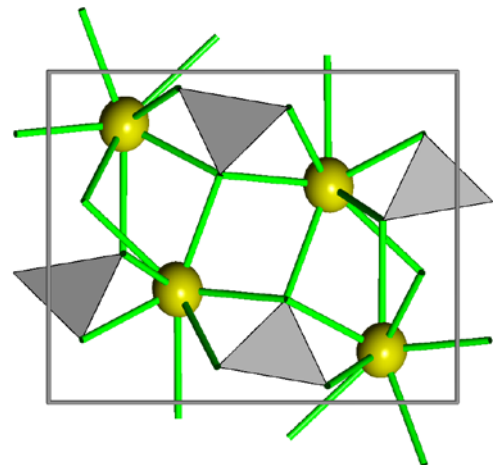
Valence strength of a P-O bond in a PO_4 -tetrahedron is $5/4$. If there were two tetrahedra sharing one oxygen atom, the sum of valence strengths on that atom would be $2 \cdot 5/4 = 2.5$, which is significantly different from the valence of the oxygen atom (2) and therefore unlikely.

On the other hand, the bond strength in a BO_3 -triangle is $3/3 = 1$, and in a BO_4 -tetrahedron it is $3/4$. Therefore, it is possible to have corner sharing of two BO_3 -triangles (the sum of bond strengths on O atom is exactly 2), two BO_4 -tetrahedra (sum of 1.5 – the rest is easy to make up by additional cations) or one triangle and one tetrahedron (bond strength sum of 1.75 – again easily compensated by additional cations).

Since chemically and structurally borates, carbonates, phosphates and sulphates are extremely diverse, while their abundance is relatively low, only a few structure types are illustrated below.



a calcite, b – aragonite (CaCO_3).

Structure of dolomite $\text{CaMg}(\text{CO}_3)_2$.Structure of inyoite $\text{Ca}_2\text{B}_6\text{O}_6(\text{OH})_{10} \cdot 8 (\text{H}_2\text{O})$.a Structures of a) apatite $\text{Ca}_5(\text{PO}_4)_3(\text{OH}, \text{F}, \text{Cl})$, b) barite BaSO_4 .**Crystal chemistry of silicates.**

Silicates dominate the composition of the Earth's crust and mantle. Crystal chemistry of silicates is a particularly fascinating subject, because the variety of structures of silicates is almost unlimited. This is due to a combination of two factors:

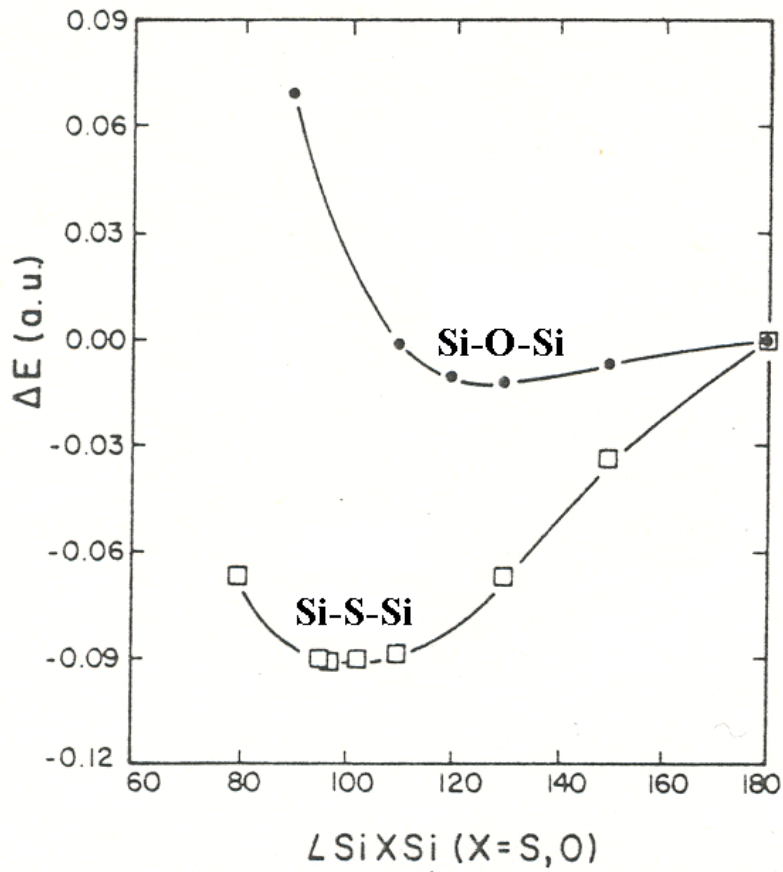
1) silicate tetrahedra $[\text{SiO}_4]$ can polymerise, forming polyanions – in the form of chains, sheets, and frameworks,

2) silicate polyanions are incredibly flexible and can easily adjust to the cations – hence the enormous diversity of silicate polyanions (a few hundreds are known) and silicate structure types (many hundreds).

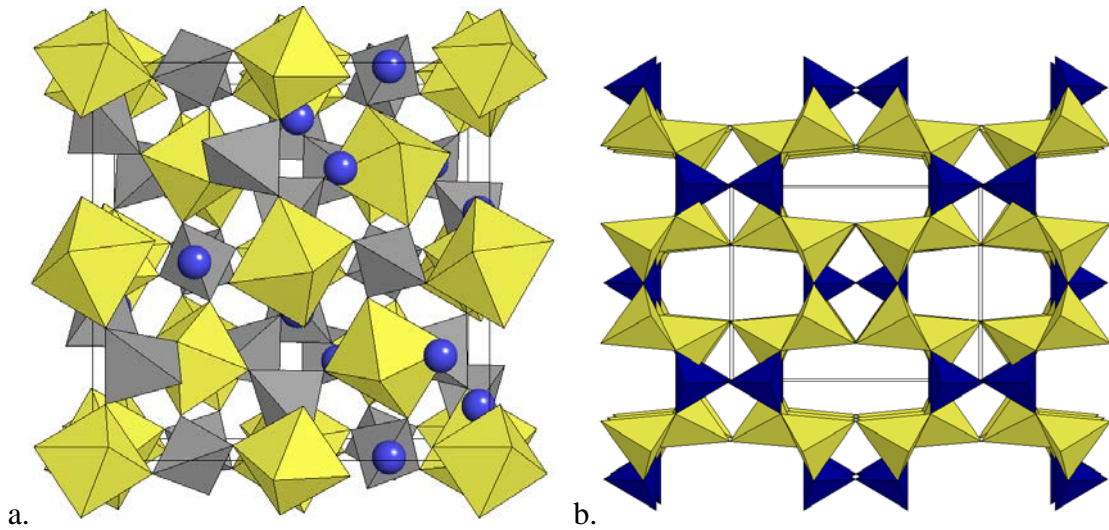
The ability of silicate tetrahedra to polymerise is remarkable, especially compared to sulphates and phosphates, in which the anion tetrahedra $[\text{PO}_4]$ and $[\text{SO}_4]$ almost never polymerise. Borates, on the contrary, also have a huge variety of polyanions. Why? The answer, as we have seen above, is given by Pauling's second rule, from which it follows that at most two SiO_4 -tetrahedra can share a particular corner. Three silicate tetrahedra having a common O-atom are forbidden by this rule and are never observed. Sometimes the tetrahedra have no common vertices with each other (as it happens in orthosilicates) – in this case other cations must satisfy the balance of valence strengths. Pauling's rules were originally formulated for ionic crystals (because for ionics they have a more or less transparent explanation), but afterwards it was realised that they are perfectly valid for significantly covalent crystals as well. Metallic and almost entirely covalent crystals require different approaches for the explanation of their structures.

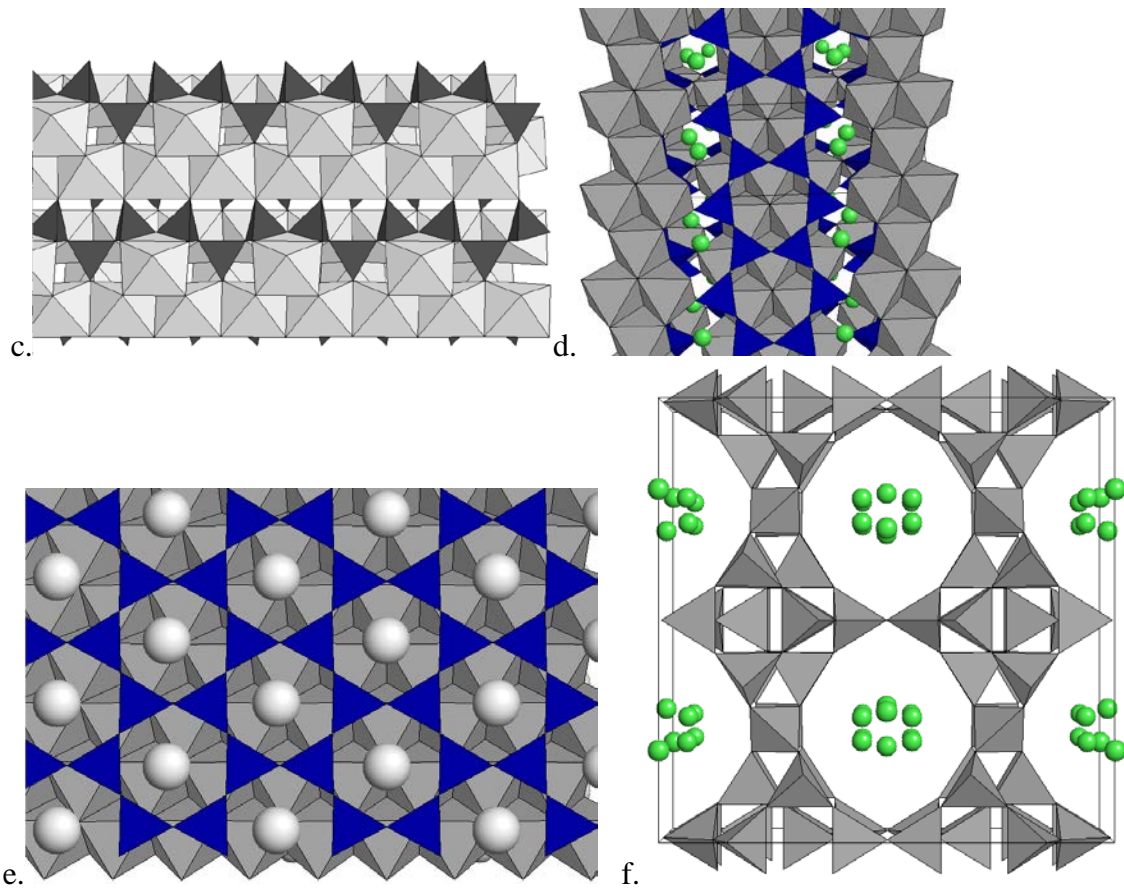
Now let us discuss the second major structural feature of silicates – the remarkable flexibility of silicate polyanions. The Si-O bonds are very rigid, so at first the idea that silicate polyanions adjust themselves to the cations looked strange when initially proposed by a Russian crystallographer N.V. Belov. Eventually it proved to be the only explanation of the structural features of silicates. According to Belov, silicate polyanions are formed when a large cation is present – it would be difficult for a single tetrahedron to grip the large atom. Larger polyanions, on the contrary, can 'prepare' a cavity of the necessary size for any cation, however large. This is particularly clear in zeolite minerals or feldspars, where there are large cations such as Na^+ , K^+ , Ca^{2+} , Sr^{2+} , etc. in the large cavities of the aluminosilicate framework. Silicate polyanions also adjust themselves to the cation motifs – e.g., to the layers of cation octahedra in micas – parameters of the silicate sheets in micas are completely controlled by the dimensions of the octahedral layer.

The incredible flexibility of the silicate polyanions comes from the flexible Si-O-Si angles: as quantum-mechanical calculations of G.V. Gibbs and co-workers (1980s-1990s) have shown, there is almost no energy cost associated with changing this angle between 120° and 180° . These calculations gave a clear rationalisation to Belov's observation, and allow us to understand many fundamental features of silicate minerals – their structures, dynamics, behaviour under pressure, and phase transitions.



Energy change due to the change of Si-O-Si angle in silicates (and Si-S-Si angle in analogous sulphur-containing materials). One can see that the energy is almost insensitive to the Si-O-Si angle. (Gibbs et al., series of works in 1980-s).





Some silicate crystal structures: a) Garnets $A^{2+}_3B^{3+}_2[SiO_4]_3$ (A=Ca, Mg, Fe; B=Al, Fe, Cr) (orthosilicate, i.e. with isolated silicate tetrahedra),
 b) Hemimorphite $Zn_4Si_2O_7(OH)_2 \cdot (H_2O)$ (diorthosilicate, i.e. with paired tetrahedra),
 c) Wollastonite $CaSiO_3$ (chain silicate),
 d) Amphibole (chain silicate) $A_{0-1}B_2Y_5[Si_8O_{22}](OH,F)_2$ [A=Ca, Na, K; B=Ca, Fe, Li, Mg; Y=Al, Cr, Fe, Mg]
 e) Mica (sheet silicate) $AB_{2-3}[Si_4O_{10}](OH,F)_2$ [A=K, Na; B=Al, Cr, Fe, Li, Mg]
 f) Zeolite stilbite $NaCa_4[Al_8Si_{28}O_{72}] \cdot 30(H_2O)$ (framework silicate).

Orthosilicates	Diorthosilicates	Ring Silicates	Chain silicates	Sheet Silicates	Framework silicates
Zircon	Hemimorphite	Beryl	Pyroxenes	Micas	Feldspars
Garnets	Thortweeite	Benitoite	Pyroxenoids	Talc	Zeolites
Olivine	Wadsleyite		Amphiboles	Chloritoids	
Ringwoodite			Biopyriboles	Clays	
Kyanite, andalusite, (sillimanite)					

The degree of polymerization of the silicate anions depends on the concentration of SiO_2 in the system – the more silica is present, the greater extent of polymerization. Below's principle implies that large cations (Na^+ , K^+ , Ca^{2+} , Sr^{2+} , Ba^{2+} , Pb^{2+} , ...) will be present in such highly polymerized

silicates. The two trends happen at the same time during magmatic crystallization: it turns out that orthosilicates usually have very high melting temperatures, and the melting temperature goes down with the increase of degree of polymerization. Therefore, orthosilicates containing smaller cations and having higher melting temperatures will crystallize first. Such silicates (e.g., olivine) are the dominant minerals of the upper mantle and of mafic/ultramafic rocks. After their crystallization magma becomes more enriched in SiO_2 and in large cations (which are “incompatible” in mantle minerals and thus prefer to stay in the melt), and on decreasing temperature more and more polymerized silicates crystallize – pyroxenes, amphiboles, micas, feldspars, quartz. Studies of magmatic crystallization and mineral reactions (occurring between the already crystallized minerals and silica-enriched melts) have resulted in the so called Bowen reaction series, which has the form of a “fork” with two branches, one starting with olivine and one beginning from Ca-feldspar anorthite.

Bowen's Reaction Series

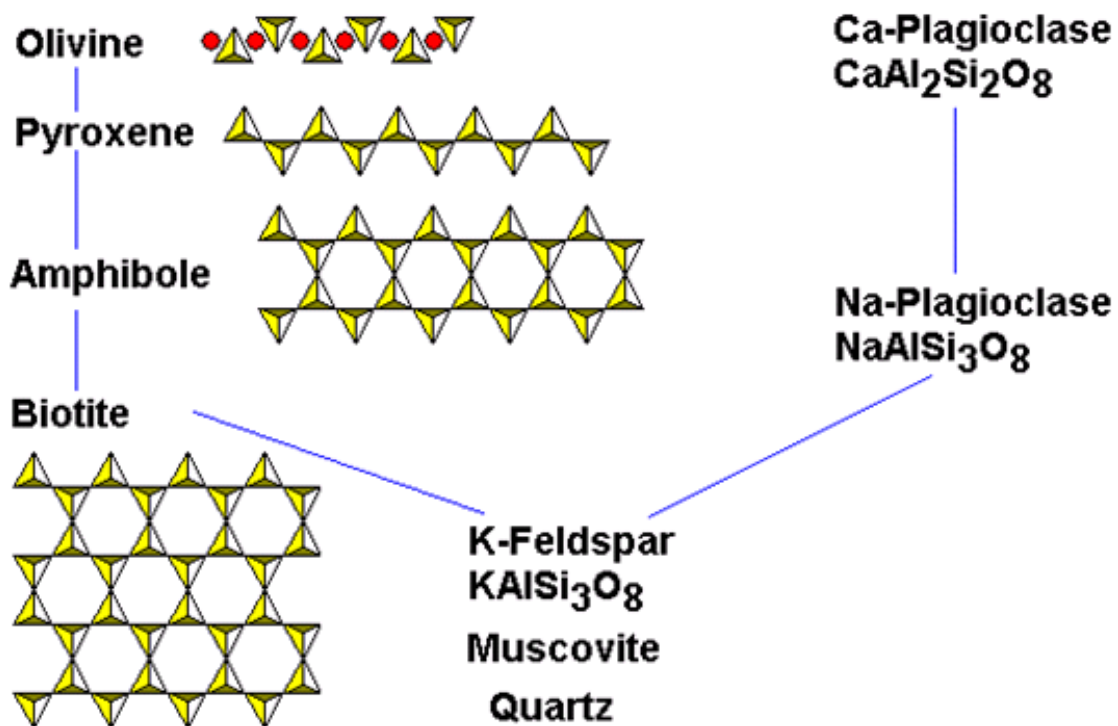


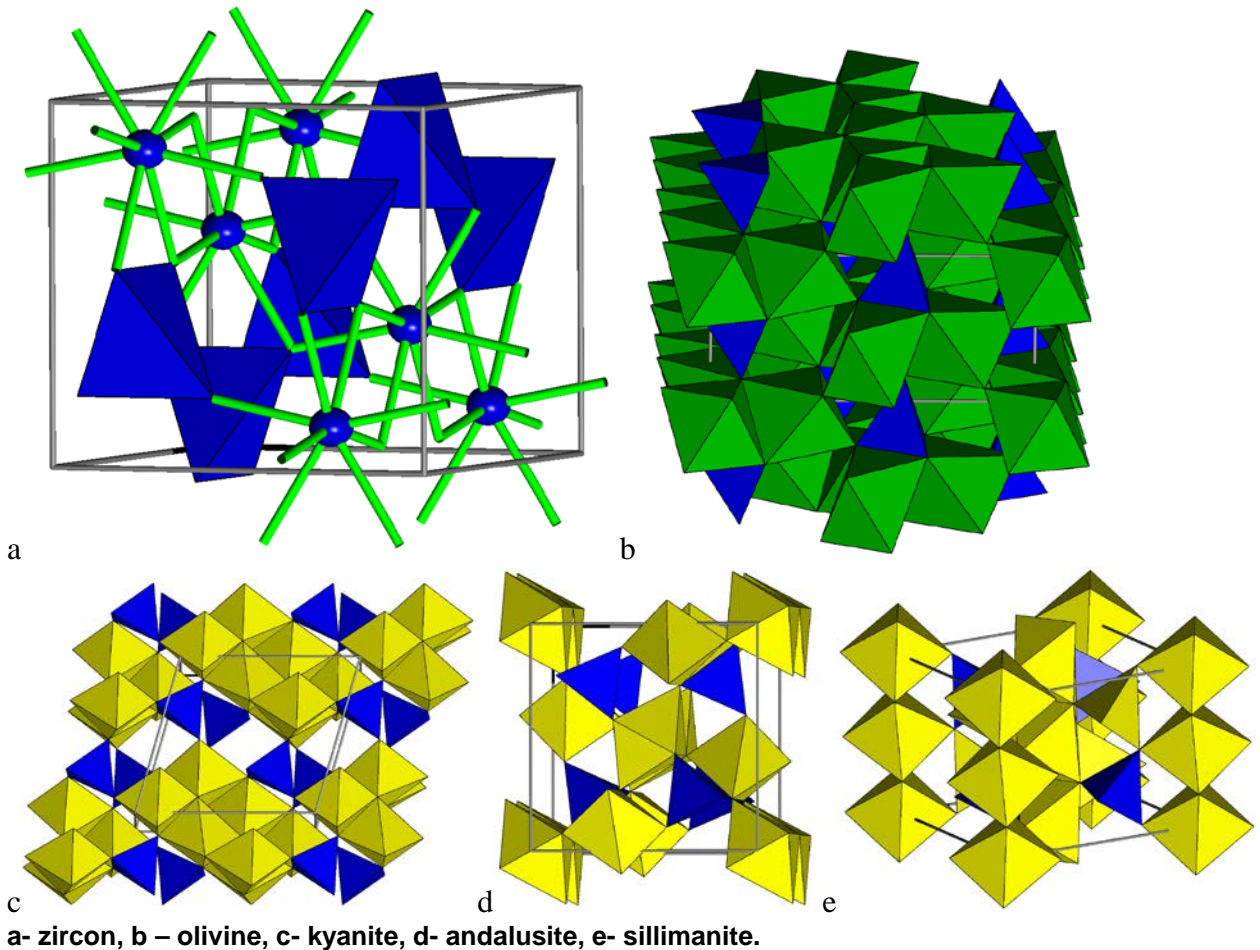
Illustration of the Bowen Reaction Series (figure courtesy of S. Dutch).

At high pressure, crystal chemistry of silicates changes in that it becomes based on six- and (very rarely) five-fold coordinated Si. High-pressure crystallography is the subject of next chapter; here we discuss structures of some of the most important silicate minerals.

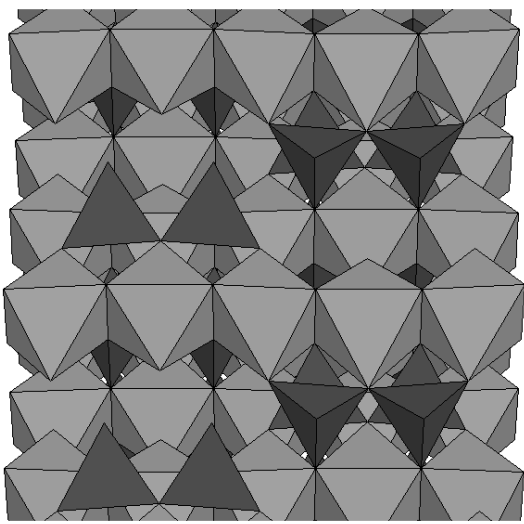
Orthosilicates: zircon ZrSiO_4 , garnets $\text{A}_3\text{B}_2(\text{SiO}_4)_3$ [A=Ca, Mg, Fe; B=Al, Fe, Cr], olivine and ringwoodite $(\text{Mg,Fe})_2\text{SiO}_4$, Al_2SiO_5 polymorphs. These minerals are rather dense and hard and have high melting temperatures; olivine even can be described as based on hexagonal close packing of oxygen atoms and ringwoodite has a cubic close packing. According to Belov’s principle, only relatively small cations can form orthosilicate structures – large cations prefer polysilicate constructions.

Olivine and garnet, along with chain silicates from the pyroxene group, are the main minerals of the Earth's upper mantle (24-410 km), whereas ringwoodite is the major mineral between 520-670 km depths. Ringwoodite has the spinel structure type.

Kyanite, andalusite and sillimanite are important metamorphic minerals, kyanite is stable in the upper parts of the Earth's mantle.

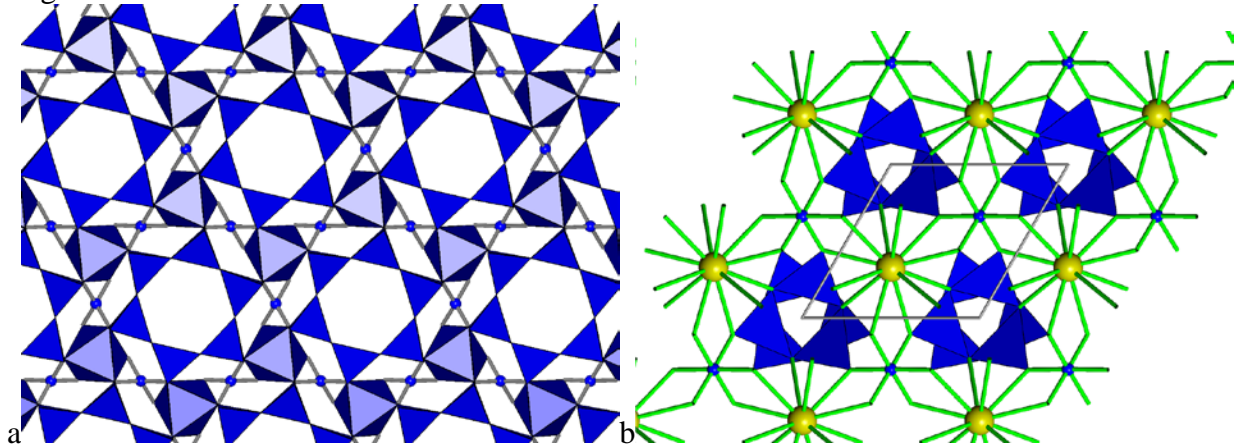


Diorthosilicates: wadsleyite. Only wadsleyite is a major Earth-forming mineral, it is the main phase of the Earth's mantle between 410 and 520 km depths. Its structure is related to spinel (can be considered as its polytype – see above) and is often called β -spinel. It has been found that wadsleyite structure can incorporate significant amounts of water (up to about 0.1%), thus making the Earth's transition zone a possible reservoir of water inside the Earth. Wadsleyite has been discovered in meteorites.



Crystal structure of wadsleyite.

Ring silicates: beryl $\text{Be}_3\text{Al}_2\text{Si}_6\text{O}_{18}$, benitoite $\text{BaTiSi}_3\text{O}_9$. SiO_4 -tetrahedra can be easily joined in a large possible variety of rings, from the smallest 3-membered to very large 12-membered or even larger.

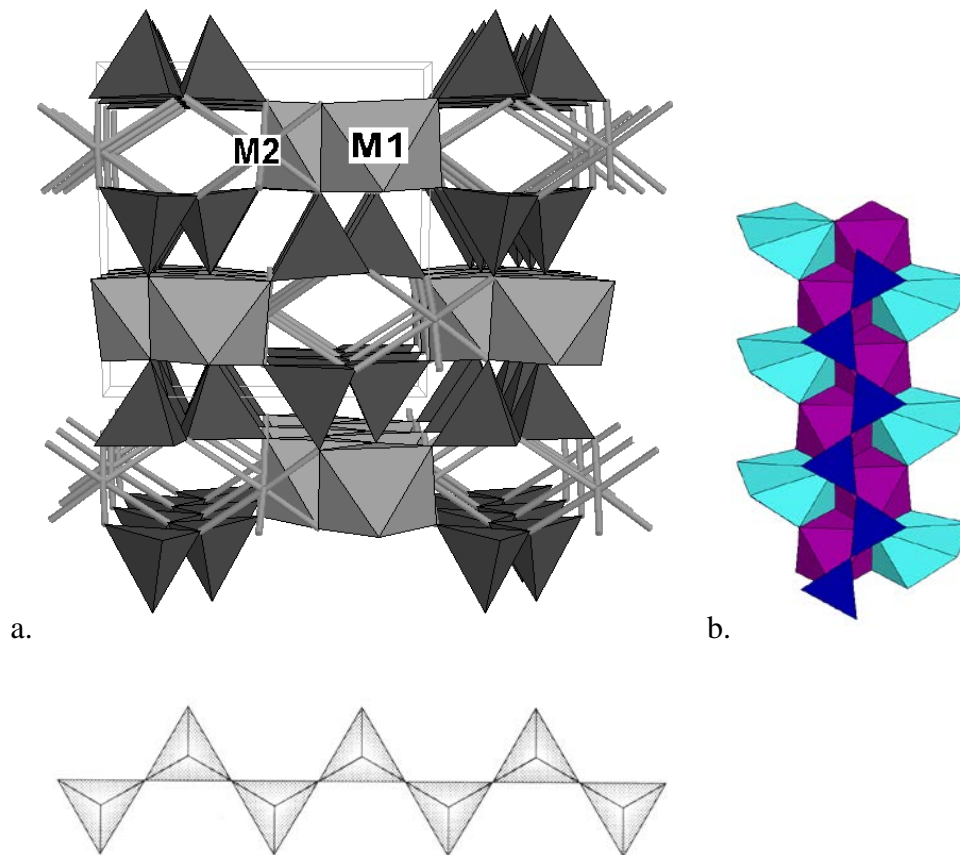


Structure of a) beryl, b) benitoite.

Chain silicates: pyroxenes, pyroxenoids, amphiboles, biopyriboles.

Pyroxenes will be discussed in a greater detail to provide an illustration of many general concepts that we have encountered before.

Pyroxenes $\text{AB}[\text{SiO}_3]_2$ [A=Ca, Fe, Li, Mg, Mn, Na; B= Al, Cr, Fe, Mg, Mn] - their structure is based on the cubic close packing of the oxygen ions – this explains the relatively high density of pyroxene minerals and pyroxene-bearing rocks, as well as their stability in the upper mantle of the Earth. The chemical formula is ABSi_2O_6 . The pyroxene structure contains silicate chains $[\text{SiO}_3]$ and two types of cation positions – M1 (octahedrally coordinated) and M2 (with an octahedral or 7-fold or 8-fold coordination). The M1 site is smaller and more regular; the M2 site therefore is more convenient for larger ions (because of the size of the site) and transition metal ions (which sometimes prefer distorted coordinations).



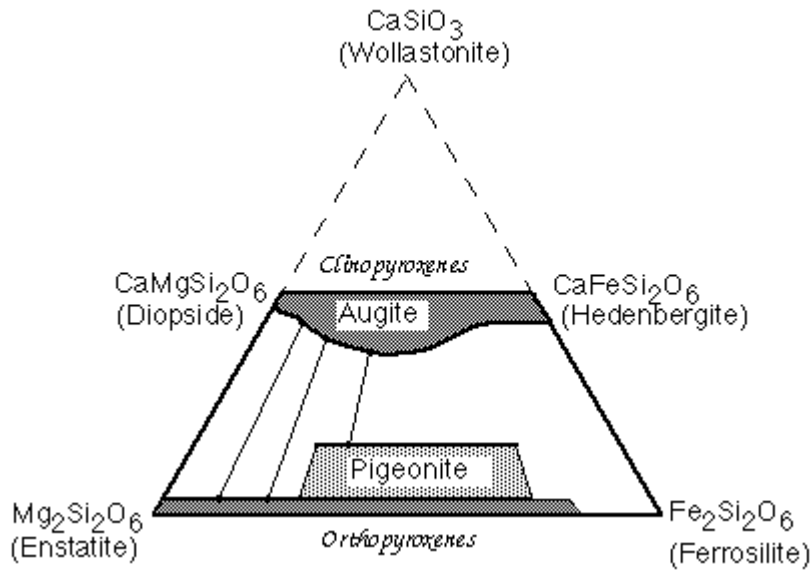
Pyroxene structure. a) Chains of silicate tetrahedra run perpendicular to the plane of the drawing. There are two types of cation sites in this structure – M1 (shown by octahedra) and M2 (for M2 only bonds to oxygens are shown). b) View of the silicate chain (blue). *Purple octahedra* M1 positions, *turquoise irregular polyhedra* M2 positions. c) Single SiO_3 chain.

The following pyroxenes are of importance – either as abundant rock- and Earth-forming minerals, or (spodumene) as industrially important materials:

Enstatite MgSiO_3
 Ferrosilite FeSiO_3
 Diopside $\text{CaMgSi}_2\text{O}_6$
 Hedenbergite $\text{CaFe}^{+2}\text{Si}_2\text{O}_6$
 Aegirine $\text{NaFe}^{+3}\text{Si}_2\text{O}_6$
 Jadeite $\text{NaAlSi}_2\text{O}_6$
 Spodumene $\text{LiAlSi}_2\text{O}_6$

Often, a distinction is drawn between clinopyroxenes (monoclinic) and orthopyroxenes (orthorhombic). Solid solutions are very common within (and much less between) these families.

The Pyroxene Quadrilateral

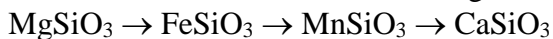


On slow cooling we get exsolution of cpx from opx and vice versa. This can proceed in several stages in pigeonites and produces lamellar structures. Careful study of exsolution phenomena in pyroxenes (by X-ray or transmission microscope methods) has the potential to yield a great deal of information about the thermal histories of exsolved pyroxenes.

Pyroxenes can adopt many different space groups depending on cation sizes, silicate chain configuration, and possible ordering of the cations. The pressure-induced $C2/c$ - $Pbca$ transition in $(Mg,Fe)SiO_3$ pyroxenes (which are very abundant in the Earth's upper mantle) at ~ 7 GPa is thought to be responsible for the seismic discontinuity at the 220 km depth. This is one of a number of impressive examples of the link between crystallography and geophysics, between microscopic structure and macroscopic and even global behaviour and properties of materials.

There is a size limit for M-cations in pyroxenes. One of such criteria is simply given by the ionic sizes necessary to form the required coordination polyhedra – in pyroxenes, octahedral coordination for M1 cations and 6-8-fold coordination for M2. Magnus-Goldschmidt rules require the ratio of ionic radii of the cation and anion to be between 0.414 and 0.732 for the cation to have an octahedral coordination, and between 0.732 and 1 to be 8-coordinated. With a table of ionic radii at hand, we can immediately say that Al^{3+} , Mg^{2+} , Fe^{2+} and Fe^{3+} would be able to adopt the octahedral coordination, while Si^{4+} is too small and K^+ is too big for that (Note, however, that anions are usually more compressible than cations, and at high pressures the cation/anion radius ratio increases and the cations generally adopt higher coordination numbers – e.g., Si^{4+} becomes 6-coordinate).

Let's look at a series with increasing radius of the M-cation in pyroxenes:

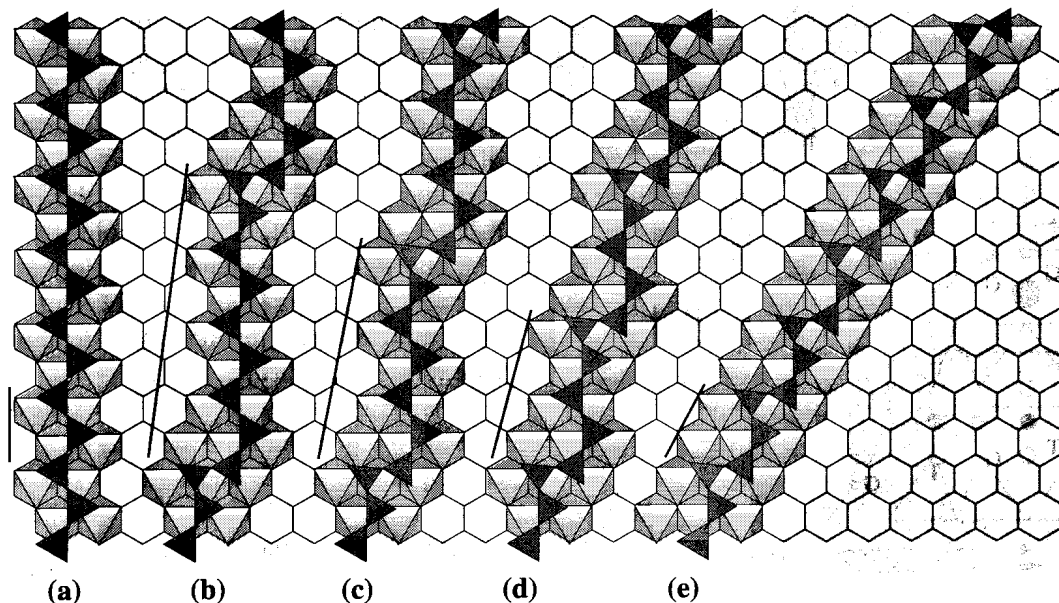


The former two minerals are pyroxenes, while the latter two are not. Pyroxmangite and rhodonite ($MnSiO_3$) and wollastonite ($CaSiO_3$) are pyroxenoids; their structures are similar to the pyroxene structure, but differ in the cation motif and configuration of the silicate chain, which has 3 tetrahedra per period in wollastonite, 5 in rhodonite, and 7 in pyroxmangite. This is a typical case of morphotropy.

Pyroxenoids. Because of the restriction on the size of the M1-cation, many potentially pyroxene compositions adopt one of a number of different, but related pyroxenoid structures. Here is a list of pyroxenoid minerals classified by the length (number of tetrahedra in a repeat unit) of the silicate chain:

Pyroxenoid subfamily3 chains supergroupWollastonite CaSiO_3 Bustamite $\text{CaMn}^{+2}\text{Si}_2\text{O}_6$ 4 chains groupSuzukiite BaVSi_2O_7 5 chains groupRhodonite MnSiO_3 6 chains supergroupChkalovite $\text{Na}_2\text{BeSi}_2\text{O}_6$ 7 chains groupPyroxferroite $(\text{Fe,Ca})\text{SiO}_3$ Pyroxmangite MnSiO_3 12 chains groupAlamosite PbSiO_3

There is a correlation between the M1-cation size and configuration of the silicate chain! As pressure increases, M1-O distances contract easier than the Si-O bonds, and it becomes easier to match them in a pyroxene structure. As pressure increases, MnSiO_3 adopts the following structures (Putnis, 1992): rhodonite (5 tetrahedra per period; room-pressure phase) -> pyroxmangite (7 tetrahedra per period; stable at ~4 GPa) -> clinopyroxene-like phase (2 tetrahedra per period; stable at > 6 GPa).

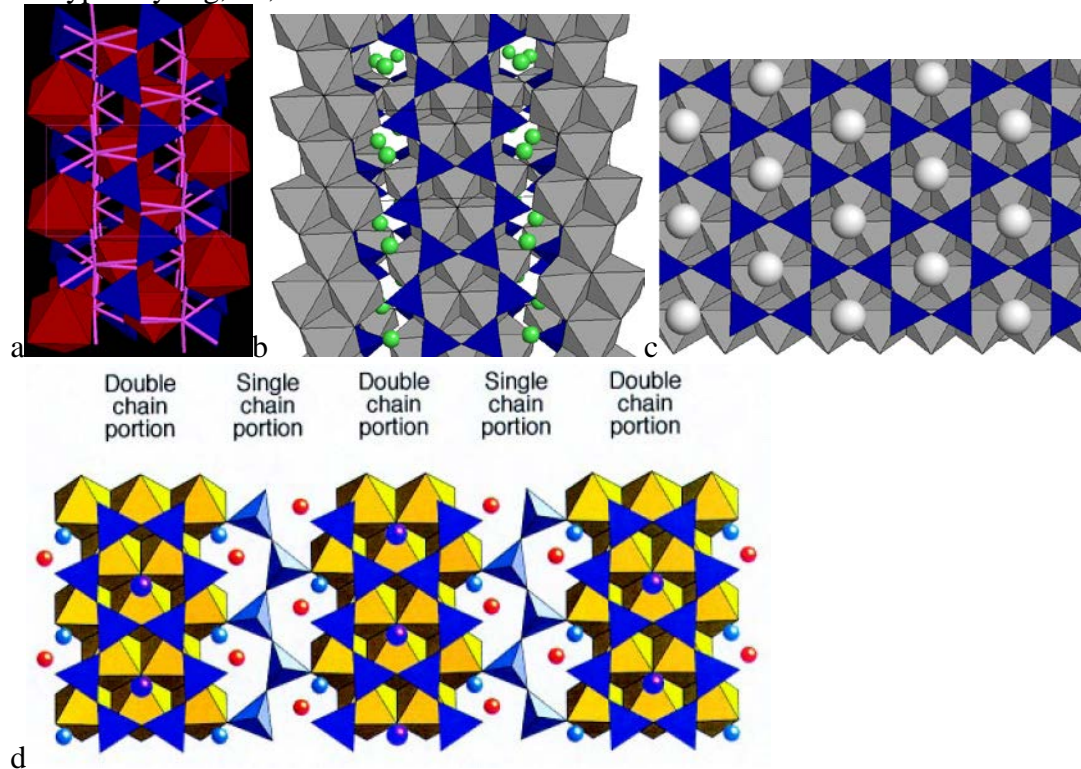


Relation between pyroxenes (a) and pyroxenoids (b-e): a) clinopyroxene, b) ferrosilite III, c) pyroxmangite, d) rhodonite, e) wollastonite. (after Liebau, 1985).

Amphiboles. This group of minerals is characterized by complex crystal structure containing double silicate chains. Amphiboles have wide variations of the chemical composition with the ubiquitous presence of solid solutions, the most important minerals are:

Actinolite-tremolite solid solutions $\text{Ca}_2(\text{Mg,Fe})_5\text{Si}_8\text{O}_{22}(\text{OH})_2$ Antophyllite - orthorhombic $(\text{Mg,Fe})_7\text{Si}_8\text{O}_{22}(\text{OH})_2$ Grunerite-cummingtonite solid solutions – monoclinic $(\text{Fe,Mg})_7\text{Si}_8\text{O}_{22}(\text{OH})_2$ Arfvedsonite $\text{Na}_3(\text{Fe,Mg})_4\text{FeSi}_8\text{O}_{22}(\text{OH})_2$

Biopyriboles. Look closely at the crystal structures of a pyroxene, an amphibole, and mica. Doubling the pyroxene silicate chain, we get the amphibole silicate chain. Sticking together such chains we get the mica silicate sheet. The same relations transform the octahedral cation motifs of these minerals. These relations become the basis of modular description of these structures. In principle, we can easily construct intermediate structures containing an arbitrary number of pyroxene chains in a band. These structures, forming a continuum between the pyroxene, amphibole, and mica structures types, are called biopyriboles (from ‘bio’ – biotite (mica), ‘pyr’ – pyroxene, and ‘bole’ – ‘amphibole’). The octahedral cations in pyroxenes, amphiboles, and micas are typically Mg, Fe, Al.

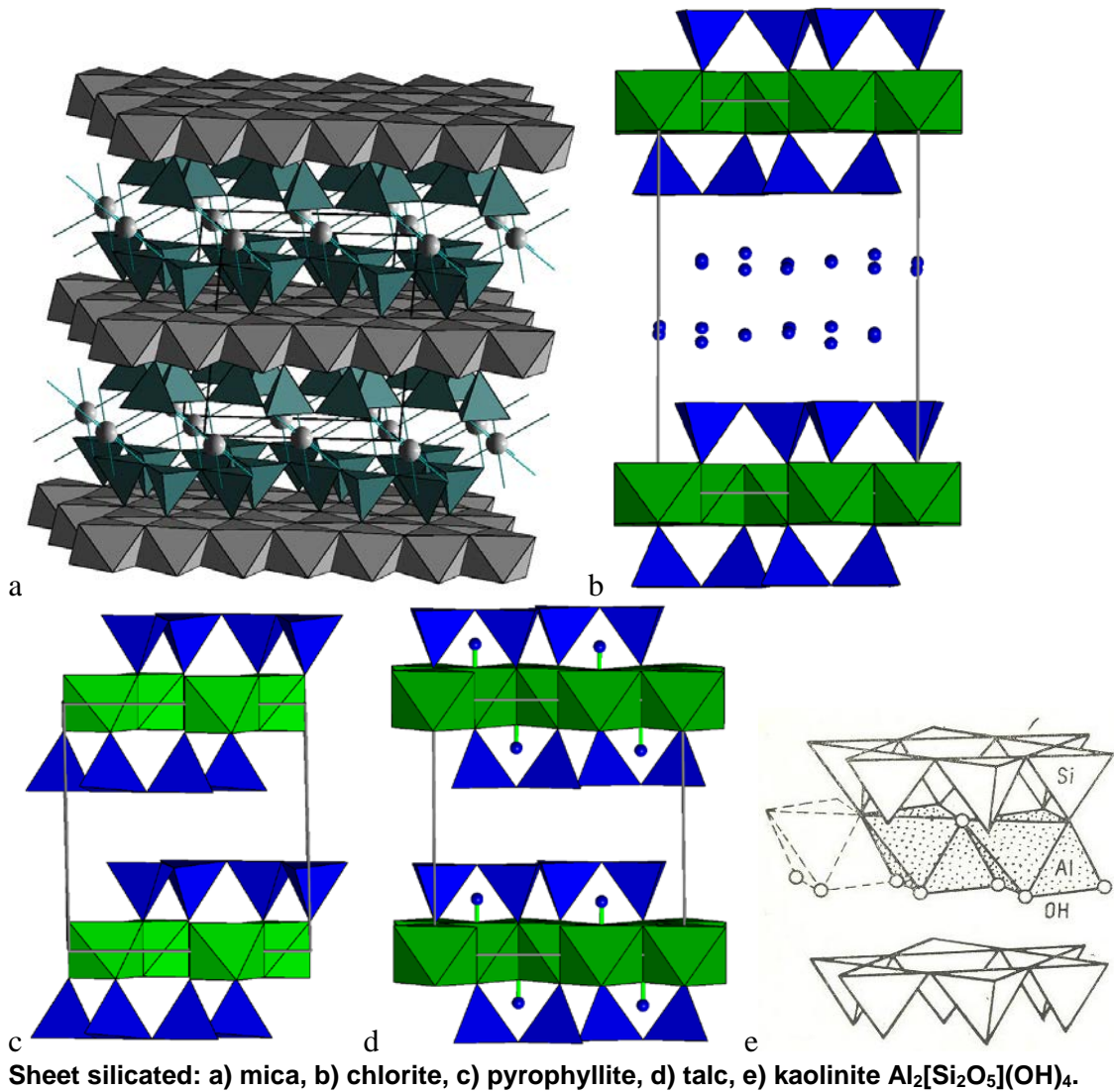


Structures of a) pyroxene, b) amphibole, c) mica, d) biopyribole. The biopyribole structure corresponds to the so called “21 clinopyribole” containing modules of pyroxene and amphibole structures (Yang et al., 2001).

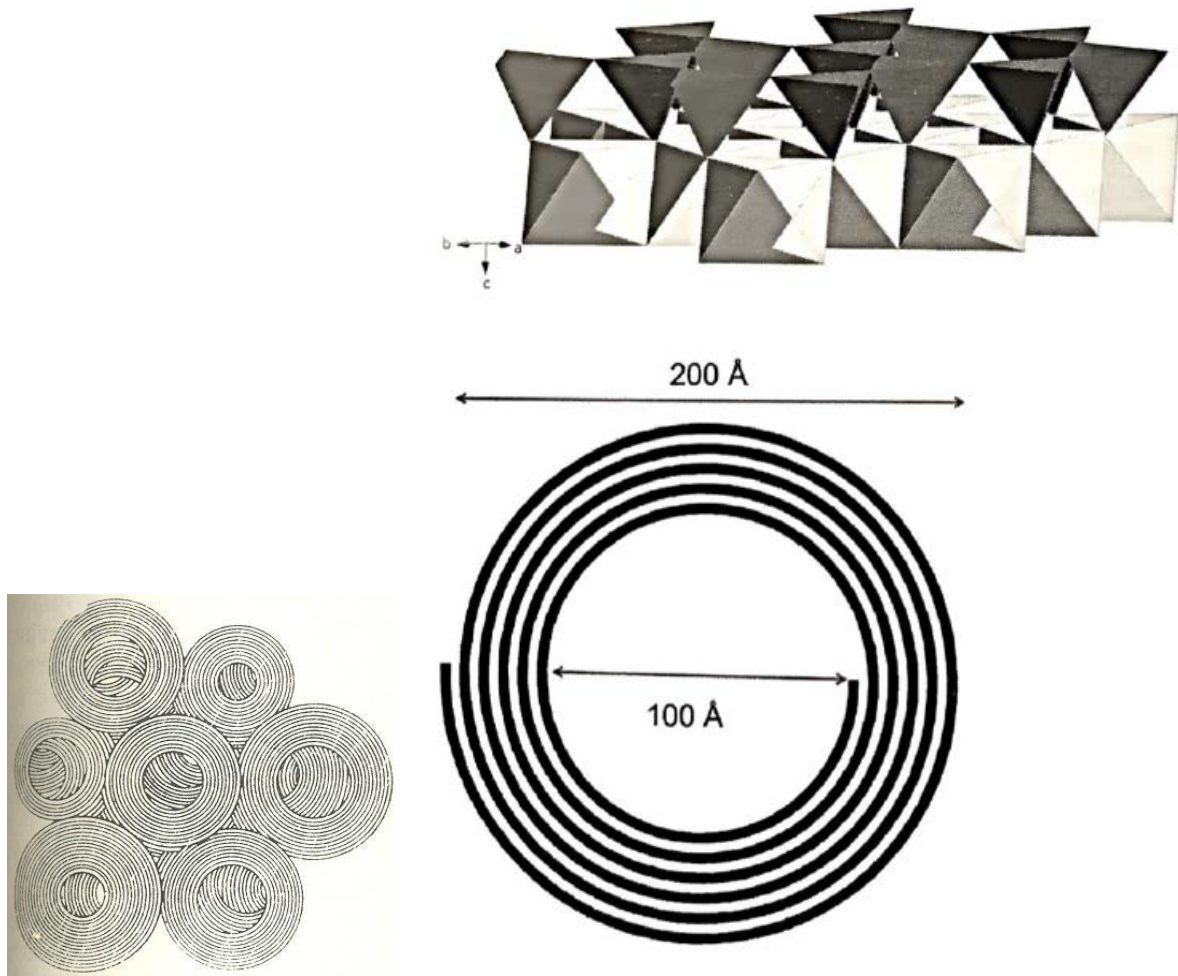
Sheet silicates: micas, clays, talc $Mg_3Si_4O_{10}(OH)_2$, pyrophyllite $Al_2Si_4O_{10}(OH)_2$, chlorites.

There is an enormous diversity of sheet silicates, to a large extent because in such structures one often has polytypes and hybrid mixed-layered structures.

Kaolinite is a prototype clay mineral. Pyrophyllite and talc have similar structures, except that octahedral cations are divalent in talc (Mg^{2+}) and trivalent in pyrophyllite (Al^{3+}). Chlorites have an additional layer of atoms between the “talc layers”: this can be represented as a brucite layer $Mg(OH)_2$.



An important issue is commensurability between the octahedral and tetrahedral sheets. When commensurability is not perfect, significant strains occur in the structure. In chrysotile-asbestos $\text{Mg}_3[\text{Si}_2\text{O}_5](\text{OH})_4$, because of these strains, the mineral itself is found in the form of thin tubes ~10 unit cells thick. Because of this, asbestos has a large surface area and can act as a catalyst for various reactions – hence its cancerogenic properties.



Chrysotile-asbestos.

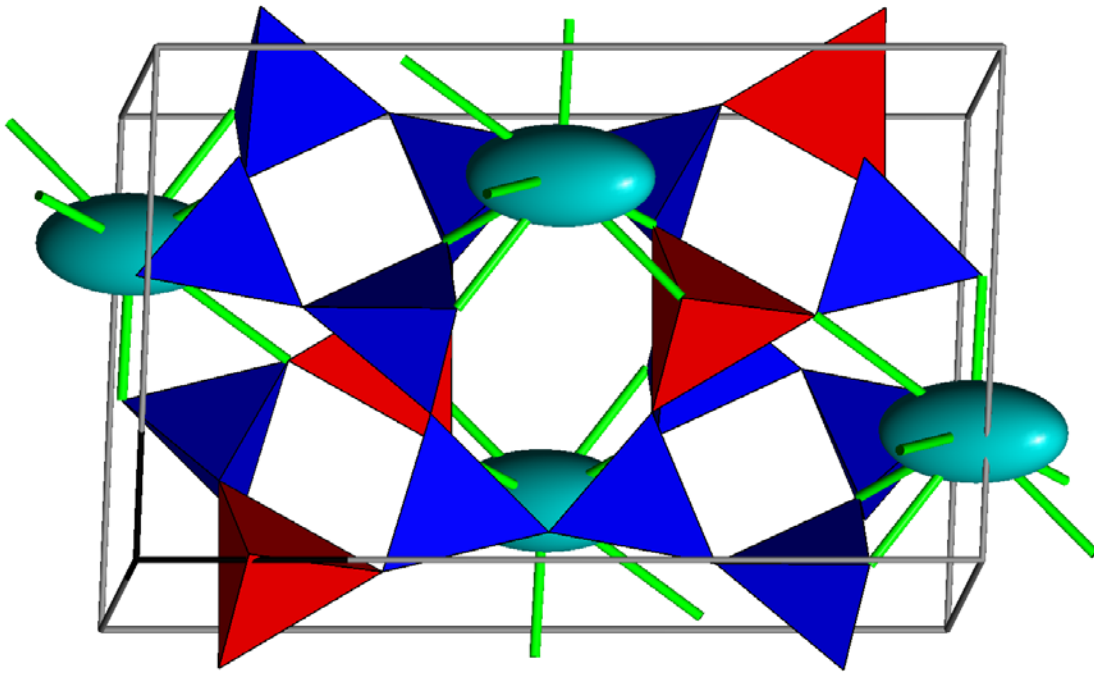
Framework silicates and aluminosilicates: feldspars, zeolites.

Feldspars:

Two main solid solution series exist in feldspars:

Plagioclases: albite $\text{NaAlSi}_3\text{O}_8$ - anorthite $\text{CaAl}_2\text{Si}_2\text{O}_8$.

Alkali feldspars: (microcline, orthoclase, sanidine) KAlSi_3O_8 – albite $\text{NaAlSi}_3\text{O}_8$.

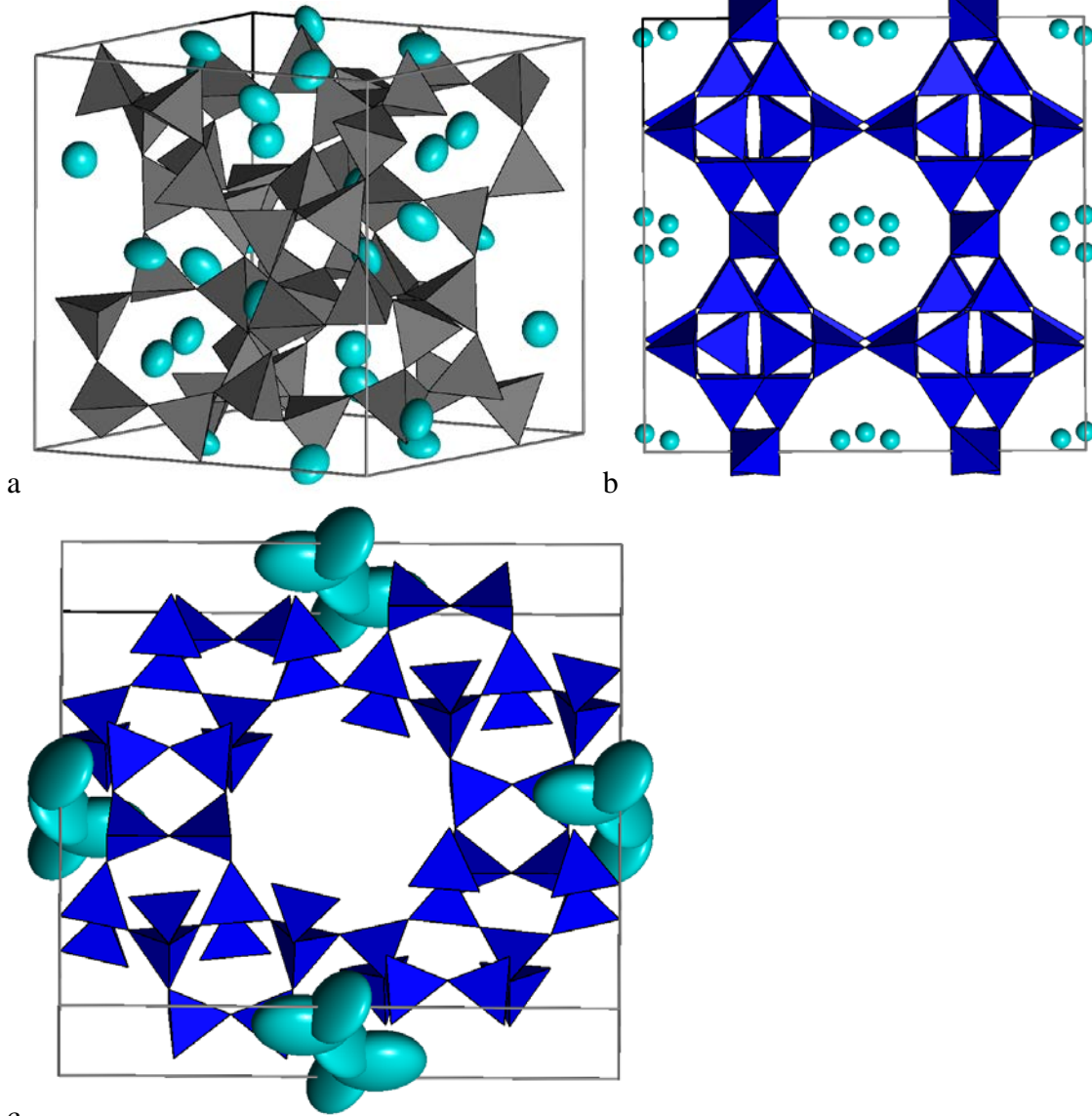


Structure of albite $\text{NaAlSi}_3\text{O}_8$. Green ellipsoids show the positions of Na atoms and their amplitudes of thermal vibrations.

At high temperatures, in many feldspars Al and Si are statistically distributed over tetrahedral framework-forming positions, but on slow cooling the distribution of these atoms becomes ordered, which leads to symmetry lowering. Fast cooling can keep the high-temperature disordered structure. Among K-feldspars, low-temperature triclinic microcline has nearly complete Al-Si ordering, monoclinic orthoclase has some positions preferred by Al and some by Si, but within each position the Al-Si distribution is statistical, and high-temperature sanidine has practically complete Al-Si disorder. The degree of Al-Si order is determined by the speed of cooling of magmatic rocks after their crystallization. Therefore, studying Al-Si ordering in feldspars can be used to determine the cooling history of rocks containing feldspars.

Zeolites:

Framework silicates, the structure of which contains large cages that can incorporate water molecules and/or large cations. Because of their peculiar structures, zeolites are widely used as materials for ion exchange, for water purification, catalysis, and hydrocarbon cracking. There is now a whole industry of zeolite synthesis. Which is more, scientists have learned to synthesise new zeolite structures with the needed cage sizes.



c
 a) analcime $\text{NaAl}(\text{Si}_2\text{O}_6) \cdot (\text{H}_2\text{O})$, b) stilbite $\text{NaCa}_4\text{Al}_8\text{Si}_{28}\text{O}_{72} \cdot 30(\text{H}_2\text{O})$, c) mordenite $(\text{Ca}, \text{Na}_2, \text{K}_2)\text{Al}_2\text{Si}_{10}\text{O}_{24} \cdot 7(\text{H}_2\text{O})$.

10. Crystallography at extreme conditions.

Units of pressure: The standard unit is 1 Pascal (Pa), which corresponds to a very low pressure. Often pressure is given in gigapascals (GPa), kilobars (kbar) or megabars (Mbar). 1 bar is equal to the standard atmospheric pressure, approximately 10^5 Pa.

1 bar = 1 atm $\approx 10^5$ Pa.

1 Mbar ≈ 100 GPa

1 GPa ≈ 10 kbar

Most of material inside the Earth experiences high pressures (up to 3.65 Mbar) and temperatures (up to 6000 K), and these extreme conditions of pressure and temperature greatly alter the structures and properties of materials.

Did you know that:

- 1) *At the lowest point of the oceanic floor (Mariana Trench, 11 km depth) pressure is > 1 kbar. Amazingly, some forms of life survive this pressure.*
- 2) *According to computer simulations, shock pressure exerted by the stone thrown by David into Goliath's head, should have been >1.5 kbar in order to break Goliath's head.*

There are several approaches to the study materials at such extreme conditions: 1) static compression (e.g., in diamond anvil cells pressures up to ~4 Mbar can be generated), 2) shock-wave compression (for very short times, pressures of ~100 Mbar can be achieved), 3) theoretical simulations (see Chapter 12).

Thermodynamics.

The Gibbs free energy:

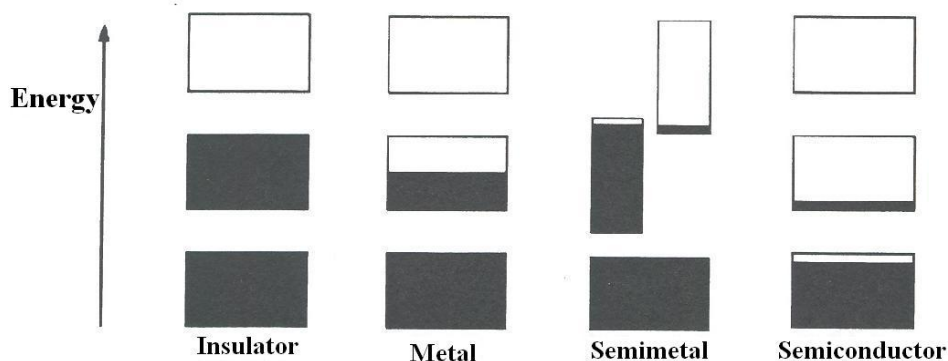
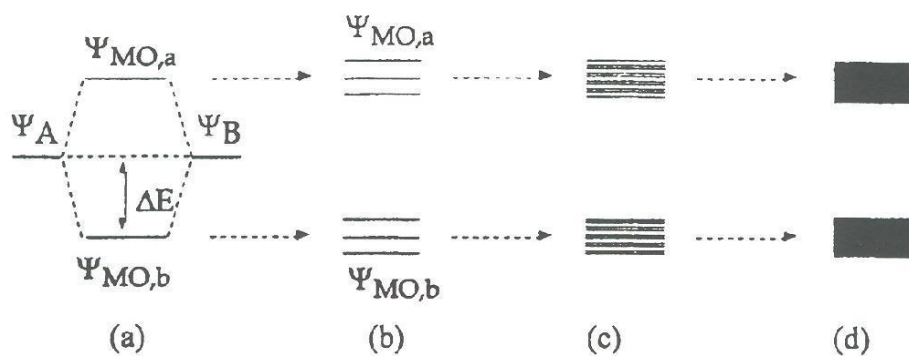
$$G = E + PV - TS$$

always attains the minimum in the equilibrium state. The increase of pressure always leads to a decrease of volume, and increase of temperature always raises the entropy. Phase transitions under pressure lead to denser phases, temperature-induced transitions lead to high-entropy (often structurally disordered) phases. The effect of temperature on crystals is usually not as dramatic as the effect of pressure, in other words the TS-term (even at the melting point) is often much smaller than the PV-term at high pressure.

Since it is the density that plays a crucial role in high-pressure stability, one expects that close-packed phases will appear under pressure. This expectation is usually correct, but there are many cases where unusual open structures are formed under pressure. Additionally, one expects higher coordination numbers to appear at higher pressures.

Electronic structure under pressure.

Density increase under pressure has important consequences for electronic structure. Consider a gas of non-interacting atoms from which a crystal is formed: Such a gas has a discrete set of energy levels. As the density increases, these energy levels shift and broaden, forming bands. The width of a band formed from atomic orbitals a and b characterises the strength of overlap between these orbitals, so as the density increases, bands progressively broaden. The bandwidth is also a measure of electron delocalisation: localised core electrons correspond to flat, practically zero-width (constant-energy), bands. Bands in ionic crystals are relatively "flat", i.e. the different orbitals constituting the band have nearly the same energies, as a result of which the band is narrow in energy, or (in physical jargon) "flat". In covalent crystals, significant degree of electron delocalisation between bonded atoms is responsible for rather wide bands. In metals, bands are even broader.



Genesis of band structures in solids.

It is to be expected that under pressure valence bands (occupied) and conduction bands (unoccupied) of a non-metal will broaden, and the band gap will decrease – eventually vanishing and producing a metallic state. Metallisation under pressure is a fundamental and universal phenomenon, important for understanding planets. The observation of strong magnetic fields in giant planets Jupiter and Saturn (which consist almost entirely of a H-He mixture) can be explained only if one assumes that liquid interiors of these planets are electrical conductors (it is currents in these conducting liquids that generate planetary magnetic fields). Recent experiments showed that liquid H (and H-He mixtures) become metallic at pressures ~ 100 GPa and temperatures ~ 2000 K and, therefore, most of Jupiter is metallic.

The Earth's magnetic field is likewise generated by convective currents in the liquid outer core. Now it is well established that the core is made of Fe-rich alloys, but W.H. Ramsey has conjectured in 1949 that it is possible that the core consists of the same materials as the mantle (e.g., oxides and silicates of Mg), but that at core pressures these materials become ultradense and metallic. It turned out, however, that pressures needed to metallise these materials are 10-100 times higher than those in the Earth's centre.

Among the most important effects of pressure are the increase of packing density of crystal structures (often leading to close packed structures and structures with higher coordination numbers), suppression of magnetism (for example, Fe in the core of the Earth is non-magnetic!), and changes in the electronic structure of the atoms (e.g., $s \rightarrow d$ transitions in K, Rb, Cs).

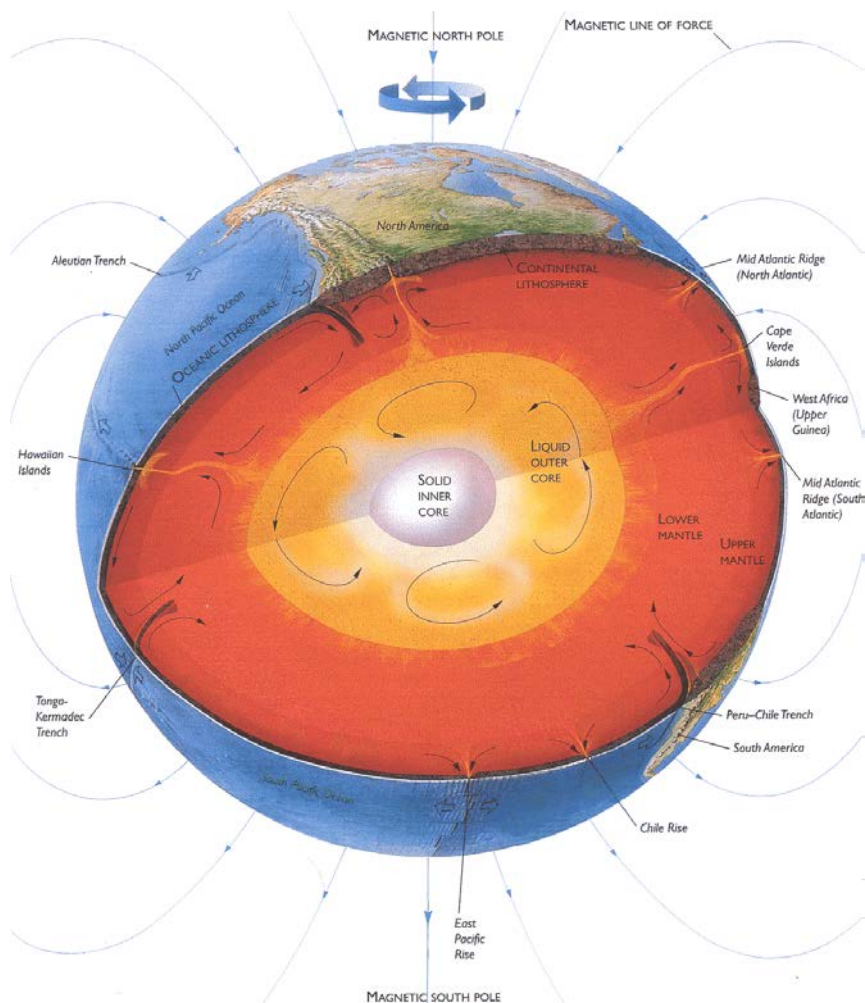
Introduction to the Earth's internal structure.

The Earth is one of the 9 planets in the Solar System. It is the largest of the 4 planets (Mercury, Venus, Earth, Mars) known as terrestrial (or rocky) planets; the other 5 planets are known as gas planets. Like any other terrestrial planet, the Earth 1) is believed to have a nearly chondritic composition, and 2) is deeply chemically differentiated (into the metallic Fe-rich and silicate-oxide fractions) and stratified (metallic Fe forms the core, while oxides and silicates form the mantle and crust).

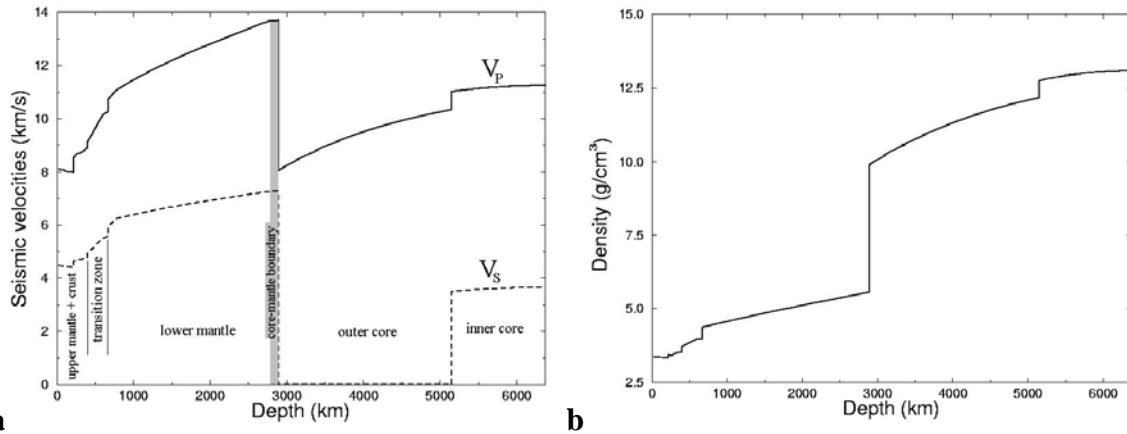
Estimates of elemental abundances (in atoms per 1 atom Si).

Element	The Universe	Whole Earth	Earth's Crust	Upper Mantle	Lower Mantle	Pyroclitic Homogeneous Mantle
O	20.10	3.73	2.9	3.63	3.63	3.68
Na	0.06	0.06	0.12	0.03	$2 \cdot 10^{-3}$	0.02
Mg	1.08	1.06	0.09	0.97	1.09	1.24
Al	0.08	0.09	0.36	0.17	0.06	0.12
Si	1	1	1	1	1	1
P	0.01	-	$4 \cdot 10^{-3}$	$6 \cdot 10^{-4}$	$4 \cdot 10^{-5}$	$4 \cdot 10^{-4}$
S	0.52	-	$8 \cdot 10^{-4}$	$6 \cdot 10^{-4}$	$5 \cdot 10^{-5}$	$2 \cdot 10^{-3}$
Ca	0.06	0.06	0.14	0.12	0.05	0.09
Cr	0.01	-	$1 \cdot 10^{-4}$	$5 \cdot 10^{-3}$	0.01	0.01
Fe	0.9	0.9	0.11	0.14	0.14	0.16
Ni	0.05	-	$3 \cdot 10^{-5}$	$3 \cdot 10^{-3}$	$4 \cdot 10^{-3}$	$3 \cdot 10^{-5}$

Further stratification of the planet is determined by structural transitions in the mantle and core minerals – these are responsible for the discontinuities of elastic properties, observed in seismological studies. Spherically averaged seismological models of the Earth (e.g., PREM – Preliminary Reference Earth Model), in view of the lack of direct sampling, comprise the central piece of information on the deep regions of the planet.



Scheme of the Earth's internal structure. (taken from Lamb S., Sington D. Earth story: the shaping of our world. London: BBC Books, 1999, 240 pp.)

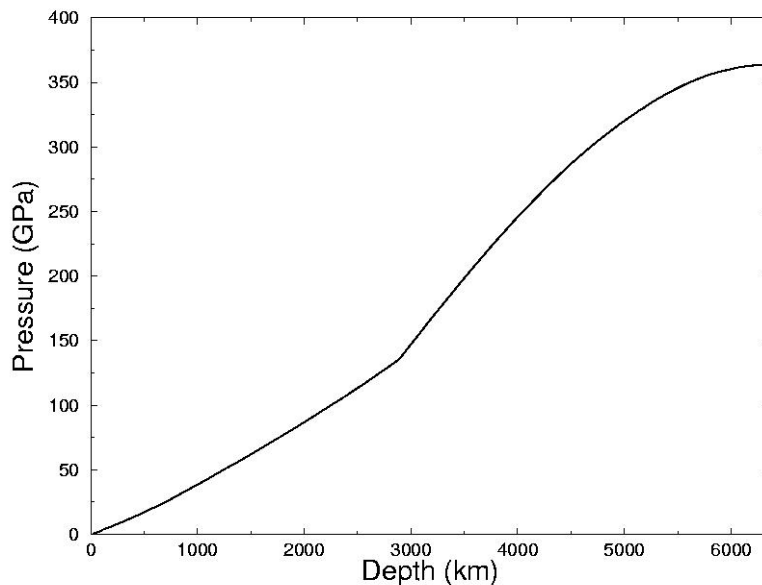


a **b**
PREM profiles: a) seismic wave velocities, b) density. Major regions of the Earth are specified. The core-mantle boundary region D' (grey shading) is the major seismic boundary in the Earth and has many anomalous and poorly understood properties.

Pressure distribution can be calculated using the following equation:

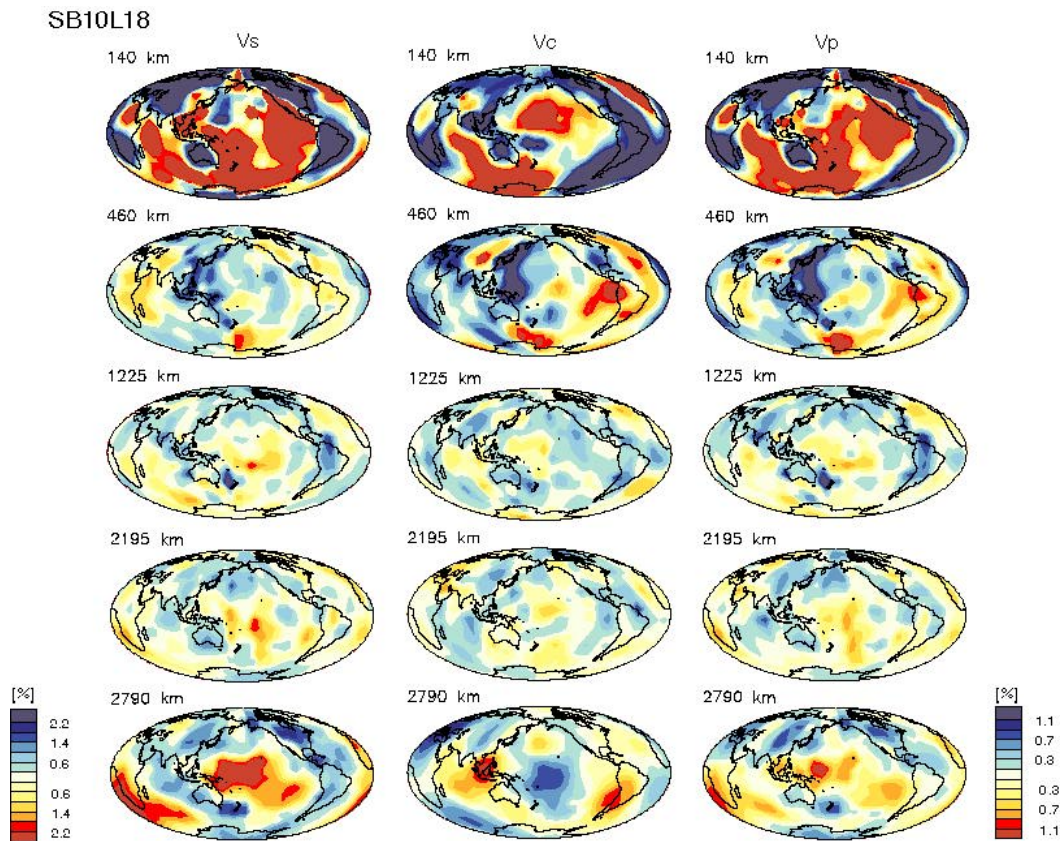
$$dp/dr = -4\pi G \rho r^2 \int_0^r \rho r^2 dr = -g\rho,$$

where G is the gravitational constant, r is the radius, and g is the acceleration due to gravity.



PREM pressure profile.

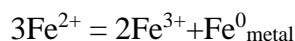
The energy balance of the Earth is known only very approximately, the main mechanism of the heat transport in the Earth is thermal convection. Convection of the liquid outer core also generates the magnetic field of the Earth, which shields the planet from the solar wind. Solid-state convection in the mantle is responsible for plate tectonics, and is the ultimate cause of the continental drift, earthquakes, and volcanism. Seismic tomography enables a visualisation of this convection and can in principle give information on the underlying temperature anomalies (Oganov et al., 2001).



Seismic tomography images of Masters et al. (2000). V_c is the bulk sound velocity, not directly observed, but easily obtained from the observable V_s and V_p and often convenient for analysis.

The core must be mainly made of Fe, with minor siderophile (particularly Ni) content. Its density, however, is too low compared to pure Fe at the core conditions (by ~6-10% in the outer core). This is explained by the presence of lighter alloying elements – S, Si, O. It was long believed that the phase of Fe stable at the inner core conditions is hcp-Fe. However, preliminary experiments show the possibility that the stable form of the (Fe,Ni) alloy in the inner core has the bcc structure. Previously, this was predicted by Belonoshko (2003) for pure Fe and by Vocadlo (2003) for Fe-Si and Fe-S alloys. From seismic observations it follows that the inner core is highly seismically anisotropic, with the fastest direction of seismic waves along the axis of the Earth's rotation. This anisotropy implies a high degree of crystal alignment, the cause of which is unknown. Currently, the composition and temperature of the core are still under debate. Perhaps the best estimates (Alfe et al., 2002) have the liquid outer core containing 10% Si+S and 8% O, and crystallizing from it solid inner core with 8.5% Si+S and 0.2% O. The temperature at the inner-outer core boundary is estimated to be 5500 K. The temperature of the core at the boundary with the mantle is ~4300 K.

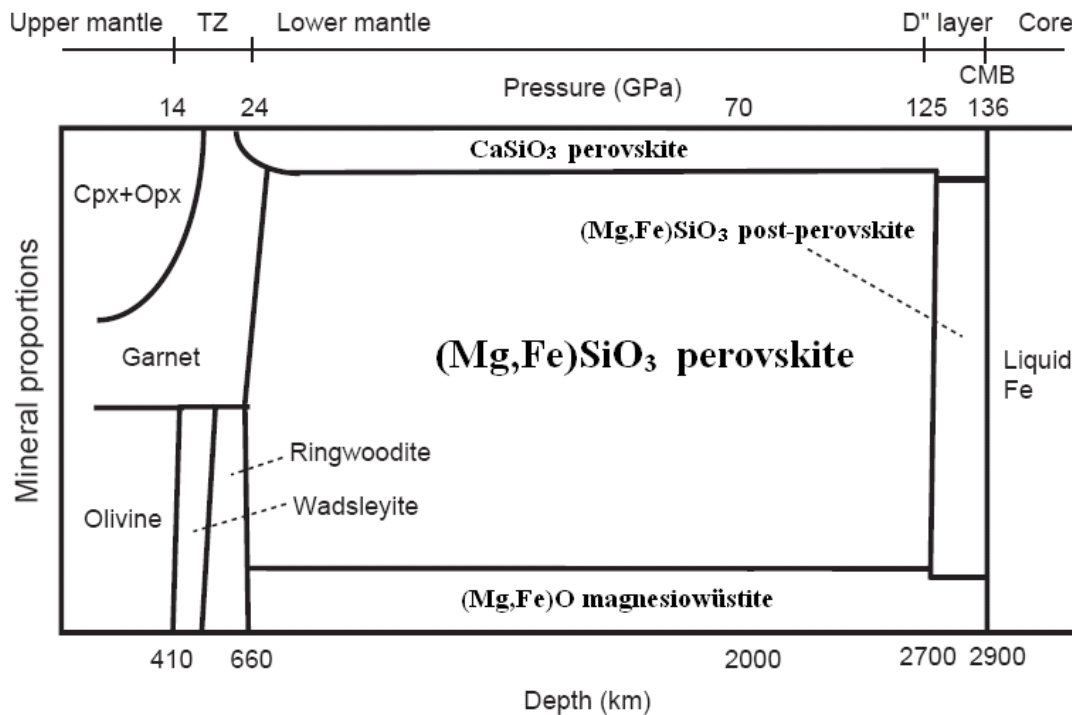
The Earth's mantle consists mainly of Mg-silicates, with ~10-15% of Mg^{2+} substituted by iron. In the upper mantle and transition zone we have high-spin Fe^{2+} , but in the lower mantle the picture changes dramatically: Fe^{2+} disproportionates producing Fe^{3+} impurities and free metallic Fe:



This reaction, first observed (Frost et al., 2004) and theoretically justified (Zhang & Oganov, 2006), is due to peculiarities of the perovskite and post-perovskite structures. Fe^{3+} impurities undergo at least partial transition from the high-spin to the low-spin state at conditions of the

lower mantle. Effects of such transitions on the physical properties of these silicate minerals are still not well understood.

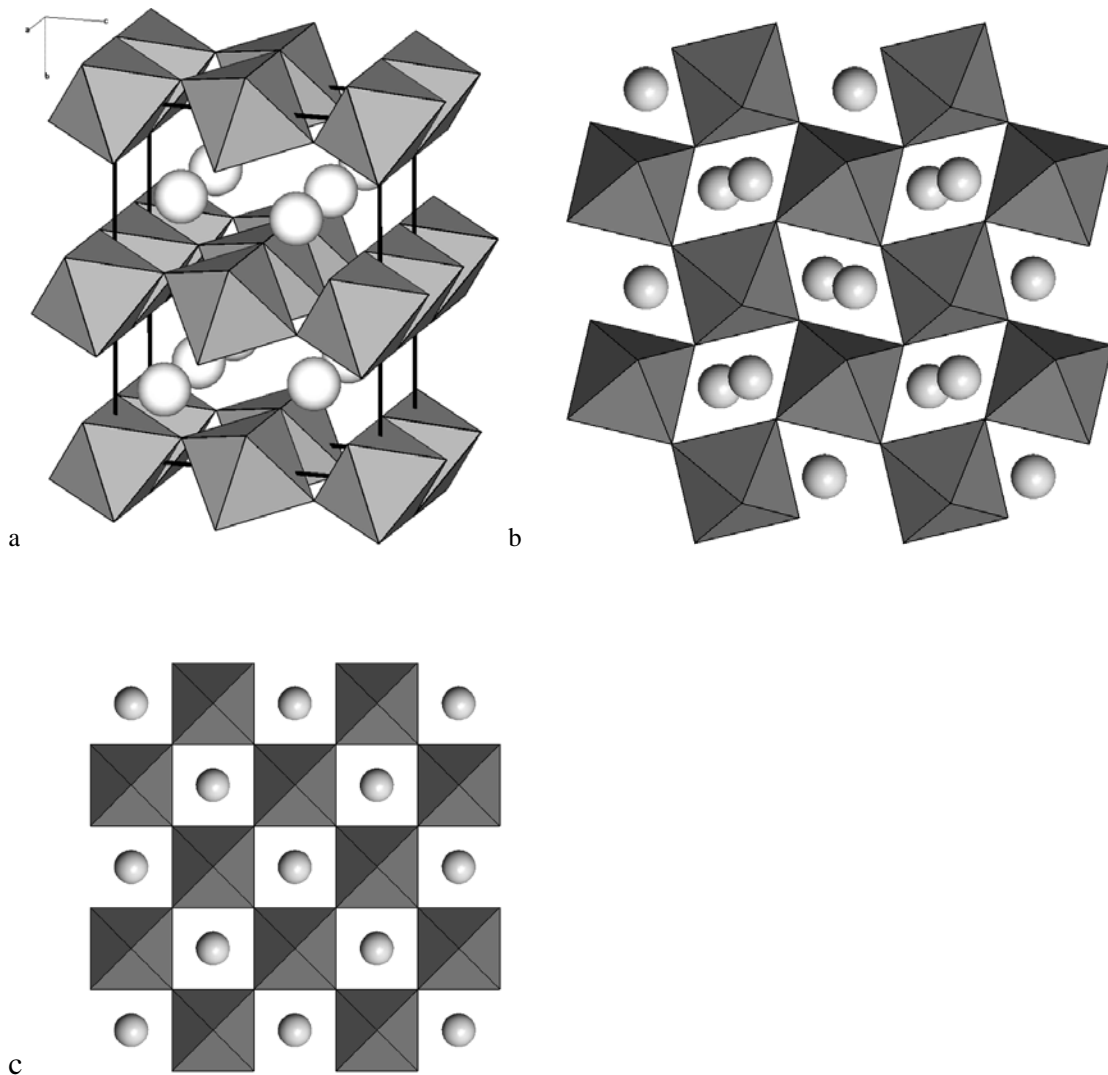
Phase transitions of Mg-silicates determine the seismic stratification within the mantle. Currently, it is believed that the lower mantle would consist of $(\text{Mg,Fe})\text{SiO}_3$ perovskite (~75 vol. %), magnesiowüstite $(\text{Mg,Fe})\text{O}$ (~20 vol. %), and CaSiO_3 perovskite (~5 vol. %).



Schematic phase relations in pyrolite (adapted from Ono & Oganov, 2005). Cpx and Opx ortho- and clinopyroxene, ILM is MgSiO_3 ilmenite (akimotoite), MW is magnesiowüstite $(\text{Mg,Fe})\text{O}$, 'Mg-perovskite' and 'Ca-perovskite' stand for MgSiO_3 and CaSiO_3 perovskites.

The electrical conductivity of the lower mantle is indeed very high ($\sim 10^0$ - 10^2 S/m); apart from partial melting it could be due to ionic diffusion in MgSiO_3 perovskite (O'Keefe & Bovin, 1979; Matsui & Price, 1991).

The core-mantle boundary region (called D'' layer) has many anomalous properties, which for many years could not be explained. The explanation came with the discovery of a new phase of MgSiO_3 (Oganov & Ono, 2004; see also Tages Anzeiger, 22 July 2004). This new phase has a layered CaIrO_3 -type structure. Its elastic anisotropy explains the seismic anisotropy of the D'' layer, and the phase transition itself explains the D'' discontinuity and the thickness of the D'' layer (on average, 150 km) as well as the variations of this thickness in different regions.



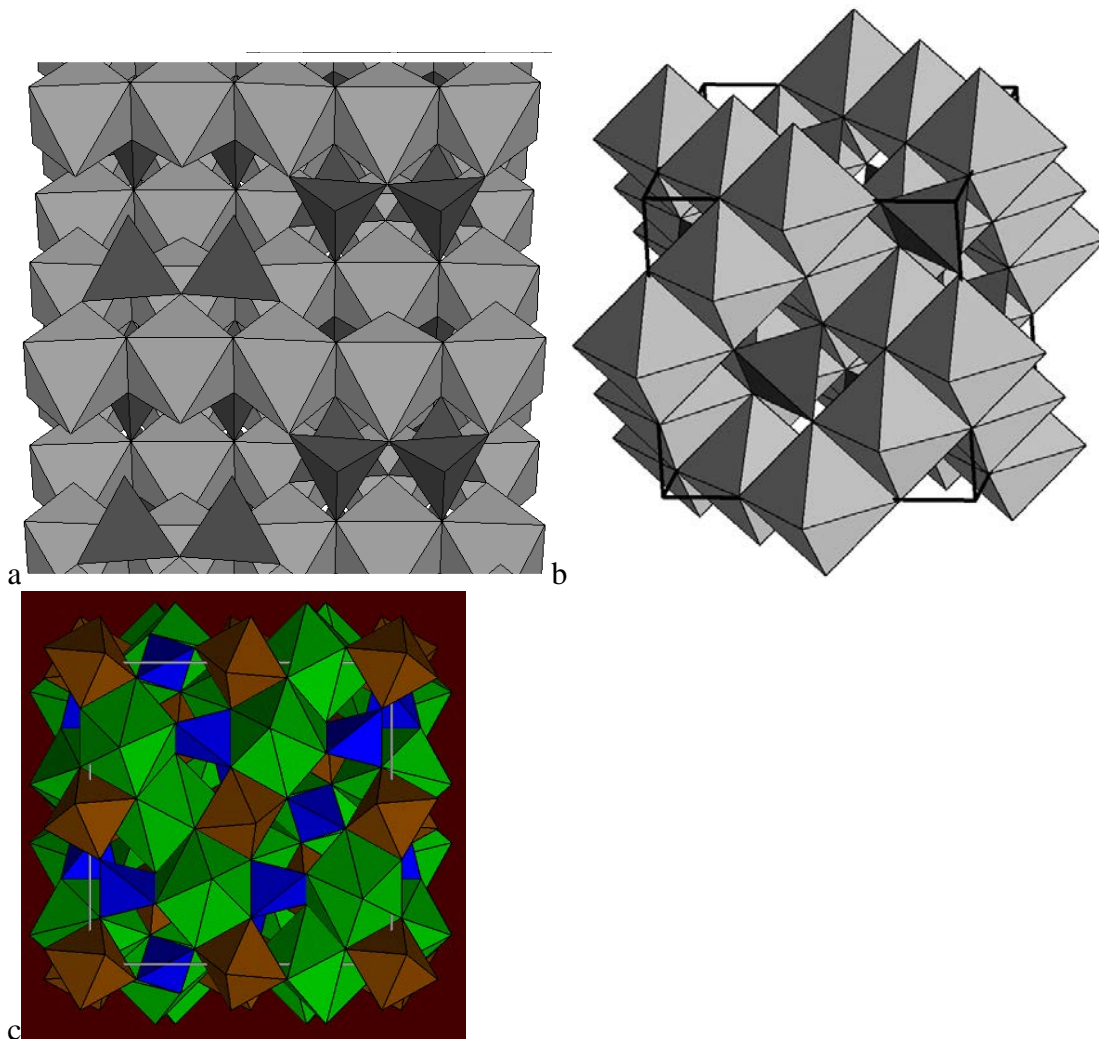
a) CalrO₃-type phase of MgSiO₃, b) perovskite-type phases of MgSiO₃. c) cubic perovskite structure of CaSiO₃ in Earth's lower mantle.

Knittle and Jeanloz (1991) found that there might be a chemical reaction between the core and mantle. They experimentally observed a reaction, which can be schematically written as follows:



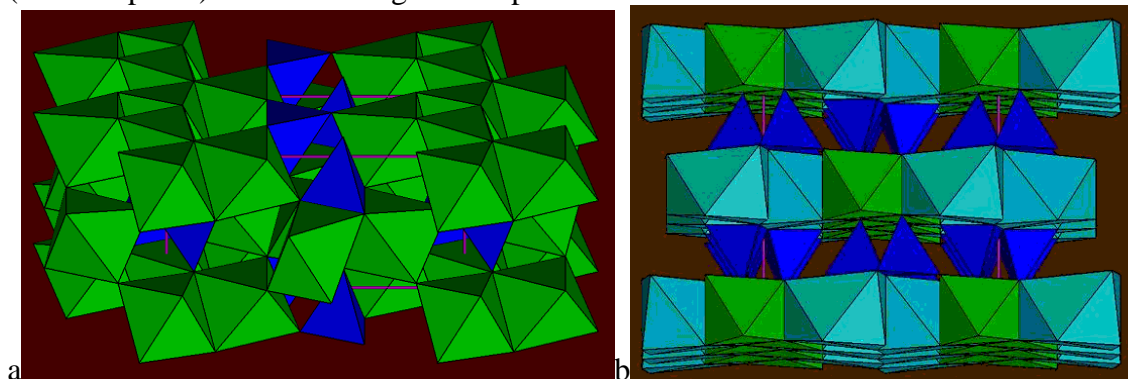
Our understanding of the mantle mineralogy can be greatly increased by studies of mantle inclusions – e.g., Harte et al. (1999) found several lower-mantle minerals (among others, they found MgSiO₃ inclusions with up to 10% Al₂O₃) in inclusions in diamonds. Most inclusions studied so far have upper-mantle or transition-zone origin, however.

The transition zone (410-660 km) is quite diverse mineralogically, and might possess exotic properties. This region can host large amounts of water: both wadsleyite and ringwoodite can contain up to 2-3 wt.% H₂O (see Fiquet, 2001 and references therein). It has also been suggested (Angel et al., 1996 and references therein) that unusual for inorganic compounds five-coordinate Si can play an important role in the transition zone, determining its transport properties.



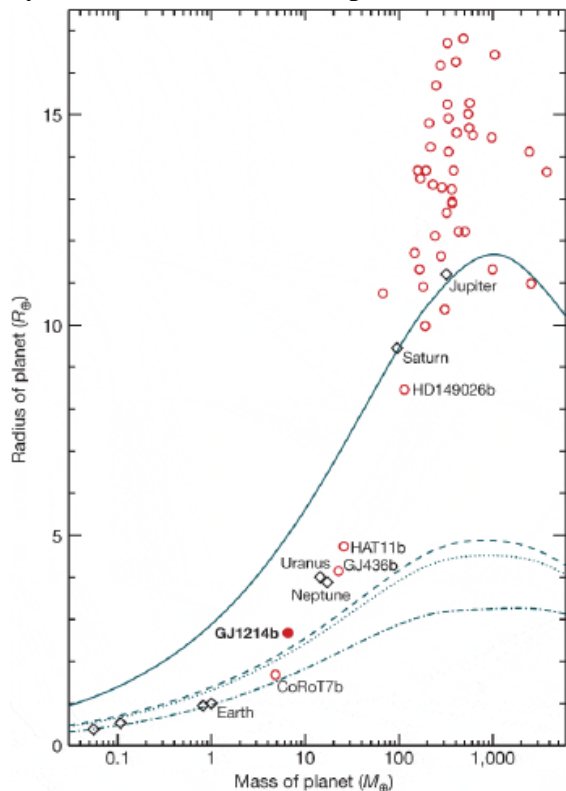
Transition zone minerals: a) wadsleyite, b) ringwoodite, c) garnet.

The upper mantle consists predominantly of olivine, garnet, and pyroxenes. There are four particularly important features of the upper mantle: 1) Ultralow velocity zone at variable depths, roughly between 50-100 km and 220 km (Anderson, 1989), 2) A seismic discontinuity (Lehmann discontinuity) at the base of the ultralow velocity zone, 220 km depth, 3) Strong elastic anisotropy above the 220 km depth, and 4) Strong compositional heterogeneity in the upper 150 km (see Ringwood, 1991). The Lehmann discontinuity is, possibly, due to the $Pbca-C2/c$ transition in pyroxenes (e.g. Mendelssohn & Price, 1997). The ultralow velocity zone is interpreted as a region of partial melting and low viscosity (asthenosphere) beneath the rigid lithosphere.



Upper mantle minerals: a) olivine, b) pyroxenes.

Planetary interiors. It is very interesting to study the structure of materials of other planets, especially giant planets Jupiter, Saturn, Uranus, Neptune, as well as planets outside the Solar System – the so-called exoplanets.

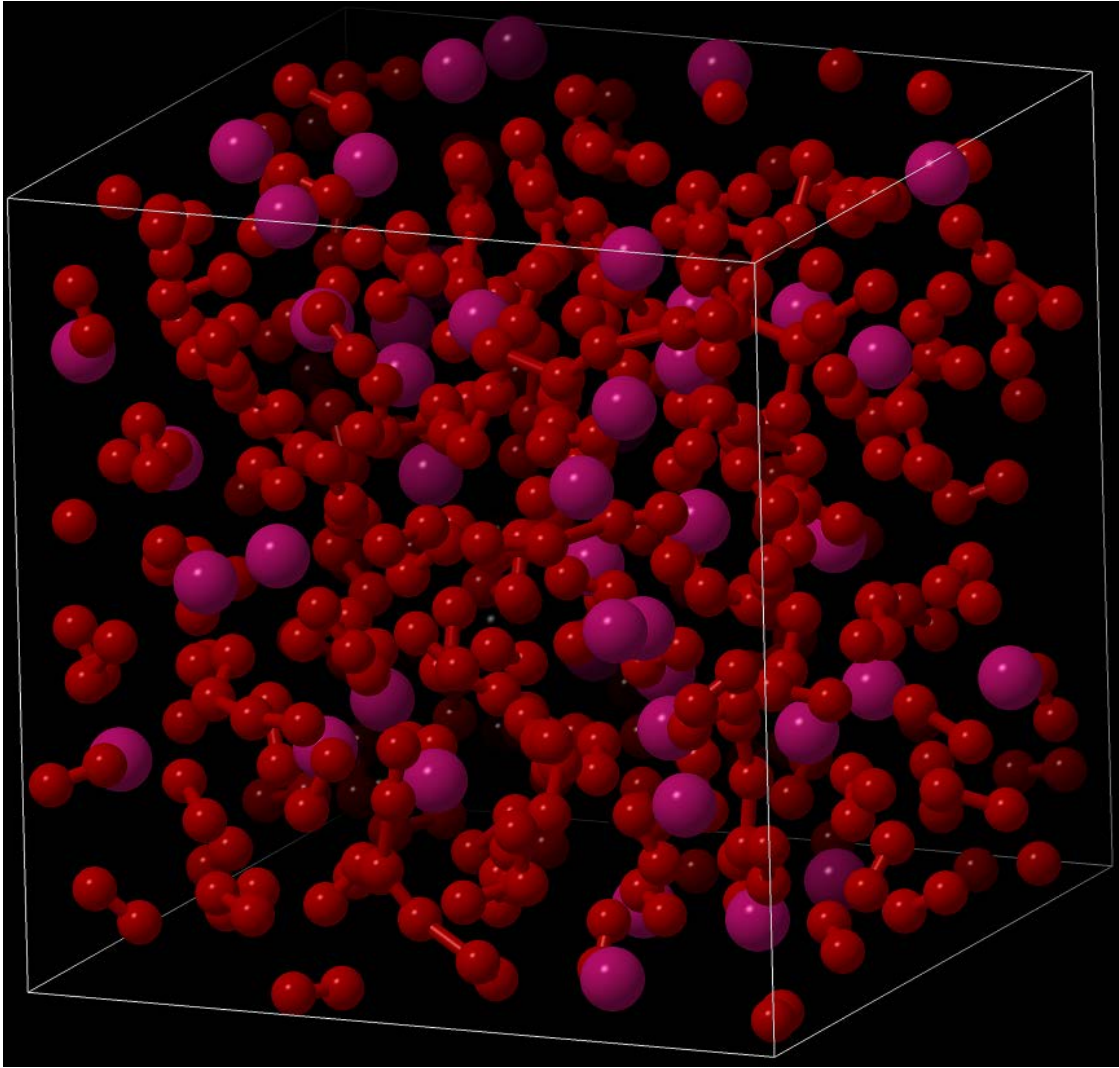


Systematics of known planets. For different compositions of planets, the radius-mass correlation is different. Solid line – H+He mixture, dashed line – water, dotted line – water-silicon-iron, dash-dotted line – silicon-iron (terrestrial planets). Exoplanet CoRoT7b should be chemically similar to the Earth, but much larger and heavier.

While Uranus and Neptune consist of a mixture of water, ammonia and methane, Jupiter and Saturn are made of a mixture of hydrogen and helium. These planets possibly have small cores made of roughly the same material as the Earth, but most of their volume is liquid. Temperatures and pressures inside these planets reach extremely high values (estimates up to ~20000K and 8000 GPa have made for maximum P-T conditions inside Jupiter). Such conditions, of course, greatly change the properties of materials:

-In Neptune and possibly Uranus, there is evidence for dissociation of CH_4 with the formation of diamond. Diamond, being very dense, must sink – and this process seems to produce significant amounts of gravitational energy in Neptune (Ross, 1981).

-In Jupiter and Saturn, the H-He mixture metallises at ~100 GPa and ~3000 K. These conditions correspond to quite shallow depths in these planets, implying that most of the material in these planets is a metallic fluid. Convection of this metallic H-He fluid produces remarkably strong magnetic fields of Saturn and especially Jupiter (Jovian magnetic field is ~10 times stronger than the Earth's magnetic field). The precise nature of this metallic fluid is still not known.



Model of the structure of the H-He fluid before metallization. One can clearly see H₂ molecules. These molecules would be broken in the metallic phase.

11. Structure-property relations.

Crystal structure is the basis for physical properties of a material. A primary important characteristic of all the physical properties of crystals is their anisotropy. Anisotropy of the structure determines the anisotropy (i.e. dependence on direction) of physical properties.

Crystals with a molecular type of structure with weak bonds between the molecules have, in general, low hardness, low melting temperature, high compressibility.

Materials with layered structures usually have perfect cleavage and platy habit of crystals.

Metals and crystals with significant delocalisation of electrons (e.g., semiconductors such as graphite, pyrite, nickeline, galena) have metallic luster and often are ductile.

Here we consider only a few examples of physical properties, most relevant to mineralogy:

- 1) link between crystal symmetry and several properties (optical activity, pyroelectricity, piezoelectricity) of crystals,
- 2) colour of minerals.

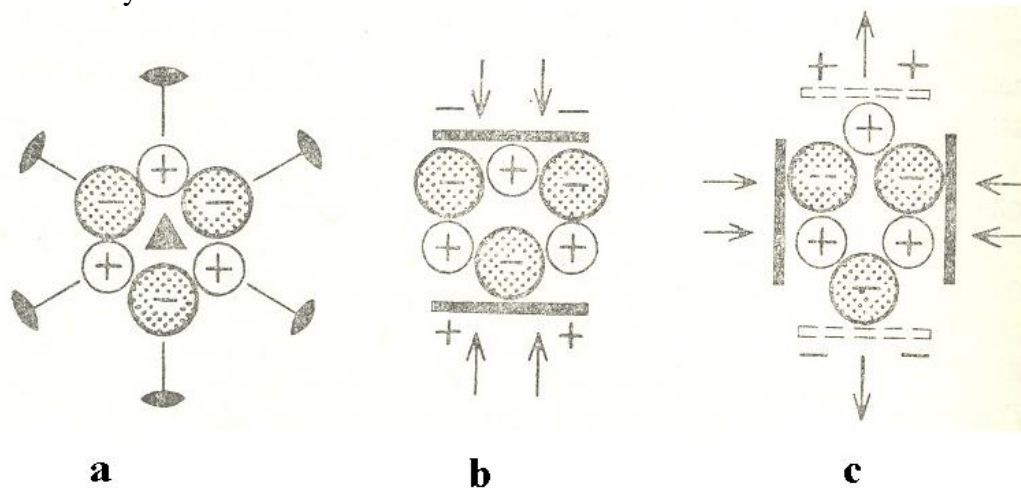
Link between symmetry and properties.

Optical activity: often, when polarised light travels through a crystal, the polarisation plane of light changes orientation (it rotates). In this case, we deal with an optically active crystal. Optical activity can be present only in chiral crystals – the direction of rotation (“left” or “right”) depends on whether the crystal is left or right. In chiral crystals, symmetry planes,

inversion centre, and $\bar{4}$ axis cannot exist. All symmetry classes that do not contain these elements, can be optically active. Among minerals, the most famous examples of optical activity are quartz and cinnabar (HgS).

Pyroelectricity: many crystals, e.g. tourmaline, when heated on fire, become electrically polarised (hence the name of the phenomenon – pyroelectricity, “pyros” means “fire” in Greek): opposite ends of a crystal acquire opposite electrical charges. On cooling, the charges reverse signs. This phenomenon can exist only in non-metallic crystals. For electrical polarisation to exist, there must be a unique polar direction in the structure not related by the symmetry elements to any other direction in the crystal. This automatically rules out all crystals with an inversion centre, and many acentric classes as well. Out of 32 crystallographic point groups, 21 are acentric (i.e. have no centre of inversion), but only 10 are pyroelectric – 1, 2, 3, 4, 6, m , $mm2$, $3m$, $4mm$, $6mm$.

Piezoelectricity is a similar phenomenon, where electrical polarisation appears as a result of mechanical deformation. Crystals belonging to 20 point groups can be piezoelectric – all acentric classes, except for 432. Like pyroelectricity, this phenomenon occurs only in non-metallic crystals.



Piezoeffect in quartz – a) undeformed structure, b) compressed along a twofold axis, c) stretched along a twofold axis. Under stress along the twofold axis, this direction becomes polar. (after Yegorov-Tismenko, 1992).

Colour of minerals. Optical properties are also anisotropic: anisotropy of the refractive index (birefringence), is one of the manifestations of anisotropy. Colour can also be anisotropic. This latter property is called pleochroism. Perhaps, the most famous example of pleochroism is kunzite, a transparent precious variety of spodumene ($\text{LiAlSi}_2\text{O}_6$). In this rather extreme case of pleochroism, the difference in the colour can be easily seen when the crystal is viewed in different directions. Kunzite crystals from Afghanistan are truly beautiful! Look at the pictures to see pleochroism and a cut kunzite gemstone.



Demonstration of pleochroism of kunzite – its colour parallel to [001] is much stronger than in a perpendicular direction.



Cut kunzite. The colour is delightful, but unfortunately it gradually fades away when kunzite is exposed to daylight. It can be restored by radiation. This indicates that the colour of kunzite is due to point defects and the associated electronic centres in its structure. Another interesting feature: irradiated by UV- or visible light, kunzite absorbs the energy and then radiates it back – creating impressive glowing effect in the dark! Such a glowing effect is called *luminescence* when its duration is long, or *fluorescence* if its duration is short.

As mentioned above, the colour of kunzite is due to point defects in the structure, and this is a very common origin of colour of minerals. An example of an electronic centre is Cl vacancy in NaCl – the position of the vacant Cl⁻ ion is occupied by a bare electron playing the role of the anion to maintain charge balance. This is the simplest electronic centre. Since the energy levels in such a defect differ from those in the bulk crystal, it can cause colour in crystals which are colourless in the absence of electronic centres. In NaCl, e.g., very small concentrations of electronic centres create deep blue colour – it can be seen in many natural samples. The colour is determined by the transition energies from one energy level to another – these determine the frequencies of the absorbed light. E.g., if yellow light is absorbed, crystals will be transparent for blue light and therefore will have blue colour. Other examples of colour due to the electronic centres – amethyst (variety of quartz, SiO₂), fluorite (CaF₂, having green, blue, violet colours), pink, black and smoky quartz varieties. Colours generated by electronic centres can disappear and reappear during irradiation, heating, etc. – unlike colours of other types.

Another cause of colour – transition metals. The energy levels of many transition metal ions in the crystal field are often close to the energies of quanta of the visible light – and thus can determine colour. Even small impurities of transition metals can often give very strong colours – e.g., the deep-red colour of ruby is created by just a fraction of a percent of Cr^{3+} ions in corundum (Al_2O_3). No wonder that most minerals of transition metals are coloured. It is interesting that even small variation in the crystal field strength can produce different colours – depending on the crystal field, chromium ions (Cr^{3+}) can give red colour (ruby), green (emerald), or blue colours. Likewise, copper ions Cu^{2+} can give blue (azurite $\text{Cu}_3(\text{CO}_3)_2(\text{OH})_2$) or green (malachite $\text{Cu}_2(\text{CO}_3)(\text{OH})_2$) colours. Such ions are called chromophores (greek ‘carrying colours’).

Yet another cause – electronic band transitions. This is a very common cause of colour in semiconductors, where energy band gap between the valence and conduction bands is sometimes similar to the energy of the visible light – again, defining which frequencies will be absorbed. No defects or ions-chromophores are necessary for this type of colour. Examples of colour of this origin – e.g., deep-orange realgar AsS , yellow orpiment As_2S_3 , deep-red cinnabar (HgS). Note that ionic insulators with wide band gaps ($>1\text{-}2\text{ eV}$) will be always colourless (unless they contain transition metal ions or electronic centres). So, colour can tell us something even about the chemical bonding and band structure!

Finally, colours can be simply due to microscopic coloured inclusions – e.g., inclusions of green amphiboles in quartz can make quartz green! Non-crystalline bitumen inclusions in (normally yellow) sulphur crystals are responsible for the black and brown colours of such varieties, and give important information about the conditions under which the crystals of sulphur grew!

12. Simulating & predicting structure and properties of crystals.

Crystals choose their structure so as to minimise their free energy. The most stable structure of a compound at given conditions has the lowest possible free energy. Many properties of crystals can be found by calculating the derivatives of the free energy – e.g., the elastic constants are second derivatives of the free energy with respect to lattice parameters.

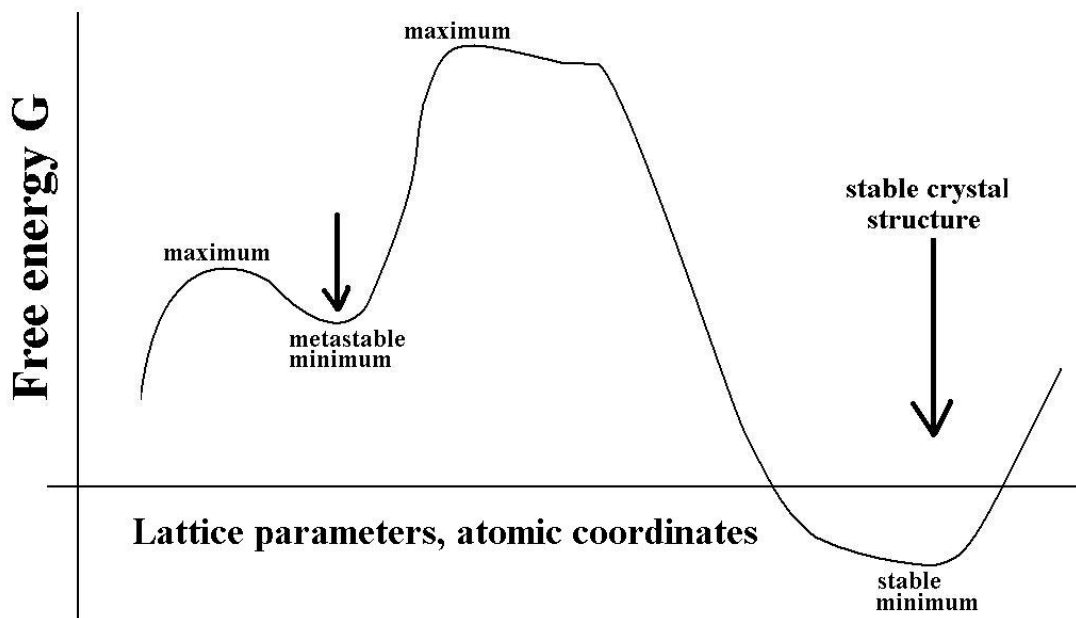


Illustration of how the deepest free energy minimum determines the stable crystal structure. Metastable crystal structures correspond to local minima.

The Gibbs free energy:

$$G = E + PV - TS$$

(E is the internal energy, P , V , T , S are the pressure, volume, temperature and entropy, respectively), when minimised with respect to lattice parameters and atomic coordinates at given pressure P and temperature T , yields the equilibrium crystal structure at given P - T conditions.

Statistical physics guarantees that if we can calculate the internal energy as a function of structure, we can calculate all the other thermodynamic properties including the entropy and the free energy. Therefore, the ability to calculate the energy of each given structure is crucial. There are two ways of calculating the energy: 1) quantum-mechanical, by solving the Schrödinger equation or its analogues, 2) semiclassical, by expressing the total energy as a sum of atom-atom potential energy terms. In the first approach, one explicitly considers electrons and nuclei (and hence it is possible to calculate electron density maps, study the electronic and magnetic structure, etc.), but since the Schrödinger equation cannot be solved exactly for many-electron systems like crystals, the solution is always approximate. In the second approach, one only considers the atoms as entities – this makes calculations much faster, but also much more approximate. Additionally, all information about the electronic and magnetic structure is lost.

For example, when modelling silicates, we can assume that the atoms interact in a pairwise fashion, so that the total energy is just a sum of pair interactions:

a. Coulombic energy between charged atoms. Experimental studies of electron distribution in silicates usually reveal charges of +1.5 to +2.5 for Si. Although this is much smaller than the formal 'ionic' charge of +4, ionic forces are essentially important

(the best model of the Si-O bond would be about half ionic and half covalent – see, e.g., L. Pauling's classical book 'The nature of the chemical bond').

b. Atom-atom repulsion. Apart from Coulombic repulsion between like-charged atoms, we also have shorter-range repulsion due to the overlap between electron clouds belonging to neighbouring atoms.

c. Van der Waals forces. In ionic systems, although always present, they are not crucial – unlike in solid noble gases, graphite, and many molecular crystals.

The energy of interaction of two ions is then:

$$E_{ij} = \frac{Z_i Z_j}{R_{ij}} + b_{ij} \exp\left(-\frac{R_{ij}}{\rho_{ij}}\right) - \frac{C_{ij}}{R_{ij}^6},$$

where the first, second, and third terms represent contributions a, b, c, respectively. Z_i and Z_j are atomic charges, R_{ij} the interatomic distance, and b_{ij} and C_{ij} parameters. These parameters can be fitted to experimental data (structures, properties) or quantum-mechanical calculations.

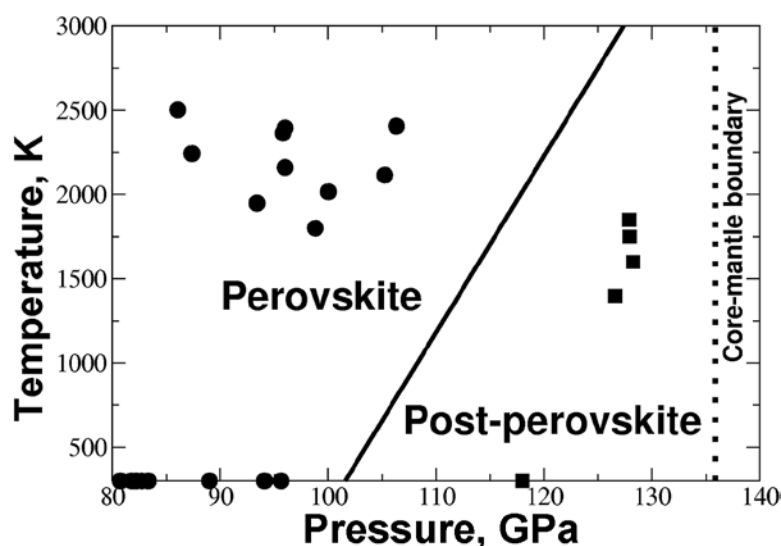
Lattice energy is found by summing over all pairs of atoms; optimal crystal structure is then found by minimising this energy with respect to atomic positions. Studying crystals at high pressures and temperatures, we have to minimise the free energy, i.e. include the entropy term ($-TS$) and the PV -term.

Differentiating the free energy with respect to lattice parameters, we get the elastic constants. By similar procedures, dielectric and piezoelectric properties can be easily studied as well. Such simulations play an important role in explaining and predicting properties of materials, mechanisms and thermodynamics of phase transitions, etc.

Over the last 10 years, the accuracy and capabilities of quantum-mechanical calculations increased dramatically. Now it is possible, with routine calculations, to predict lattice parameters within 1%, elastic and dielectric properties within 15%, vibrational frequencies within 5% of their experimental values. At high pressures and temperatures, when experiments become more difficult and for many properties there is a large uncertainty, theory can provide a more convenient route for exploring materials. Just to list some key applications:

- Discovery of a post-perovskite phase of MgSiO_3 , the main mineral of the core-mantle boundary region (Oganov & Ono, 2004).
- Determination of the high-pressure melting curve of iron (Alfe et al., 1999-2002) and of the temperature of the Earth's core – about 5600K in the centre.
- Elucidation of the thermal structure of the Earth's mantle (Oganov et al., 2002).
- Explanation of the elastic anisotropy of the Earth's solid inner core (Gannarelli, 2003).

To demonstrate the accuracy of such calculations, I show two examples – MgSiO_3 post-perovskite (its stability field and crystal structure – Oganov & Ono, 2004) and CaO (phase transition pressure and equation of state – Jung, 2004).



High-pressure phase diagram of MgSiO₃. Line – theory, symbols – experimental data (circles – perovskite, squares – post-perovskite).

Table. Lattice parameters (in Å) of MgSiO₃ post-perovskite at 120 GPa (orthorhombic, *Cmcm*)

	Theory	Experiment
<i>a</i>	2.474	2.471
<i>b</i>	8.121	8.091
<i>c</i>	6.138	6.110

Table. Comparison of theory and experiment for CaO – transition pressure (from NaCl- to CsCl-type structure) and the equation of state (for the NaCl-type phase)*.

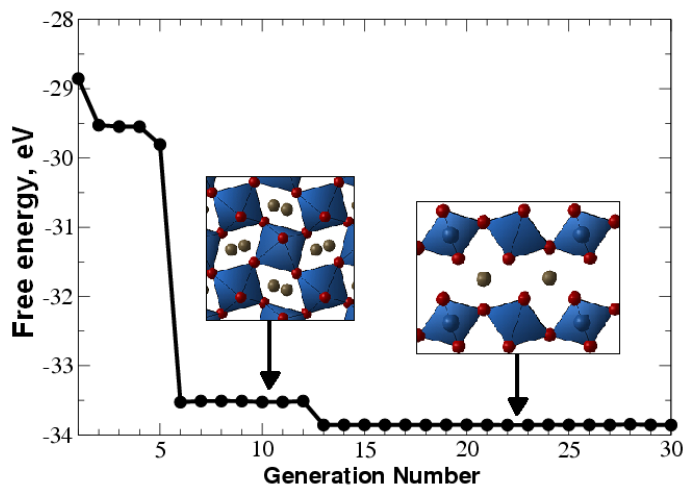
	Theory	Experiment
P_{tr} , GPa	64	65 ± 5
V_0 , Å ³	28.31	27.75
K_0 , GPa	109	125
K'_0	4.22	3.6

* V_0 , K_0 , K'_0 are the volume, bulk modulus, and its pressure derivative at zero pressure.

(bulk modulus is the inverse of the compressibility $\beta = -\frac{1}{V} \frac{dV}{dP}$).

Crystal structure prediction. Once a starting model of a crystal structure is known, it is easy to optimize it – e.g. by moving the atoms in the direction of forces acting on them. Now, what if one does several such optimizations starting with several very different initial structures? Generally, the results will be different depending on the starting structure – this way one obtains a number of different structures corresponding to *local* minima of the energy. How many different local minima are possible? In principle, an infinity, but it is the lowest, so called global, minimum that is of main interest. How to find the most stable structure at given P - T conditions knowing just the chemical formula? Rules of crystal chemistry are definitely helpful in restricting the class of possible structures, but these rules are not enough to obtain one most stable structure. One could compare the (free) energies of all possible structures and find the lowest-energy structure, but this requires an unfeasible computational effort – to predict the structure containing only 10 atoms in the unit cell would take about 1000 years on today's computers! Such computing costs can in principle be avoided. Several methods have been

devised to solve this problem, but none seem to have showed satisfactory results. In fact, this problem is often considered to be impossible to solve. A very promising method was developed recently (Glass et al., 2006; Oganov & Glass, 2006). This method combines an evolutionary strategy and quantum-mechanical simulations. In this method, one starts with randomly generated structures, which are evaluated using quantum-mechanical calculations of their free energies. The best structures are selected to produce the next generation of structures – using “genetic” crossover of their elements, as well as through mutation. From generation to generation, increasingly favourable structures are found this way.



Prediction of the crystal structure of MgSiO₃ at 120 GPa (20 atoms/cell). Free energy of the best structure as a function of generation is shown, together with perovskite and post-perovskite structures. Between 6th and 12th generations the best found structure is perovskite, but at the 13th generation the global minimum (post-perovskite structure) is found. This simulation used no experimental information and found both the stable and good metastable structures in a single simulation. Blue polyhedra – SiO₆ octahedra; gray spheres – Mg atoms.

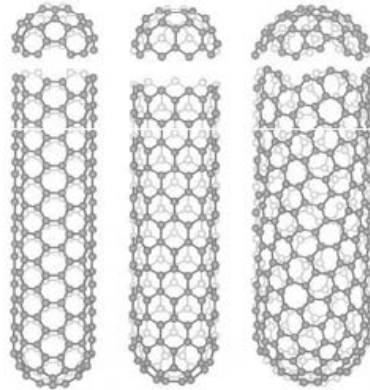
Crystal structure prediction is very important for computational design of new materials, for investigating state of matter at extreme pressures and temperatures, etc. It is amazing that this problem – the central problem of crystal chemistry – remained open until so recently. Even now there are many open issues in this field.

13. Supplementary lecture: Crystallography of nanoparticles.

By nanoparticles we understand atomic assembles, the size of which ranges between 1 and 100 nanometres ($1 \text{ nm} = 10 \text{ \AA}$). Nanoparticles thus occupy an intermediate position between typical molecules and bulk materials. By the number of atoms, the following rough order-of-magnitude estimates can be given: molecules: 1-10 atoms, nanoparticles: $10\text{-}10^6$ atoms (radius up to 1000 \AA), bulk materials $>10^6$ atoms.

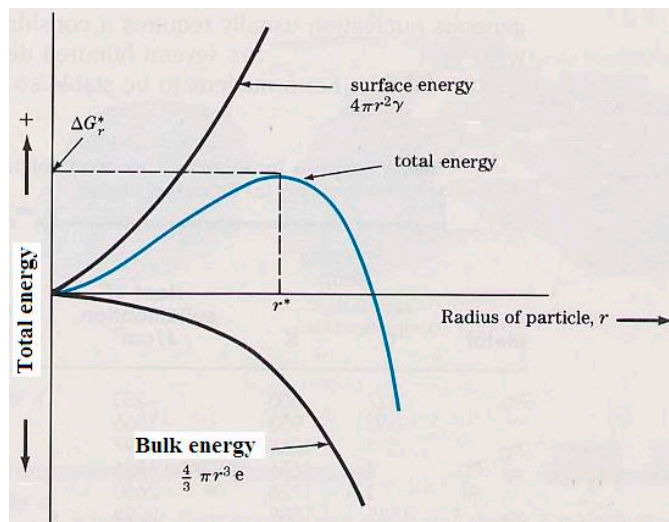
Studies of nanoparticles are important for several reasons:

- (i) They open up unique technological perspectives, if we can learn to manipulate atoms on nanoscale. Properties of nanoparticles depend on their size and structure and thus can be tuned, or manipulated. Nanoparticles often have unique properties. E.g., dislocations cannot exist in particles smaller than $\sim 300 \text{ \AA}$ in diameter. In such particles deformation occurs through non-dislocation mechanisms, and such nanomaterials are mechanically much stronger than bulk crystalline materials. A striking example is given by carbon nanotubes, which display extremely interesting properties. Young's modulus of carbon nanotubes is 1.2-1.8 TPa, the value for steel is 0.21 TPa. Yield stress of a nanotube is 45 GPa, that of steel is 2 GPa. The presence of carbon nanotubes in Damascus steel is believed (Reibold, 2006) to be one of the secrets of the unique mechanical properties of this material. Finally, depending on their structure, carbon nanotubes can be metallic or insulating. Metallic nanotubes have extremely high electrical conductivity, because these nanotubes are almost defect-free.



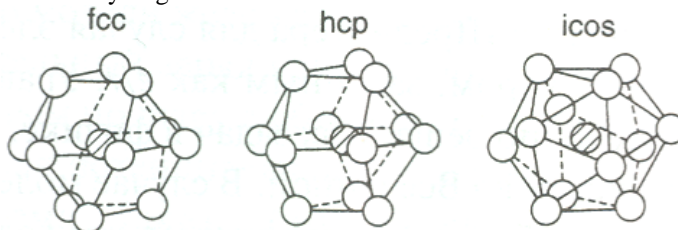
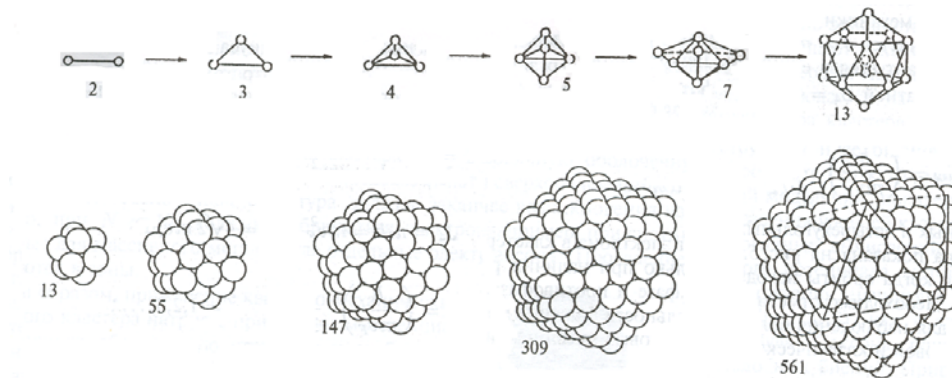
Carbon nanotubes.

- (ii) Fundamental importance – theory of molecules and solids is well developed, whereas for intermediate sizes it is not mature and many new phenomena are expected. Structures of nanoparticles often differ from those of crystals and molecules (the same is often true also for surfaces), and can therefore bring new understanding of chemical structures and bonding. E.g., see discussion below on “magical numbers”.
- (iii) Processes of crystal growth and phase transformations involve nucleation – i.e. formation of a nanosize “critical nucleus” of the new phase. The total energy of a nucleus consists of two parts – surface energy (positive, proportional to r^2) and volume energy (negative, proportional to r^3). At small sizes surface term dominates and nuclei are energetically unfavourable and increases up to the critical radius r^* . At large sizes the volume term dominates and crystals above certain size are energetically favourable. This model, however, is simplified – the structure of small particles may drastically differ from the bulk structure and that affects energetics.



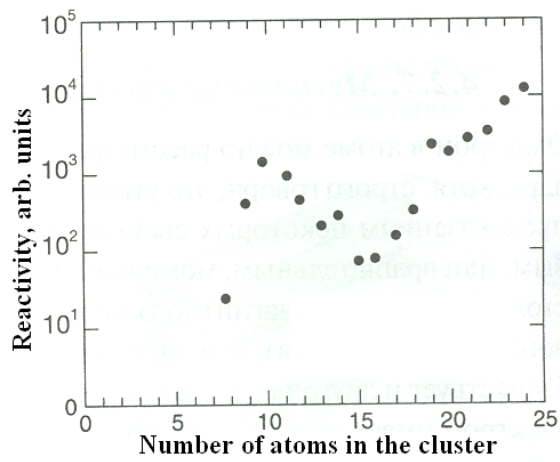
Energy contributions for a nanoparticle, as a function of its radius.

One of the radical differences between crystals and nanoparticles is that the latter can have non-crystallographic symmetry elements. For instance, Al_{13} clusters (experimentally known to be particularly stable) can be either cuboctahedral (as in fcc- or hcp-structures) or icosahedral. Theoretical studies showed that icosahedral clusters (containing fivefold axes) are the most favourable ones. Icosahedral clusters are known to be stable for many other clusters (e.g. noble gases), which means that as these clusters grow, there must be a reconstruction into a crystal-like structure at sufficiently large cluster size.

Possible structures of Al_{13} clusters (from Poole & Owens, 2003).

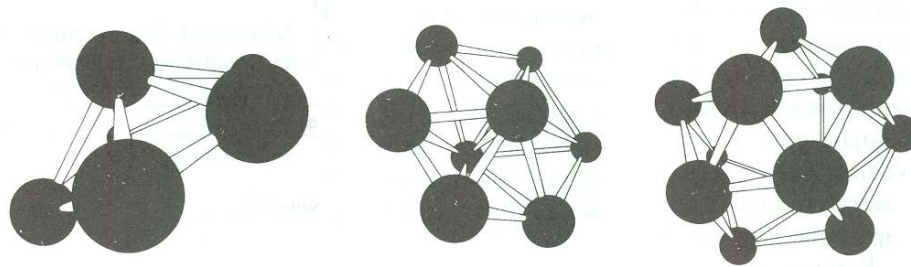
Structures of noble gas clusters (from Suzdalev, 2005).

Properties depend on the size – properties of an isolated atom are not the same as properties of a small molecule, or of clusters of various sizes, or of a large crystal. Both atomic and electronic structure change with size, sometimes quite dramatically. An example of reactivity is illustrated below for Fe nanoparticles. Japanese researchers have found that Au nanoparticles smaller than 3-5 nm in diameter are catalytically very active and have an icosahedral structure (unlike the fcc-structure of the bulk), and this was used in the design of a new air freshening device using Au nanoparticles on the Fe_2O_3 substrate.

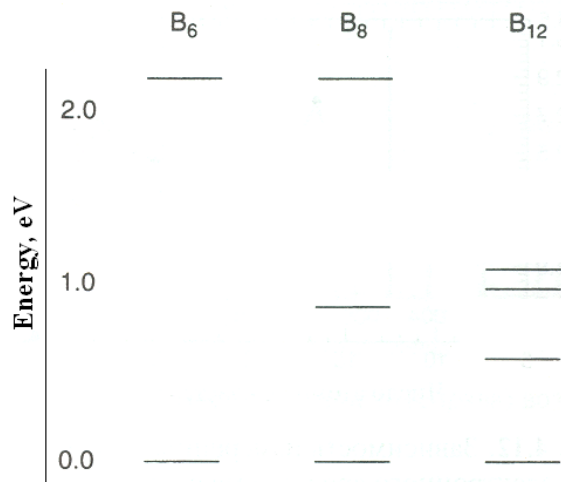


Reactivity of Fe nanoparticles with hydrogen (from Poole & Owens, 2003).

Since structure of nanoparticles depends on their size, electronic properties will also be size-dependent, as illustrated below for boron clusters.



Structure of boron clusters (from Poole & Owens, 2003).



Theoretically calculated energy spectra of boron clusters (from Poole & Owens, 2003).

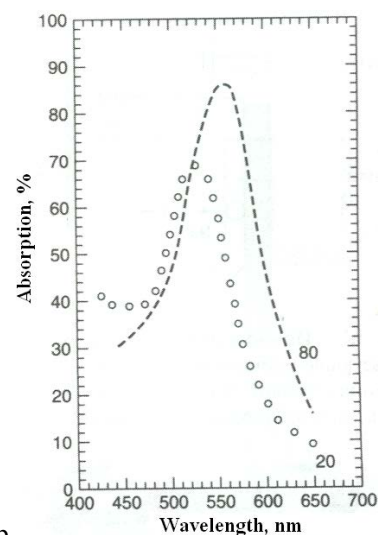
Such variations of electronic structure imply variations of many other properties, e.g. optical properties, with size. For instance, the colour of Au nanoparticles is strongly size-dependent, as illustrated below.

Different sizes of colloidal gold particles



2 5 6 12 16 18 24 60 90 150 nm

a



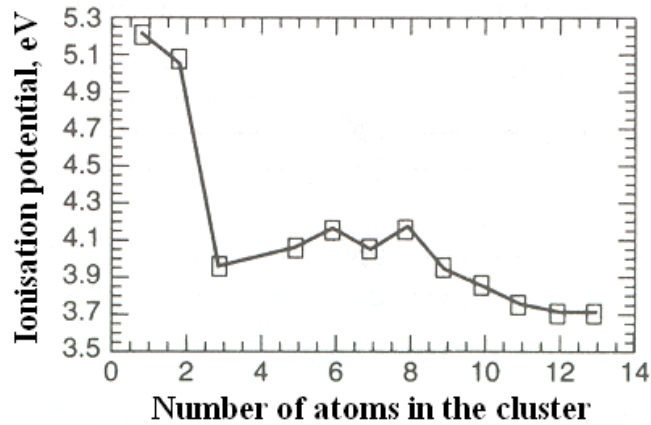
b

(a) Dependence of colour on the size of Au nanoparticles. (b) Optical absorption spectra of gold nanoparticles of two sizes (20 nm and 80 nm diameter) in glass (from Poole & Owens, 2003).

This is related to a masterpiece of ancient Roman art, the famous Lycurgus cup, which remained a mystery for nearly 2 millenia. The cup is red when the source of light (candle) is placed inside it, but is green otherwise. The reasons for this have been understood only recently. The color of transmitted light (red in this case) is due to the absorption spectrum of gold nanoparticles – around 10 nm in this case. The green color is due to scattered light – the phenomenon of Rayleigh scattering, when wavelength of light (380-780 nm) is many times greater than the fluctuations of density, on which light is scattered (here, the size of gold nanoparticles, about 10 nm). Rayleigh scattering cross-section depends on the wavelength of light (it is inversely proportional to the fourth power of the wavelength, i.e. blue color is scattered more than red – this is why the sky is blue, when you don't look at the Sun). Combination of scattered blue color and transmitted red color gives green color.

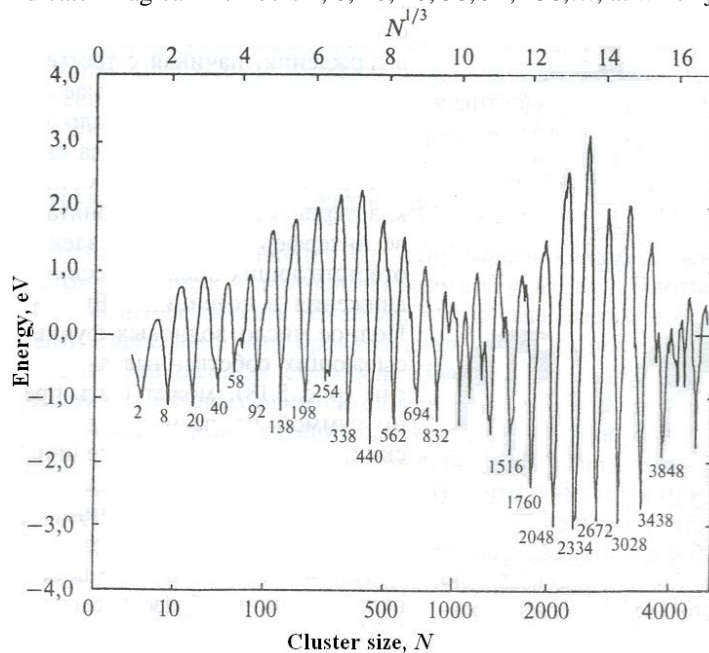


As figure below shows, for Na clusters the ionisation potential is a non-monotonic function of the number of atoms. In particular, there are peaks at $N=2,6,8$. Peaks at $N=2$ and 8 can be explained if one considers a cluster as a “superatom” – in that case, they correspond to filled electronic shells.



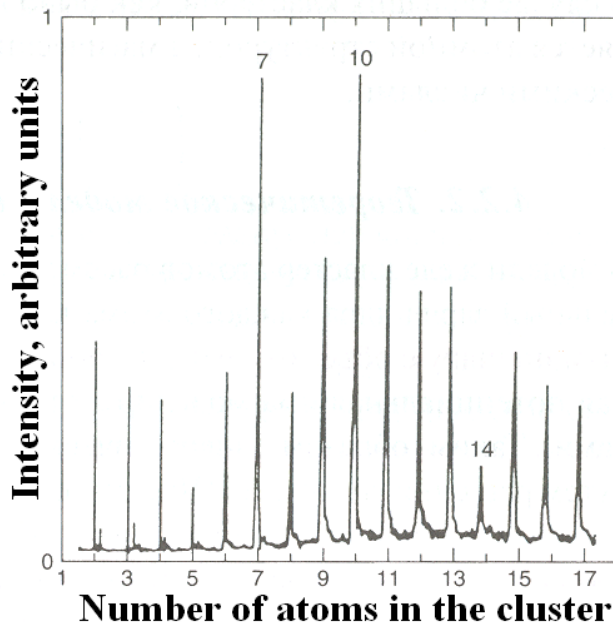
Ionisation potential of Na clusters (from Poole & Owens, 2003).

The idea of clusters-superatoms has been used to formulate the so-called “jellium” model, where the cluster is represented as a free-electron drop of finite size. Results of this model are shown below and indicate “magical” numbers 2, 8, 20, 40, 58, 92, 138, ..., at which jelly particles are particularly stable.



Energy of Na nanoclusters in the “jellium” model (from Suzdalev, 2005).

“Magical numbers” (i.e. the numbers of atoms in a nanoparticle, at which the particle is especially stable) are a general feature of nanoparticles. As figure below shows, for Pb, the most stable clusters contain 7 and 10 atoms.



Mass-spectrum of Pb nanoclusters (from Poole & Owens, 2003).

For small nanoparticles the magical numbers are determined by electronic effects (“electronic magical numbers”, providing optimal occupation of bonding orbitals), for large particles – by geometric effects (“structural magical numbers”, providing minimisation of the surface energy and creating maximally dense particles with maximally spherical shapes).

E.g. for Na nanoparticles all the predicted magical numbers have been experimentally observed – electronic up to $N=1220$, and structural at $N>1415$. Noble gas clusters are an interesting special case – consisting of atoms with filled electronic shells, these clusters do not have electronic magical numbers, only the structural ones. Experiments confirm that particularly stable clusters of Ar and Xe contain $N=13, 19, 25, 55, 71, 87, 147$ atoms. For He quantum effects create a slightly more complicated case. ^3He has stable clusters at $N=7, 10, 14, 23, 30$, while magical numbers for ^4He are $N=7, 10-11, 14, 22, 26-27, 30$. ^4He clusters containing 64 and 128 atoms were experimentally found to display superfluidity, which was previously observed by P.L. Kapitsa for liquid ^4He .

14. Supplementary lecture: Structure of crystalline surfaces.

In this course we mainly considered the ideal crystal. This simplification (infinite, strictly periodic defect-less solid) enables deep understanding of solids, but of course in reality we never deal with infinite crystals and periodicity is perturbed by atomic motion and defects. Defects can be 0-D (substitutions, vacancies, interstitials), 1-D (dislocations) and 2-D (surfaces). Here we consider surfaces. In fact, in the very beginning of this course we already discussed surface energies and their role in defining the equilibrium morphology of crystals. Now let us explore the structure of surfaces of crystals – this knowledge is more recent compared to the knowledge of bulk structures, because special experimental methods (in particular, electron microscopy) had to be developed in order to obtain this knowledge.

Surface is a special case of an *interface* – the former term is usually applied to the boundary layer between a crystal and gas, and the latter means the boundary between two solids, or between a solid and a liquid. Solid-solid interfaces are more difficult to study, and our knowledge about them is still not well developed.

Surfaces (and interfaces) are important for many reasons:

- (i) Surface energies determine the morphology of crystals and the size of the critical nucleus.
- (ii) Most catalytic processes occur on solid surfaces. Understanding of catalysis without understanding surface structures is impossible.
- (iii) Surfaces often have structures and properties different from the bulk, and different surfaces of the same crystal may possess very different properties – this opens up avenues for engineering the desired properties.
- (iv) Surfaces and interfaces are particularly important for microelectronics – for instance, to increase the density of transistors in computer chips, already by end of 2000s computer companies are pushed to the nanometer scale where surface effects are crucial.

- (v) Understanding surface structures will lead to a more complete understanding of the structure of matter, and structure-property relations. In many ways, surface crystallography is just a 2D-extension (or reduction) of our usual 3D-crystallography and many of the concepts we have developed can be applied to surfaces as well.

Surface can be viewed as a „suffering“ crystal – a crystal where many bonds have been broken. These „dangling bonds“ are unfavourable - as we know, surface energies (measured in units of energy per area – e.g. J/m^2) are always positive (i.e. destabilising) and there are several ways to minimise this surface energy:

1. *Relaxation* – in this case, the structure of the surface is very similar to the bulk structure, the only differences are small shifts of the atoms, mainly in the direction perpendicular to the surface. Almost all known metals surfaces and surfaces of ionic crystals belong to this category.
2. *Reconstruction* – bonding topology differs from that of the bulk. Surfaces of covalent crystals (semiconductors) are typically reconstructed.
3. *Chemisorption and physisorption* – in these cases foreign atoms or molecules attach themselves to the surface, either by van der Waals (physisorption) or stronger (chemisorption) interactions. In the latter case, this allows „dangling bonds“ to be saturated and one can talk about the formation of new compounds at the surface – *surface phases*. One example of a surface phase is the oxidised layer (Al_2O_3) on the surface of aluminium – it is because of this layer that aluminium is chemically relatively inert (without it, Al would vigorously react with water!). Another example – $\text{Al}(\text{OH})_3$ layer on the $\{0001\}$ surfaces of corundum – it is because of this layer that corundum crystals grown in basic OH-rich environment have platy habit.

Relaxation is quite a trivial phenomenon, while chemisorption and physisorption would lead us far away from the topic of crystallography. So, let us discuss surface reconstruction as an example of the fascinating phenomena in surface science. Our discussion will closely follow the book of Oura et al. (2003), where the reader is referred for more details (and discussions of physisorption and chemisorption).

One of the few metals whose surfaces reconstruct is Pt, in its normal fcc-phase. The unreconstructed Pt(100) surface is not close-packed, and reconstruction transforms it into a nearly close-packed structure. This leads to an increase of atomic density by $\sim 20\%$. The bulk substrate and surface now have different atomic densities and symmetries, which leads to a tension - a compromise is the formation of long-period (20×5 or 29×5) or even incommensurate structures. This is a manifestation of a general principle – *competing interactions often lead to complex structures*. Similar quasi-hexagonal reconstructions were observed for Ir(100) and Au(100) surfaces.

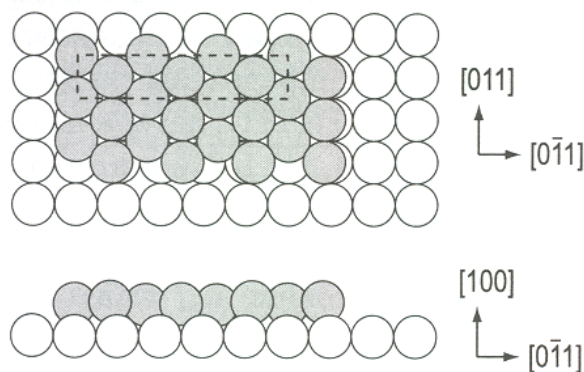
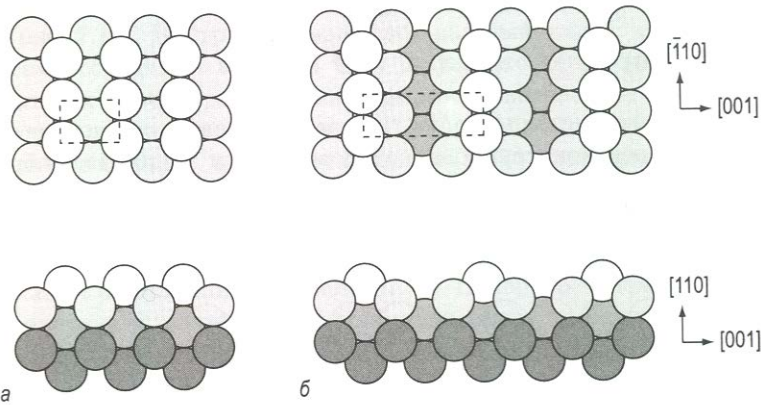


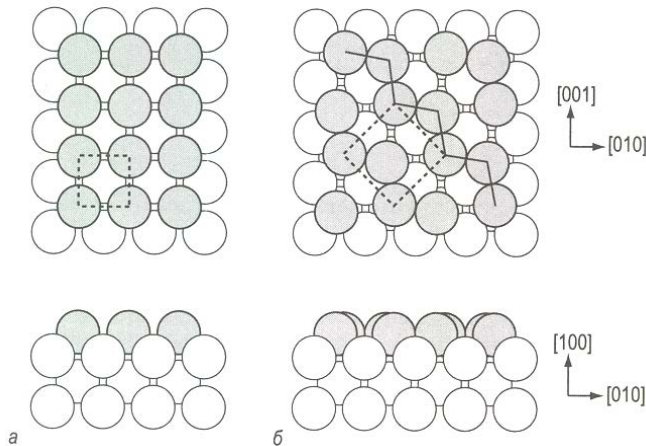
Illustration of the Pt(100) surface. Gray atoms – surface, white – substrate. From (Oura et al., 2003).

Another example is the Pt(110) surface, which is again not close-packed but reconstructs to a “missing-row” structure that can be represented as microfacets of the close-packed Pt(111) surface.



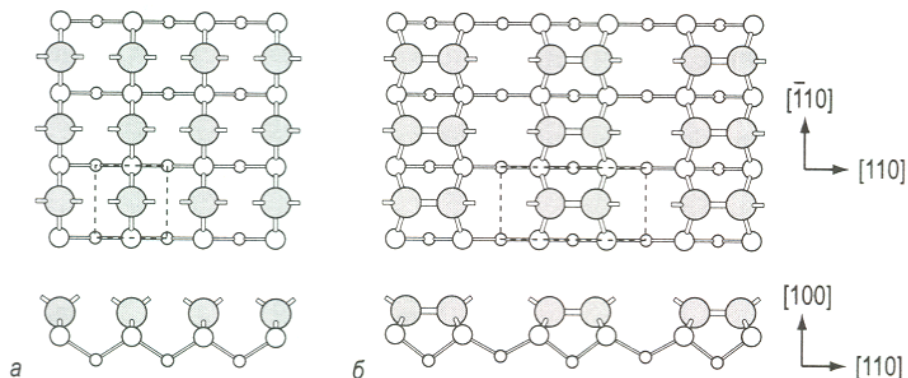
Pt(110) surface structure showing an unreconstructed surface (left) and the 1x2 reconstruction. From (Oura et al., 2003).

To finish our small tour of reconstructed metallic surfaces, we present the W(100) surface. At normal conditions W adopts the bcc structure. Below the room temperature, it adopts a 2x2 reconstruction with moderate ($\sim 0.2 \text{ \AA}$) displacements of the atoms so as to form zigzag chains along [110] directions. This is a sign of directional bonding.



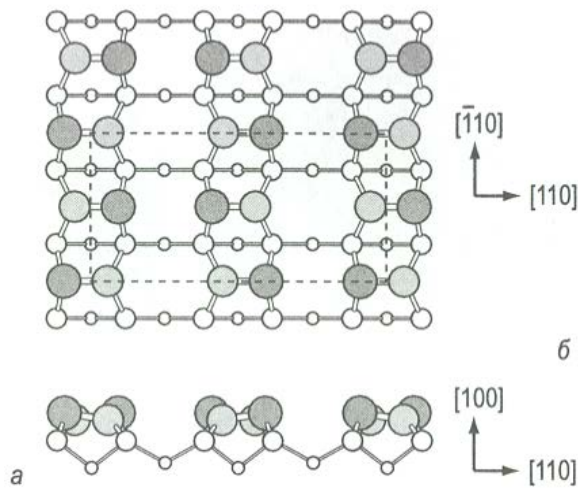
W(100) surface structure (left – unreconstructed, right – 2x2 reconstruction). From (Oura et al., 2003).

The most diverse and dramatic surface reconstructions are known in semiconductors. Without reconstruction, there would be two dangling bonds per Si atoms on the Si(100) surface. The observed 2x1 reconstruction leads to pairing of the Si atoms, which reduces the number of dangling bonds per atom to only one. Pairing is one way to stabilize surfaces. Another way is charge transfer – this has been seen in Ge(111) surfaces, where electron transfer to the most underbonded atoms lowers the energy.



Si(100) surface structure (left – unreconstructed, right – 2x1 dimeric reconstruction). From (Oura et al., 2003).

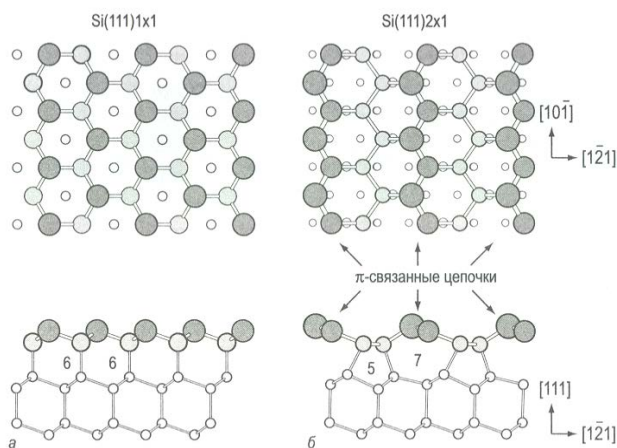
It turns out that the structure described above is only a dynamical average and on cooling the dimers adopt an inclined orientation (angle of 18° with the horizontal plane) and periodicity doubles – now the 4x2 reconstruction is formed. The same reconstruction is known for the Ge(100) surface.



Si(100)4x2 surface reconstruction. From (Oura et al., 2003).

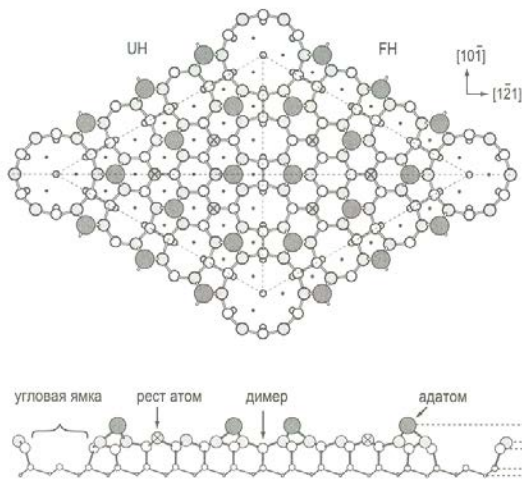
The Si(111) surface also undergoes interesting reconstructions. The 2x1 reconstruction is obtained by cleaving the crystal along (111). This reconstruction is metastable and irreversibly transforms into the 7x7 reconstruction when annealed above 700 K. The 7x7 reconstruction is stable up to 1000 K, above which it undergoes an order-disorder transformation into the 1x1 structure.

The 2x1 reconstruction contains 5- and 7-fold rings of carbon atoms between the surface and substrate. The same reconstruction is known for diamond (111) surface. Such 5+7 structure for the bulk Si and C was actually seen in calculations of Oganov & Glass (2006) and found to have rather low energy (but metastable).

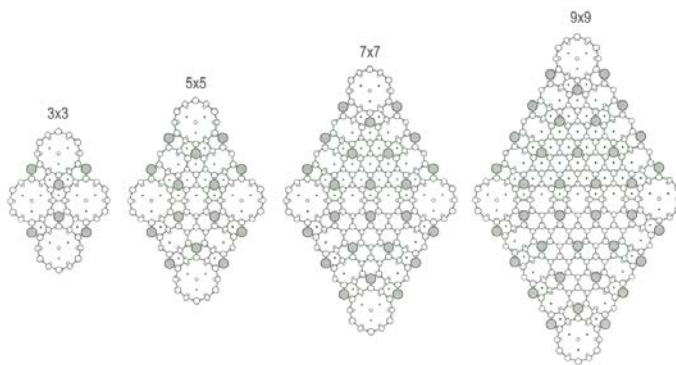


Si(111) surface structure (left – unreconstructed, right – 2x1 reconstruction). From (Oura et al., 2003).

In fact, a whole homologous series of very complex reconstructions was found for Si(111) surfaces. These $(2n+1) \times (2n+1)$ reconstructions, the most stable of which is 7x7, are shown below.



Si(111)7x7 surface reconstruction. From (Oura et al., 2003).



Family of Si(111) reconstructions (2n+1)x(2n+1). From (Oura et al., 2003).

Let us move on to a more complex case – GaAs. This material has the zincblende structure, which is non-centrosymmetric and therefore (111) and $\bar{1}\bar{1}\bar{1}$ surfaces are non-equivalent. By convention, (111) surfaces are terminated by Ga, and $\bar{1}\bar{1}\bar{1}$ surfaces are terminated by As. Let us recall that in the bulk, Ga and As occupy the same Wyckoff positions and interchanging them would change nothing. Nevertheless, these two surfaces have entirely different reconstructions!

The GaAs(111)2x2 reconstruction has every fourth Ga atom missing and the terminating layer is distorted into a flat configuration. Stability of this structure, containing Ga and As atoms in the exotic planar threefold coordination, is enhanced by additional charge transfer from Ga to As.

The GaAs($\bar{1}\bar{1}\bar{1}$)2x2 reconstruction is formed at conditions of excess of As (when the chemical potential of As is low, another reconstruction is formed - $\sqrt{19}x\sqrt{19}$) and contains As₃ trimers, in which each As atom is connected to one additional As atom outside of the trimer.

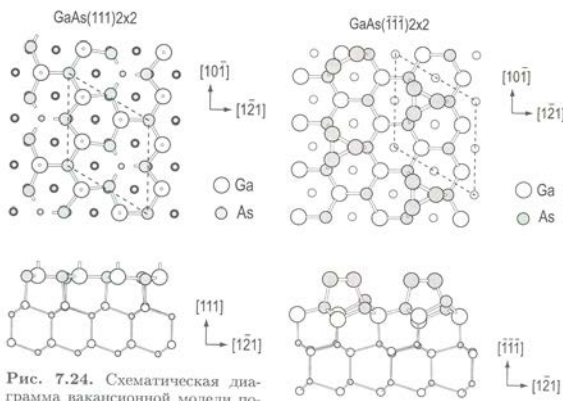
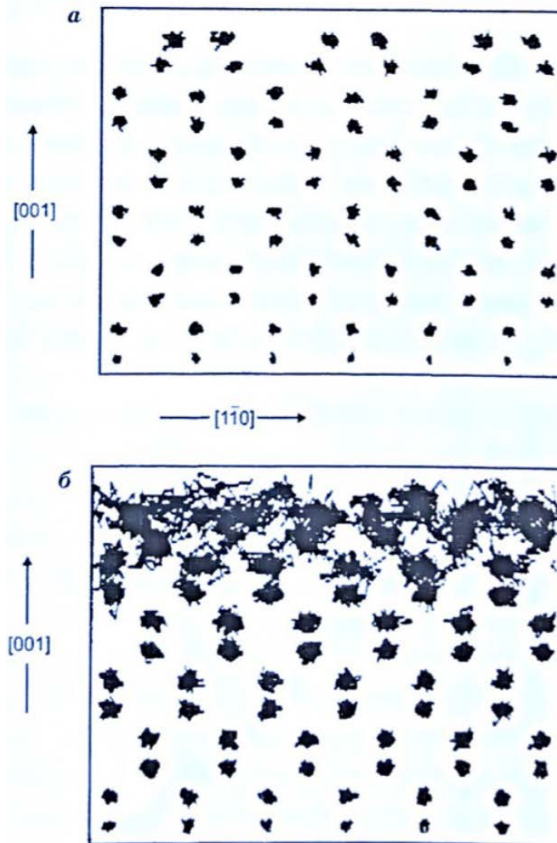


Рис. 7.24. Схематическая диаграмма вакансионной модели по

GaAs (111) and $\bar{1}\bar{1}\bar{1}$ 2x2 reconstructed surfaces. From (Oura et al., 2003).

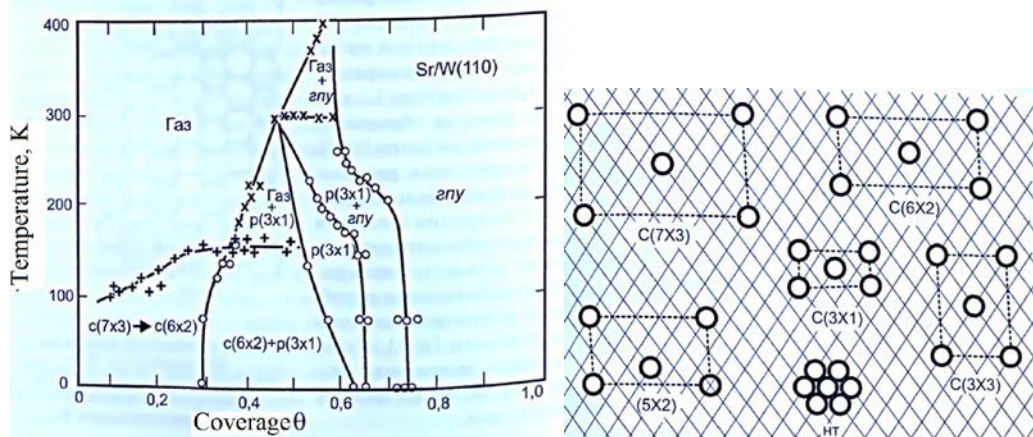
As is clear from our discussion, some of the structures we saw are extremely exotic and some phenomena seen for surfaces are new. However, many of the traditional concepts of crystallography are perfectly applicable to surfaces – we saw several examples of phase transitions and homologous structures, the formation of long-period and incommensurate structures, and a few interesting illustrations showing that metals tend to form close-packed structures also on their surfaces.

Surfaces are anomalous in many ways. For example, thermal conductivity of the surface is usually several times lower than that of the bulk. It is well known that melting begins at surfaces. Atoms experience much more vigorous thermal motion at the surface, and at temperatures well below T_m , the surface may already be molten.



Atomic trajectories in Si(100) surface at (a) 1003 K and (b) 1683 K. From [Vladimirov, 2016].

Often, new compounds (“surface compounds”) can be formed, which have no bulk analogs. E.g., Cu and B do not form bulk compounds, but do form copper borides on the surface (when a surface of Cu is bombarded by B atoms). Example of a complex surface phase diagram: Sr on W(110) surface. Ordering occurs already at low concentrations of Sr (at low T). Stoichiometric surface compounds are formed. At high concentrations, incommensurate close-packed layer of Sr is formed.



Phase diagram of Sr on W(110) surface and corresponding structures. From [Vladimirov, 2016].